astro/space

FACILITY FORM 602
N67-18003
(ACCESSION NUMBER)
158
(PAGES)
CR 91714
(NASA CR OR TMX OR AD NUMBER)
(THRU)
None
(CODE)
14
(CATEGORY)

REPRODUCED BY
NATIONAL TECHNICAL
INFORMATION SERVICE
U.S. DEPARTMENT OF COMMERCE
SPRINGFIELD, VA. 22161

U.S. DEPARTMENT OF COMMERCE
National Technical Information Service
5285 Port Royal Road
Springfield, Virginia 22151

Date: 22 June 1983

Reply to Attn of: 954.01

Subject: NASA Document Discrepancy Report

To: Dorothy Corbitt

NASA Scientific & Technical Information
Facility
P.O. Box 8757
Baltimore/Washington
International Airport, Md. 21240

Re: N67-18003 - Development of a Pressure and Force Transducer Calibration Procedure for the Hypersonic shock Tunnel. Vol. 2.

☐ 1. Page(s) are missing from microfiche and paper copy. Please provide a complete copy.

☒ 2. Portions of this document are illegible when reproduced. Please provide a reproducible copy. Not reproducible (blue prints and foldouts.)

☐ 3. A microfiche reproduction is not legible. The case file was not received. Please provide at least an acceptable microfiche.

☐ 4 Incorrectly priced at _____. It should be _____ for _____ pages. However, price will remain as announced in STAR.

☐ 5. Case file returned herewith. When correction has been made please return to NTIS or if corrections cannot be made note NASA records that the case file was returned.

☐ 6. Other:

July 28, 1983

This copy is the best available. Document contains a disclaimer concerning portions of the report being illegible.

Sincerely,

PHILIP N. FRENCH
DOCUMENT EVALUATOR

Response

Before After
___ Issue Ch. of Status___
Code_____Code
___ Comp. Ser.-No Act. ___
___Delay Ch. OF Status
___Post(ed) on Form 107___

PLEASE ATTACH COPY OF THIS LETTER WITH YOUR RESPONSE

N67-18003

FINAL REPORT
FOR
DEVELOPMENT OF A PRESSURE AND FORCE TRANSDUCER CALIBRATION PROCEDURE FOR THE HYPERSONIC SHOCK TUNNEL

CONTRACT NO. NAS8-5350

MAY 1963 THROUGH OCTOBER 1966

VOL II

Authors:

Robert F. Pickard
Project Engineer

J. R. Loyd
Engineer

Prepared for:

George C. Marshall Space Flight Center
National Aeronautics and Space Administration
Huntsville, Alabama

Date: 17 January 1967

REPRODUCED BY
NATIONAL TECHNICAL INFORMATION SERVICE
U. S. DEPARTMENT OF COMMERCE
SPRINGFIELD, VA. 22161

Astro-Space Laboratories, Inc.
2104 Memorial Parkway, S. W.
Huntsville, Alabama 35801

NOTICE

THIS DOCUMENT HAS BEEN REPRODUCED FROM THE BEST COPY FURNISHED US BY THE SPONSORING AGENCY. ALTHOUGH IT IS RECOGNIZED THAT CERTAIN PORTIONS ARE ILLEGIBLE, IT IS BEING RELEASED IN THE INTEREST OF MAKING AVAILABLE AS MUCH INFORMATION AS POSSIBLE.

ABSTRACT

This is the Final Report of the work performed by Astro-Space Laboratories for Marshall Space Flight Center on Contract NAS8-5350. The period of performance was May, 1963, through October, 1966.

The information contained in this Final Report is presented in Volumes I, II, and III. Volume I presents the summary of the work involving the area of pressure instrumentation, pressure generation, and aerodynamic damping. Volume II summarizes the work performed in the development of force balances and balance calibration procedures. Volume III comprises the summary of the work performed in the area of thin film heat sensor development and research.

VOLUME II

FORCE BALANCES AND BALANCE CALIBRATION PROCEDURES

CONTENTS

SUMMARY

This report summarized the effort expended toward the development of a Hypersonic Shock Tunnel Force Balance, the associated equipment, and calibration techniques.

A study was conducted to determine the possibility of using strain gages in a shock tunnel force balance system. The conclusion of this study indicated that semi-conductor gages could be used with adequate results, however, it was found that piezoelectric sensors offered a definite advantage. These piezoelectric sensors have high sensitivity, very high frequency response, and a very wide dynamic range.

A complete analysis was made to determine the required acceleration compensation considering the effect of the model, balance, and sting vibrations on the output of the force sensors when measuring aerodynamic forces. Included in this study phase was the design of a low pass filter which was finilized.

A through calibration study was conducted to determine the required information, equipment, and procedure. A static loading system was designed, built, and tested. This was also accomplished on a dynamic calibration system. The latter was fabricated with Astro Space Laboratories funds.

Following these detailed investigations, three bench-model force balances were designed to study the characteristics of piezoelectic type sensor force balances. Two of these balances were fabricated and tested.

Following the preliminary balance investigation, the prototype balance development program began. Three prototype balances were designed. Due to size considerations, only two balances were built. These were designated as 196 and 198. Balance 196 was staticly and dynamicly tested. The frequency response was very good, however the interactions were too great to make the balance usable in the tunnel. Balance 198 underwent complete testing and after modification, was used in the tunnel.

Balance 199 and 203 were designed, built, and tested for tunnel use. Both balances perform quite well.

A six-channel acceleration compensation analog computer was designed, built, tested, and used in the Hypersonic Shock Tunnel.

A nine-channel system was designed to provide for summing all three force sensors with the three accelerations and their interactions.

FORCE SENSOR INVESTIGATION

The measurement of aerodynamic force is probably the most difficult of all the most common parameters to determine in a shock tunnel. Since the useful test times are on the order of 2-10 milliseconds, the requirement of high frequency response is very important. The two most important considerations of any force sensor for this type of use is frequency response and sensitivity. The semiconductor could be used with adequate results if the balance is sufficiently acceleration compensated.

Due to the marginal results in the response of strain gages, a considerable effort was expended on the study of piezoelectric force sensors in force balances. A complete survey was made to determine the availability of such sensors and the limitations when used in a shock tunnel envoronment. It was found that piezoelectric force sensors have great potential for shock tunnel use. In addition, piezoelectric accelerometers can be used to acceleration compensate the balance for model inertia, thereby increasing the system response. The low sensitivity problem of conventional strain gage can be solved by the use of piezoelectric crystal load cells.

A survey was conducted to determine the availability of piezoelectric force sensors. One of the major requirements was the need for the smallest available sensor. The Kistler Instrument Company had the only small sensor available (0.500 x 0.680 inch). This was the model 912, however it should be mentioned that a smaller sensor now exists which was used later in the program.

FORCE BALANCE ACCELERATION -COMPENSATION STUDY AND SYSTEM DESIGN

The use of piezoelectric materials for sensing elements allows the design of the balance to be stiff and compact. These materials have an inherently wide dynamic range, which is somewhat matched to the characteristically large vibration in dynamic pressures encountered over the hypersonic regime.

The force measurements depend not only upon the force transducer, electrical network, and readout system, but the model, model support, and sting support are involved to a significant extent. During the useful test time, the model support system vibrates as a result of the shock load it receives during flow initiation. These vibrations cause the model-balance system to act as an accelerometer with the result that oscillations appear on the force data traces. A system is desirable which does not place a great stiffness requirement on the model, balance, and sting; yet, would reduce the detrimental effects of these vibrations on the data traces. It is thus desirable to design and develop a system which employs accelerometers to sense sting vibration and an analog circuitry to cancel its effect on the force data. This system improves the quality of the data in two ways: 1) It reduces the effects of sting vibration, and, 2) it permits the use of stiffer models.

In shock tunnel instrumentation, the short duration of test time requires that accurate measurements be made while the model-balance-sting assembly is undergoing transient oscillation due to the disturbance of the initial wave front.

For this reason, the proper design of a force-balance system and the associated instrumentation for a shock tunnel must include a thorough analysis of the transient characteristics of the balance system and provide the necessary frequency response in the instrumentation.

An analysis was conducted to define the transient behavior of the model-balance, spring-mass system and to determine the effect of the variation of several key parameters on system performance.

This information was used to optimize system design and to study various error reduction and compensation methods.

The mechanical model of the force balance system is displayed in Figure 1. This diagram represents the model and balance mass, the load cell and sting springs, and the

load cell and sting structural damping. This system is simplified in that a perfectly rigid model is assumed.

The following table lists the constants of the system and the parameter they represent:

Constant	Parameter Represented
M_m	Model Mass
M_b	Balance Mass
C_1	Sting Structural Damping
C_2	Load Cell Structural Damping
K_1	Sting Spring Constant
K_2	Load Cell Spring Constant
Fd	Aerodynamic force applied to model

From the mechanical diagram of Figure 1, the following equations of motion can be written:

$$M_m \frac{d^2x_2}{dt^2} + M_m \frac{d^2x_1}{dt^2} + K_2x_2 + C_2x_2 = F_d \qquad (1)$$

$$M \frac{d^2x_1}{dt^2} + K_1x_1 + C_1x_1 - C_2x_2 - K_2x_2 = 0 \qquad (2)$$

These equations describe the motion of M_m and M_b under the influence of a disturbing force F_d. x_1 is the motion of the sting with respect to an arbitrary fixed reference. x_2 is the motion between the model and the balance and is the actual movement that is measured by the load cells.

The Laplace transform of equations (1) and (2) is found:

$$M_mS^2x_2 + M_mS^2x_1 + C_2Sx_2 + K_2x_2 = F_d(s) \qquad (3)$$

$$M_bS^2x_1 + K_1x_1 + C_1Sx_1 - C_2Sx_2 - K_2x_2 = 0 \qquad (4)$$

Equation (3) is now solved for the highest order term of x_2:

$$x_2 = \frac{Fd(S) - K_2x_2}{M_mS^2} - \frac{C_2x_2}{M_m S} - x_1 \qquad (5)$$

Equation (4) is solved for the highest order term of x_1:

$$x = \frac{K_2x_2}{M_bS^2} - \frac{K_1x_1}{M_bS^2} + \frac{C_2x_2}{M_b S} - \frac{C_1x_1}{M_b S} \qquad (6)$$

Equations (5) and (6) are used to generate a system block diagram which presents the equivalent mechanical system and allows the simultaneous solution of the two equations. This block diagram is presented as Figure 2.

The input disturbance F_d will be a step function which simulates the initial tunnel pressure wave front.

The distance x_2 is generated at the point indicated. x_2 is the actual deflection that is measured by load cell. The sting deflection, x_1, is also available at the point indicated.

Figure 3 is the computer mechanization of the system equations of motion. The computer will solve the equations for x_1 and x_2 when a step function of F_d is applied.

Another parameter of interest is the acceleration of x_1. This value was not available directly in the program but was generated as follows. The function x_1 is available at the input of the final integrator of the second loop.

This x_1 function was used to drive a differentiation circuit and x_1 is obtained at the output. A special differentiation circuit was used to reduce noise. Although the function exhibits some noise, a usable signal is obtained. This signal simulates the output of an accelerometer on the balance which could be used for acceleration error compensation.

The results of the overall computer study reveal some significant information about the composition of the force signal waveform. Figure 4 displays a typical computer run.

The curve of X_2 represents the quantity that is sensed by the load cell. In the steady state, X_2 will assume the same form of F_D, however, the damping factors are very small and are practically negligible during normal tunnel test times.

The actual intelligence in the X_2 signal is contained in the DC portion of the curve. The A.C. components represent errors due to the force pickup acting as an accelerometer and sensing the vibration of the model and the sting. The low-frequency oscillation is due to the balance sting spring mass system, and the high-frequency oscillation is due to the model-load-cell spring mass system. It is possible to determine the D.C. level of the curve by fairing the data, however, this procedure is limited in accuracy and is further complicated for the low frequency by the fact that a full cycle may not always be available during the tunnel test time to carry out the fairing process.

For these reasons, it would be highly desirable to devise a method to remove the erroneous A.C. components form the X_2 signal and restore this quantity, as nearly as possible, to its real D.C. form.

Low-pass filtering will yield acceptable results in removing the high-frequency error, but this method is not practical for removing the low-frequency component because filtering cannot be accomplished at these frequencies and retain the necessary transient response in the overall instrumentation.

There are two methods available to detect and compensate the low-frequency A.C. component. A second load cell could be placed between the balance and sting and detect the X_1 vibration force directly and use this signal to compensate the model load cell. Another approach is to locate an accelerometer on the balance and detect the A.C. oscillations of the balance and use this signal to compensate the model load cell.

Of these two methods, the accelerometer sensor appeared to be the most promising. The load cell method would require a considerably more complicated balance and the instrumentation would be more complex. The accelerometer method would be easier to instrument and accelerometers of the required size and performance are commercially available. For these reasons, the accelerometer compensation method was studied in detail.

Compensation is accomplished by applying the proper scale factor to the accelerometer signal and summing this scaled signal with the load-cell output in the proper polarity to effect cancellation.

The degree of cancellation is limited by the accuracy of the scale factor setting and the phase shift between the two signals.

Two schemes appeared to be possible in the compensation circuitry. These two circuit configurations are shown in Figure 5. Both of these schemes are based on compensating the low-frequency oscillations by summing in the proper polarity and filtering the high-frequency oscillations.

In Scheme No. 1., the load cell output and the scaled accelerometer signal are summed and then applied to the filter circuit. The output of the filter circuit is then the filtered, compensated signal.

In Scheme No. 2, the load cell output is filtered, the scaled accelerometer output is filtered, and the two filtered signals are summed to produce the compensated, filtered signal.

These two compensation schemes were mechanized on the analog computer and studied to determine the method that would be incorporated in the instrumentation system.

After studying the initial computer transient response results, Run No. 5 seemed to offer a typical system performance. The computer program for this run was used as the system simulation, and the additional program to simulate the compensation circuitry was added to the computer setup. Figure 6 presents the additional program that was used to mechanize the compensation circuits.

A total of 12 computer runs was made. In these 12 runs, signal polarities and parameters were varied to determine the nature and quality of compensation that could be obtained. The filter configurations were tested and preliminary filter design parameters were extracted from the information.

Figure 7 displays the frequency response curves with the filtered and unfiltered summed output shown on the bottom two traces, respectively.

From the results of the compensation computer study, the following general conclusions were drawn:

1. The low-frequency oscillation can be compensated with the acceleration signal.

2. The high-frequency oscillation can be reduced to an acceptable level by proper filtering.

3. The high- and low -frequency oscillations are displaced in phase by approximately 180°.

4. The high-frequency oscillations can also be compensated by adding the accelerometer signal with the proper phase and scale factor.

5. The final system performance and accuracy will probably be limited by the filter design.

The above conclusions represent some of the important findings of the compensation study. A comparison of the results of Scheme No. 1 and Scheme No. 2 revealed that the two schemes produce approximately the same results. Scheme No. 1 represents the simpler system from a circuit and component standpoint and is the logical choice based on these results.

An important finding of these studies is the fact that the high- and low-frequency signals are displaced in phase by approximately 180°.

Initially, it was thought that compensation with the accelerometer signal might produce cancellation for both the high and low frequencies. The results show that the polarity that tends to cancel the low frequencies causes the highs to add and vice versa.

Several runs were made which proved that, with proper scaling and phasing, either the high or low frequency could be almost 100% compensated, but, in each case, the other frequency was increased by the addition.

Figure 8 shows the system functional block diagram. F_A, F_1 and F_2 are the load cell outputs and a_A, a_1 and a_2 are the accelerometer outputs. Figure 9 shows the physical arrangement of the load cells and accelerometers in a typical system.

The output of each load cell and accelerometer is fed to a charge amplifier (CA). The load cell signals are then fed to a summing amplifier (SA). The accelerometer signals are scaled and inverted, if necessary, and fed to the appropriate summing amplifier. The summing amplifier output is then filtered to remove any undesired high frequencies from the signal.

Following are brief descriptions of the system's components.

Charge Amplifier

The charge amplifier provides a voltage output proportional to the load applied to the transducer.

Phase Splitter

The phase splitter is used to provide a 180°phase-shift in the compensating signal. This provision allows either addition or subtraction of the accelerometer signal.

Scale Potentiometer

The potentiometers are used to provide the proper magnitude of the compensating signal. These pots are set experimentally during dynamic calibration of the system.

Summer Amplifier

The summer amplifiers are operational amplifiers used to combine the load cell output with the necessary accelerometer signals to accomplish the required compensation.

Filter

The filters are used to remove any unwanted frequencies from the summer output.

The final system configuration is shown in block diagram in Figure 10. This figure shows the forward channel. The aft and axial channels are identical.

This system permits the use of any combination of the three accelerometer signals to compensate each force signal. The system can be used with either strain-gage or piezoelectric instrumentation.

FILTER DESIGN

The filter chosen for use in the compensation system was a low-pass, linear-phase, shift type. The pass band can be determined for a given application and for this development a 3db frequency of 350 H_Z was used. The linear-phase characteristic was selected to improve the filter response to a step input.

This type of filter is a standard design and the circuit components can be determined from available handbook[1] data

The circuit configuration is shown in Figure 11. The input and output resistons are 600 ohms, and five reactive elements are used. Calculations based on the above noted reference yield the following circuit values:

$C_1 = 1.706\mu F$
$C_3 = 0.608\mu F$
$C_5 = 0.137\mu F$
$L_2 = 0.302$ H
$L_4 = 0.138$ H

The attenuation and phase shift characteristic of this circuit are shown in Figure 12 and 13.

BALANCE CALIBRATION - STATIC AND DYNAMIC

Because of the extremely short duration of test time and the high acceleration forces, severe performance requirements are placed on the balance and its system. Standard force balances require only a static calibration since long testing periods are available with conventional tunnels and the accelerations are damped quickly compared to the length of test. However, the shock tunnel balances require dynamic calibration as well as static calibration. The dynamic calibration requirement has evolved because of the use of accelerometers internal to the balance for inertia compensation. Since the inertia effects are different for each individual balance and model, dynamic tests must be performed for proper force sensor signal conditioning. This is accomplished by summing the acceleration signal with the force signal in such a manner that the acceleration portion of the force signal is nulled.

The first consideration in calibrating a force balance system is to determine the response to static loading and the interaction of each axis. From the static calibration, one can determine the relationship necessary to compute the applied aerodynamic forces, the pitching moment, and the center of pressure. In addition, some indication of the dynamic response and acceleration compensation requirements are obtained from the applied force interaction in each axis.

In the development of new balance systems which are built for high accuracy, a static calibration system that can apply loads at various loading positions and loading angles is a very necessary and useful research tool. A system of this type was built and tested during this program. Figure 14 is a layout of this system.

The force balance to be tested is secured to the slide table with a holding fixture. The force is transmitted to the balance through a loading sleeve. The loading sleeve actually takes the place of the wind tunnel model during static calibration. This sleeve has five equally spaced loading holes where the force can be transmitted at different positions to simulate various centers of pressure on the model. The force is generated by the air cylinder located on the rotary table. The principle of operation is to adjust the position of the slide table until the center of pressure of the model is located above the center of the rotary table. This table can be adjusted for any center of pressure. The rotary table may be rotated to simulate any axial or normal force component. The actual resultant force generated is sensed by a quartz load cell located between the balance and air cylinder. This system was designed to generate 400 pounds

force; however, due to excessive deflection of the balance holding fixture and lateral movement of the slide table, the maximum usable force is approximately 200 pounds. The pressure in the air cylinder is controlled by a micrometering valve, in such a way that any desired output force can be obtained by adjusting this valve and monitoring the load cell output.

Several tests were conducted on a balance later in the program to demonstrate the system.

This system does not lend itself accurately for low forces, however it is very promising for use with high loads.

A dynamic calibration system was designed and built for the purpose of adjusting the acceleration compensation system of the balance. A layout of this system is shown in Figure 15. The principle of operation of this system is as follows. The force balance, with the aerodynamic model, is attached with the adjustable sting which is secured to a bracket on the electromechanical shaker table. This is the only attachment position for the balance and model. The vibration fixture is fixed to the floor at the other end and provides the pivot point for the model. This pivot point is at a selected neutral accelerometer axis. This pivot point may be moved in the horizontal direction by adjusting the length of the sting.

A vibrating motion is imparted to the fixture holding the adjustable sting by the electro-mechanical shaker. The model and balance then pivots about the selected point. The output of the accelerometers are then adjusted to provide for the best possible compensation of model acceleration.

Tests were conducted with this device to isolate the accelerometer output at the pivot point or accelerometer neutral axis. This was successful.

The fabrication of the dynamic calibration system was accomplished wholly with ASL funds in an effort to contribute to the state-of-the-art.

A series of tests was conducted on a Kistler Model 912 Load Cell. Figure 16 shows the sensitivity to acceleration with frequency, Figure 17 shows the load cell sensitivity to acceleration as a function of vibration level, Table I presents the degree of actual acceleration compensation obtainable as a function of frequency.

TABLE I

FREQ. (cps)	ACC. OUTPUT (mv)	LOAD CELL OUTPUT (mv)	SUMMING AMP. OUTPUT (mv)	COMPENSATION $(1-\frac{Eout}{Ein})\ 100$ (%)
20	425	520	5	98.8
40	420	515	6	98.6
50	405	510	4.8	98.8
70	410	510	3	99.3
90	420	520	8	98.1
100	400	530	18	95.5
150	400	500	7	98.25
200	410	505	3	99.3
300	405	500	3	99.3
400	400	495	4	99.0
500	400	495	7	98.25
600	395	495	7	98.2
800	390	490	10	97.5
1000	390	490	14	96.4

PRELIMINARY BALANCE INVESTIGATION

Three basic design concepts of bench type balances were considered during the preliminary investigation. Initially, only the concepts shown in Figures 18 and 19 were considered. Because of the low natural frequency of Design No. 2, shown in Figure 2, Design No. 1 concept was built and tested.

The static calibration of this balance was accomplished as shown in Figure 20. It was found that the output of Load Cell F_3 did not function in the balance as anticipated. Further tests indicated that, if a constant force were applied at various angles, a maximum output is obtained at approximately 40 degrees. This information leads to a conclusion that moments should not be placed on the load cells or that they should be held to a minimum.

From the data obtained it was not possible to determine the quantities of drag, lift, and pitch moment or center of pressure from a simple analysis. However, it can be seen that a fixed relationship exists between F_1, F_2, and F_3. The following analysis was used.

$$\phi = f_{11}(F_1) + f_{12}(F_2) + f_{13}(F_3) \quad (1)$$

$$F_r = f_{21}(F_1) + f_{22}(F_2) + f_{23}(F_3) \quad (2)$$

$$C_p = f_{31}(F_1) + f_{32}(F_2) + f_{33}(F_3) \quad (3)$$

The actual relation can be determined from a curve fit of the exprimental data in terms of F_1, F_2, and F_3. For these solutions to have any meaningful existence, there must be a unique solution involving all 6 variables. This would mean that for a certain combination of F_1, F_2, and F_3 there will exist only one value of ϕ, F_r, C_p, F_1, F_2, and F_3 has been loaded into a computer program and a curve fit of this data was made to certain selected functions. This program has the ability to select which of the functions involving F_1, F_2, and F_3 are most significant and which can be omitted.

The relation of C_p as a function of the load cell outputs is:

$$CP = 2.091 - 0.2948F_1 + 6.88F_2 + 66.5F_3 + 1.646F_1F_2 - 334.914F_2F_3 - 34.961F_2^2$$

This equation is accurate from 5 to 8 percent of the experimental data.

The relation of F_r as a function of the load cell outputs is:

$$F_r = 14.105 + 1.548F_3 - 0.2219F_1F_2 - 3.127F_2F_3 + 0.3306F_1^2 + 6.31F_2 - 7040.1F_3^2F_1 + 454.17F_3^2F_2 - 15.713F_1F_2F_3 - 19.52 \log. F_3.$$

This equation is accurate to within 5 percent of the experimental data.

The relation of the loading angle ϕ as a function of F_1, F_2, and F_3 is as follows:

$$\begin{aligned}\text{Sin } \phi = {} & -.3379 + 0.2478F_1 - 4358.29F_3^2 - 26.91F_1F_3 \\ & -828309.22F_1^2F_2^2 + 164.161F_1^3 + 48396.99F_2^2 \\ & + 34507.12F_3^2 \\ & - 0.17669\frac{F_1}{F_2^2} + 1.465\frac{F_1}{F_3} + 1.919\frac{F_1^2}{F_2^2} - 0.4243\frac{F_1^2}{F_3} \\ & - 1.2427 \text{ Log } F_1 + 1.44 \text{ Log } F_2 - 0.5812 \text{ Log } F_3.\end{aligned}$$

This equation is exceptionally long since the computer was not instructed to delete the insignificant terms of this function.

It is now possible to compute the drag, lift, and center of pressure from these relationships from a knowledge of F_1, F_2, and F_3 without iteration as was earlier anticipated.

It was desirable that balance be built and tested which required a simpler data analysis. Consequently, a four load cell balance was designed, built, and tested. It was hoped that this new concept would eliminate the twisting of the load cells as experienced in the earlier balance. A design concept of this balance is shown in Figure 21. Tests of this balance showed great improvement, however a data analysis similar to that used in the first would have to be conducted to make the system usable.

An immeasurable amount of information was gained from this preliminary investigation about the load sensor and balance design concepts.

COMPENSATION ANALOG COMPUTER

A six-channel acceleration compensation computer was designed, built, and tested. This system was for use in the tunnel and for laboratory tests. It can be used with both load cell or strain gage balances. The design has been documented and is too envolved to place in this report.

In addition a nine-channel system was designed and documented for possible further use.

PROTOTYPE FORCE BALANCE PROGRAM

With the knowledge gained during the preliminary balance investigation, a prototype balance program was begun.

It was desired that a balance be designed that had a capacity of 400 pounds axial and 400 pounds normal force and that could be used in a 9-1/2° half-ange nose cone with a 3 inch diameter base. All prototype balances were 3-component.

Two balance concepts were analyzed and after sufficient study, a design was chosen. This balance, designated as Balance 196, is shown in Figure 22.

This balance was designed, built, and tested. It was found that this balance had very good response characteristics, however the interaction of normal force on axial force was too large. This problem caused the balance to be usable for tunnel tests.

BALANCE DESIGN OBJECTIVES OF BALANCE 198

Balance #198 was designed using an assumed total lift load of 400 lb and a drag load of 400 lb. A design objective of a natural frequency in excess of 1000 cps was coupled with the load requirements to achieve a compact, stiff force balance as shown in Figure 23 (80M41605).

Load sensing elements were placed in the conventional configuration with sufficient lift load cell spacing to allow sufficient pitching moment sensitivity.

The stiffness of the load cells, the frequency desired, and the load cell spacing limit the size and inertia of a model-support combination, as shown below.

From the differential equation (in Figure 24) for an oscillation in the lift direction, the natural frequency is seen to be

$$W_n = \sqrt{\frac{2KL^3 + 6EI}{ML^3}}$$

It can be shown, however, the $6EI \ll 2KL^3$ and, therefore,

$$W_n \cong \sqrt{\frac{2K}{M}}$$

Similarly for drag direction oscillations, (Figure 25).

$$W_n = \sqrt{\frac{K}{M}}$$

With W_n and K given values, this is the limiting relationship for system mass.

Given:

$$W = 2000 \text{ cps}$$
$$K = 5 \times 10^6 \text{ lb/in}$$
$$f = \frac{1}{2\pi}\sqrt{\frac{K}{M}}$$

rearranging the equation yields

$$M = \frac{K}{4\pi^2 f^2} = 3.17 \times 10^{-2} \text{ lb-sec}^2/\text{in}$$

therefore

$$W = Mg = (3.17 \times 10^{-2})\ (3.86 \times 10^2) = 12.2 \text{ lb.}$$

In a similar manner the system rotational inertia can be obtained. (Figure 26)

$$f = \frac{1}{2\pi}\sqrt{\frac{2Kr^2}{J_o}}$$

Given:

$f = 2000$ cps
$r = 1.000$ in
$K = 5 \times 10^6$ lb/in

The equation becomes:

$$J_o = \frac{2Kr^2}{4\pi^2 f^2}$$

$$= 6.31 \times 10^{-2} \text{ in-lb-sec}^2$$

(Small motions have been assumed throughout.)

Stress Analysis

The material, 17-4PH, was selected because of machining and heat-treating ease, as well as for strength and dimensional stability. Assumed properties of 17-4PH are as follows:

$F_{tu} = 170{,}000$ psi
$F_{ty} = 165{,}000$ psi
$F_{cu} = 170{,}000$ psi
$F_{su} = 120{,}000$ psi
Condition H 1025

$E = 28.5 \times 10^6$ psi

The balance flexures must be strong in the load carrying direction but weak in the cross axis direction.

The lift flexures are designed to be weak when subjected to a lift load. They are assumed to act as cantilever beams, as shown in Figure 27. When under a total lift load of 400 lb, the lift flexures' movement is restrained by the two normal load cells to a deflection of

$$y = \frac{400 \text{ lb}}{2\ (5 \times 10^6 \text{ lb/in})} = 4 \times 10^{-5} \text{in.}$$

The deflection at the end of a cantilever beam is given by:

$$y = \frac{PL^3}{3EI}$$

or

$$P = \frac{3EIy}{L^3} \quad \text{load felt through flexure}$$

Assumed:

$E = 28.5 \times 10^6$ psi
$I = 2.29 \times 10^{-6}$ in.^{4}
$L = 0.500$ in.
$y = 4 \times 10^{-5}$ in.

$$P = 0.0625 \text{ lb}$$

As shown, the transferred load is very small and the stress is negligible.

The lift flexures are subjected to column loading when under a negative drag load. The limiting value of L/ρ is given as follows:

$$F_w = \frac{F_{cu}}{4} = 42{,}500 \text{ psi}$$

The slenderness ratio is obtained from

$$\frac{P_c}{A} = F_c = \frac{4\pi^2 E}{(L/\rho)_c^2}$$

$$(L/\rho)_c^2 = \frac{4\pi^2 E}{F_c}$$

$F_c = 42{,}500$ psi

Substituting:

$$(L/\rho)_c^2 = 2.64 \times 10^4$$

$$(L/\rho)_c = 163$$

Radius of gyration is given by:

$$\rho = \sqrt{\frac{I}{A}}$$

$A = 1.1 \times 10^{-2}$ in^2
$I = 2.29 \times 10^{-6}$ in^4
$\rho = 1.44 \times 10^{-2}$ in.

Now since $L = 5 \times 10^{-1}$ in.

$$L/\rho = 34.7 < 160$$

Therefore, the flexure compressive stress is defined by:

$$S_c = \frac{P}{A}$$

$P = 200\#$ (on each flexure)

$A = 1.1 \times 10^{-2}$ in^2

$$S_c = 18{,}200 \text{ PSI} \ll 170{,}000 \text{ PSI}$$

Similarly, the axial flexures, as shown in Figure 28, are treated as built in beams. The analysis can be simplified by assuming two cantilever beams as shown below:

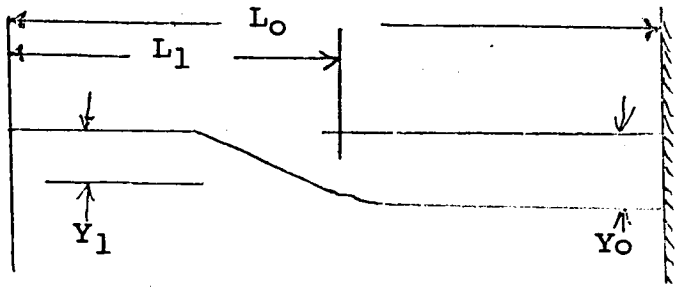

$L_o = 0.150$ in.
$L_1 = 0.075$ in.
$Y_1 = 1/2\ Y_o$

Under a 400 lb axial load, the axial load sensor allows a deflection of 8×10^{-5} in. (y_o). The load transferred under this condition is given by

$$P = \frac{3EIy_1}{L_1^3}$$

Substituting:

$$P = 0.1137 \text{ lb. for each flexure}$$

The stress is negligible.

The axial flexures are also subjected to shear stresses when a normal load is present. For a normal load of 400 lb each flexure feels 100 lb.

$$S_s = \frac{P}{A_s}$$

$A_s = (0.230\ (0.020) = 0.0046\ in^2$

$P = 100\ lb.$

$$S_s = 21{,}750\ PSI < 120{,}000\ PSI$$

The sting side of the balance, as shown in Figure 27, is the supporting base for the balance and should be as stiff as possible. The size (diameter) limitations of the balance did not allow for the stiffness desired. The worst loading condition was selected for analysis, i.e., a 400 lb load at the forward end. Assuming the base as a cantilever, end-loaded, the deflection and stress are determined as follows:

$$Y = \frac{PL^3}{3EI}$$

$L = 2.44\ in.$
$P = 400\ lb.$
$I = 3.622 \times 10^{-3}\ in^4$

Substituting:

$$Y = 0.0187\ in.$$

The deflection proved to be excessive (as will be discussed in the data analysis). The stress becomes

$$\sigma_b = \frac{MC}{I}$$

$M = PL$
$C = 0.217\ in.$

$$\sigma_b = 58{,}400\ PSI < 170{,}000\ F_{tu}$$

The allowable balance loading was reduced as a result of testing, but since #198 was a "bread-board" model, time was not spent on redesign.

ANALYSIS OF CALIBRATION DATA (BALANCE NO. 198)

A standard calibration was performed on Balance 198 with a load range of 25 to 150 pounds. These loads were placed on the balance in both the negative and positive force directions. (Figure 27)

Figure 29 is a plot of the forward load cell output at the various loading positions. The data points all lie on the constant load lines and show a linear relationship with both position and magnitude of force. This data was taken with negative normal force. It can be seen from this figure that the load center is located very accurately and is directly over the center of the aft load sensor.

Figure 30 is a plot of the forward load cell output for the positive loading direction. A comparison of Figures 27 and 30 indicate that the forward sensor reacts the same to a negative or positive force and the output at each station is practically the same. The load center is located at the same position in both tests. The conclusion would have to be that the forward sensor performs very well throughout the range tested and at all positions.

Figure 31 is a plot of the aft load cell output for negative normal loading. The lines drawn through the data for constant load are "best straight lines" and should be considered as such. The points at position 1 are definitely "off" the line except for the 25 pound load. The remaining data points define the constant loading quite accurately as well as the forward load center. By observing Figure 31, one can see that the load center is approximately 0.030-inch aft of the center of the forward load cell.

Figure 32 is a plot of the aft load cell output for positive normal loading. The lines drawn through the data for the constant loads are "best straight lines" and should be considered as such. These are not data scatter but are repeatable trends. Figure 33 is a plot of the same data; however, the constant load lines are located by the first three positions. All of the remaining data points are above the line in an increasing amount as the position moves forward. Point No. 3 is also above the line but only a very small amount. However, it is obvious that the non-linear reaction which occurs must begin near position No. 3. The result of this reaction is a tension force on the aft load cell in excess of the applied load. At position 6, which is in compression, the tension force still exists since the output

of the load cell is less positive than it should be. This reaction force causes the forward load center to shift forward approximately 0.150 inch. A discussion of this phenomenon will be made later in this report.

Figure 34 is a plot of the axial load cell output as a function of load. The maximum load presented here is 80 pounds, however, data has been presented earlier in excess of 150 pounds without change in sensitivity.

Figure 35 presents the percent of normal load interaction on the axial load cell output for negative normal loading. At each position, the bar represents the spread of data from 25 pounds to 150 pounds normal force. The line drawn through the bars show the mean or possible best representation of this interaction relationship. Observation of this data shows that the action of normal force on axial output can be accounted for within ±1 percent at all positions and better than ±0.5 percent between the forward and aft load cells.

Figure 36 presents the percent of the axial force interaction on the forward and aft load cell outputs. The action of the aft load cell places it in tension, and compression on the forward sensor. One can observe that the sum of the two normal sensors (plus and minus) would cause the total interaction to approach 1 percent at loads greater than 25 pounds and approximately 2-1/4 percent at 10 pounds. However, the two sensor outputs will be used separately for normal force correction. The dashed lines represent "best straight lines" as shown in Figure 36.

As mentioned earlier in the report, the variation in the data from a straight line as obtained from the aft sensor is not scatter but repeatable trends. The shift in the load center shown by the positive loading data is certainly not a desirable reaction; however, it is explainable.

Figure 23 is an assembly drawing of Balance 198. In view D-D, the numbered points indicate the location of the load positions. A load downward on the balance as shown would be a negative normal load or force. The data in Figure 23 shows that the forward load center is slightly aft of the center of the forward load cell; however, this does not create any difficulty. The load center shift is only of concern in the positive loading direction. The phenomenon that causes this shift is present in both loading positions; but as stated previously, this creates problems only in the positive loading direction.

The weakest section of the base of the balance is located under the aft load cell. Also, it is realized that the entire

balance base is not sufficiently strong based on the deflection. At the time the balance was designed it was not known quantitatively how much the load cells would be affected by base deflection.

The action of the balance base at the aft load cell location when under negative normal loading would possibly appear as follows:

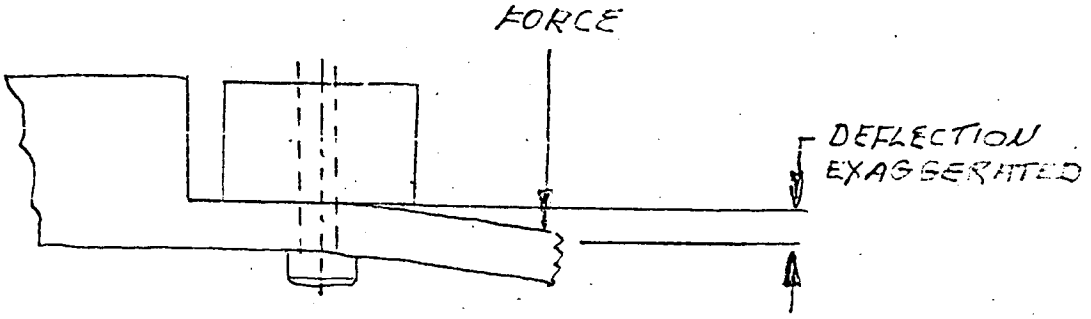

The effect here would be small; however, it could move the pivot point slightly aft of the center depending upon the flatness of the base and the possibility of the screw head causing a small moment on the screw thereby creating a force on the sensor. The data shows the result of this effect to be small even though the deflection is large.

The action of the balance base at the aft load cell location when under positive loading would possibly appear as follows:

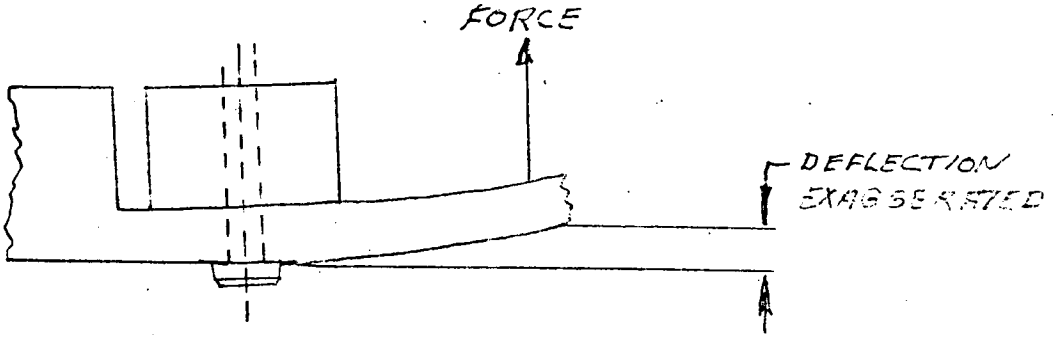

This effect would produce a tension force on the screw by trying to pivot about the corner of the sensor. This effect could be large since the moment arm creating the tension force would be larger and the actual point of loading would no longer be at the center of the load cell. The actual excessive tension force is 4.95 pounds at position 5 with 100 pounds normal force and 6.18 pounds at position 6. The ratio of these excessive loads is 1.25. Using the position of the aft load cell as the pivot point the position ratio is 1.28. This does not mean that this source of force transfer is the only contributing factor.

Another possible source of this reaction would be through the drag load member. This member is in tension when a negative normal load is present and in compression when a positive normal load is present. This is evident from the interaction of normal force on drag. This would be considered as a beam under simultaneous axial and transverse loading. Axial tension tends to straighten the beam and thus reduce the bending moments produced by the transverse loads, but axial compression has the opposite effect and may greatly increase the maximum bending moment and deflection.

Regardless of the various contributing factors, the primary reason for the shifting of the load center is the excessive deflection of the balance base.

It is recommended that Balance 198 be used in the negative direction only. This is based on two facts; 1) The error is quite small when used in this direction and certainly well within any accuracy requirements of the Hypersonic Shock Tunnel and, 2) The shift of the load center when used in the positive loading direction.

To transfer the load sensor outputs into usable force data, it is necessary to establish relationships between outputs and applied loads. The relationships should also include corrections for interactions between axial and normal outputs. The general equations can be written as follows. (Shown in Figure 37):

$$F_n = F_A + F_f - K_{AI}A_f - K_{fI}A_f$$

F_A - Aft load cell output (mv.)

F_f - Forward load cell output (mv.)

F_n - Normal resultant load (mv.)

K_{AI} - Ratio of interaction of drag on aft output

K_{fI} - Ratio of interaction of drag on forward output

A_f - Axial load cell output (mv.)

To determine normal load in pounds, the load cell calibration factors must be included.

$$F_n = \frac{F_A - K_{AI}A_f}{C_A} + \frac{F_f - K_{fI}A_f}{C_f}$$

Where C_A and C_f are load cell calibration constants (mv/lb)

3.2 Load Position

$$X_L = \frac{\frac{(F_A - K_{AI}A_f)\ (2.410)}{C_A} + \frac{(F_f - K_{fI}A_f)\ (4.370)}{C_f}}{\text{Normal Load}}$$

Where the lengths 2.410 in. and 4.370 in. are the distances of the aft and forward load cell centerlines with respect to the 1.10 in. diameter of the balance taper.

3.3 Axial Load

$$F_{AX} = \frac{A_f}{C_{AX}} - K_{NI}\ F_N$$

K_{NI} - Ratio of interaction of lift on axial output

C_{AX} - Axial load cell calibration factors (mv/lb)

For use in equations (1), (2), and (3), the constants K_{AI} and K_{fI} can be determined from the percent interaction of drag on lift versus applied axial load (Figure 35). The equations of the "best lines" are used to determine the constants and the actual axial load cell output is used to determine slope.

$$K_{fI} = \frac{-0.00919A + 6.60}{100}$$

$$K_{AI} = \frac{0.00979A - 7.90}{100}$$

The terms in the numerator are percentages. The constant K_{AI} is opposite in sign, since its plot should be in the negative direction.

The constant K_{NI} for equation (1) can be obtained from Figure 35:

$$K_{NI} = \frac{0.966X_L - 4.65}{100}$$

since the interaction is due more to load position that to load.

Substituting the constants into the original equations yields the desired relationships.

$$F_N = \frac{F_A-(0.0000979A_f-0.0790)A_f}{C_A} + \frac{F_f-(0.0000919A_f-0.0660)A_f}{C_f}$$

$$X_L = \frac{\frac{F_A-(0.0000979A -0.0790 \quad (2.410)}{C_A} + \frac{F_f-(0.0000919A_f-0.0660)A_f(4.}{C_f}}{F_N}$$

$$F_{AX} = \frac{A_f}{C_{AX}} - (0.00966X_L-0.0465)F_N$$

Where:

C_A = 4.85 mv/lb
C_f = 4.86 mv/lb
C_{AX}= 3.75 mv/lb

The computations can be simplified considerably by assuming C_A and C_f as being equal.

When only a normal force exists the maximum error in determining this force is 1.5% at all positions and the maximum error in determining the location of this force is 0.6%. The error introduced by the combined loading interactions are dependent only upon the error introduced by considering these as straight lines or linear. For example, the axial force due to the normal force on drag interaction can be corrected to within ±0.5% of the normal load when the load is applied between the two normal force sensors. The normal force sensors can be corrected for drag interactions to within ±0.25 percent at 15 pounds of axial force and above.

It would be extremely difficult to state a true accuracy value based upon a combination of the above described errors. It would have to be based upon the ratio of anticipated lift to drag forces. However, the balance is capable of giving sufficiently accurate results in a range of 25 to 150 pounds normal force and 15 to 150 pounds axial force. The balance is to be operated in the negative normal direction only and the C.P. should be located between the forward and aft load cells for best performance.

RESPONSE TESTS

Before this balance was placed in the tunnel for testing, drop tests were performed to determine the response time and acceleration compensation. Three oscilloscope records are shown to illustrate balance rise time and output wave form.

The response time was determined by simulating a shock load and photographing its oscilloscope trace. The force balance was attached to a heavy string and a weight was hung from the balance in the normal force direction. The wire holding the weight was cut and the weight was allowed to fall. This rapid release of lift force was the simulated shock load. The time required for the balance to respond to the simulated shock load was obtained by photographing the oscilloscope trace and recording the time per cm variable.

The scope trace was photographed when the balance had no load and with the load applied. The trace was triggered manually with the horizontal display on single sweep. The triggering mode for these lines was on automatic. An external D. C. voltage was used to trigger the scope for the force balance response trace. The D.C. voltage (about 6 volts) was connected across the wire supporting the weight and to the External trigger input on the scope. With the horizontal display on single sweep and the triggering mode on D.C., the wire supporting the weight was cut. When the wire was cut the D.C. external circuit was broken triggering the scope trace and the load on the force balance was released.

Figure 38a shows the uncompensated trace. The time per cm variable was 1 millisecond per cm. The top line represents the D.C. level when the force balance is loaded with the 10 lb. weight. The bottom line is the no-load condition. The time required for the load cell output to become zero appears to be about 0.8 millisecond from this photo. Figures 38b and 38c show the compensated signal without the filter. The response time in these pictures appears to be about 0.5 milliseconds or better. The time per cm variable for these pictures is as follows:

B-Upper - 0.2 milli-sec/cm.
B-Middle- 0.1 "
B-Lower - 0.2 "
C-Upper - 0.2 "
C-Lower - 0.2 "

SUMMARY DESIGN LIMITS

Outside Dia. - 1.440"
Length from sting end - 4.785"

Load cell spacing - 2.000"

Design Loads:

Normal - 400#
Axial - 400#

Recommended Loads:

Normal: 25# - 150#
Axial : 15# - 150#

C. P. Location - between load cells
Loading Mode - negative normal only

BALANCE DESIGN OBJECTIVES OF BALANCE 199

Extensive testing of an earlier balance, (#196), and balance #198 show that excessive balance base deflection is the major cause of normal load washer output nonlinearity and lift on drag interactions. Balance #199 is the outcome of an attempt to apply the results of the above mentioned research in developing a force balance with a very stiff sting side while retaining an outside diameter of 1.5 inches and supporting an axial load of 200 pounds and a total lift load of 200 pounds.

The areas of foremost importance in the design of balance #199 were the load sensor mounting method and the deflection limiting design of the balance base.

Kistler's Model 901 Load Washer was selected for use because of its size, rigidity, and preload capability, as described in Figure 39. It was determined that the preloading bolt stiffness should be less than the load washer stiffness for optimum performance. The initial attempt at preload utilized a shoulder screw, as shown in Figure 40, with the load washers in a standard configuration, Figures 41 & 42. The load washer stiffness is given as 6.67×10^6 lb/in and the screw is determined, as follows, using assumed dimensions.

$$e = \frac{PL}{AE}$$

or

$$K = \frac{P}{e} = \frac{AE}{L} \qquad \text{(Stiffness)}$$

$$A = \pi/4\ (0.218)^2 = 0.0373\ \text{in}^2$$

$$L = 0.533\ \text{in.}$$

$$E = 2.9 \times 10^7\ \text{lb/in}^2 \quad \text{(17-4 PH Stainless Steel)}$$

$$K = 2.03 \times 10^6\ \text{lb/in.} < 6.67 \times 10^6\ \text{lb/in.}$$

After subsequent testing and disassembly it was discovered that the initial preload of 900 lbs had dropped 300 - 400 lbs and nonreturn problems were evident in the data. Further analysis indicated that the shoulder screw design was a contributing factor. Due to the shoulder and undercut complexity, the elongation was not uniform throughout loading. The problem was solved by simplifying the design to allow the shank to expand more uniformly and by changing to Beryllium Copper material to reduce stiffness while retaining ductility and strength. The redesigned shoulder screw is shown in Figure 43, and its stiffness is 0.61×10^6 lb/in. as compared to 6.67×10^6 lb/in. for the washer. The 1000 lb preloading force tends to prevent localized bending by the balance base in the load washer vicinity.

Balance Base Design

Force balance #199 has a base utilizing a semicircular lower segment enclosed in a cylinder with screws and dowel pins joining the two pieces. The use of the cylinder allows maximum stiffness by retaining balance size while allowing flexure and load washer mounting through cut-out sections, as shown in Figure 44. The cylinder is connected to the base around a complete circumference in two locations which further increases stiffness.

The base segment is assumed as a semicircle:

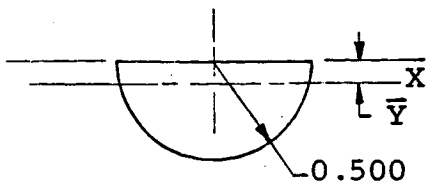

For a semicircular area:

$$\bar{y} = 0.4244\ R$$

$$I_{xx} = 0.1098\ R^4$$

$$\bar{y} = (0.4244)(0.500) = 0.212 \text{ in.}$$

$$I_{xx} = (0.1098)(0.500)^4 = 0.686 \times 10^{-2} \text{ in}^4$$

The cylinder cross-section assumed without cutouts:

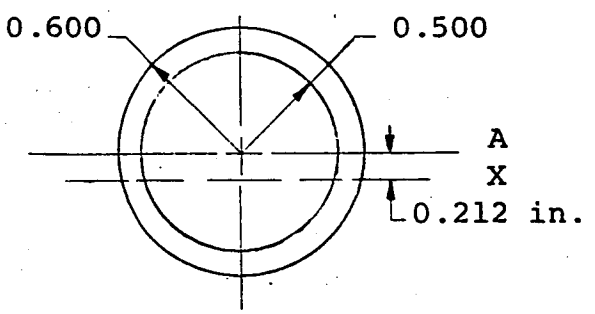

$$I_{AA} = \Pi/4\ (R^4\ r^4)$$

$$= 5.26 \times 10^{-2} \text{ in}^4$$

$$I_{xx} = 5.26 \times 10^{-2} + Ad^2$$

$$= 6.82 \times 10^{-2} \text{ in}^4$$

Therefore:

$$I_{xx}\ \text{Total} = 6.82 \times 10^{-2} + 0.686 \times 10^{-2}$$

$$= 7.51 \times 10^{-2}\ \text{in}^4$$

Assuming the combination cantilevered and end-loaded.

$$y = \frac{PL^3}{3EI}$$

$P = 200\#$

$L = 3.22$ in.

$E = 2.9 \times 10^7$ lb/in^2

$I = 7.51 \times 10^{-2}$ in^4

$y = 1.02 \times 10^{-3}$ in.

This represents a simplified stiffness of

$$K = \frac{200}{1.02 \times 10^{-3}} = 1.96 \times 10^5\ \text{lb/in}$$

The saddle for balance #199 was designed using a cylindrical element, once again, to retain the balance design diameter (1.5 in.) while increasing strength. The saddle is simplified somewhat, as shown, for analysis:

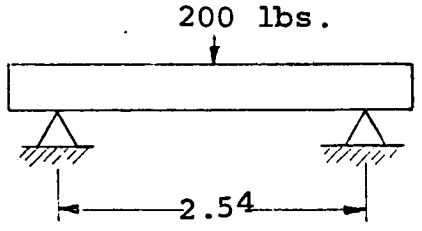

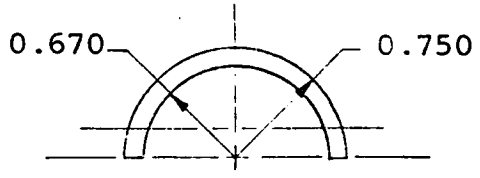

$$I_{xx} = 7.4 \times 10^{-3}\ \text{in}^4$$

The deflection at the midpoint is given as:

$$y = \frac{PL^3}{48EI}$$

$P = 200$ lb.

$E = 2.9 \times 10^7$ lb/in^2

$L = 2.54$

$y = 3.08 \times 10^{-4}$ in.

The stiffness in this mode is:

$$K = \frac{200}{3.08 \times 10^{-4}} = 6.5 \times 10^5 \text{ lb/in.}$$

The flexures are designed as shown in Figure 41. For simplified analysis purposes they can be illustrated as below:

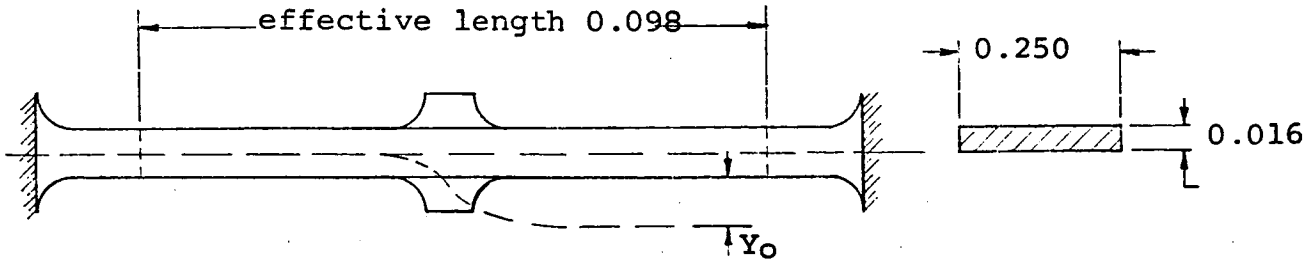

Where

$L_o = 0.098$ $\qquad$ $y_1 = 1/2\ y_o$

$L_1 = 0.049$

By assuming the flexures as two cantilever beams joined in the center, the deflection becomes:

$$y_1 = \frac{PL_1^3}{3EI}$$

or

$$P = \frac{3EI\ y_1}{L_1^3}$$

Under an axial load of 200 lb the axial load washer allows the lift flexures to each see a deflection of 200 lb/ 6.67×10^6 lb/in., which is 3×10^{-5} in. This results in a load transferred through the lift flexure of:

$I = 8.53 \times 10^{-8}$ in^4

$E = 2.9 \times 10^7$ lb/in^2

$P = 1.89$ lbs

Under a total normal load of 200 lb., the axial flexure would see 1.5×10^{-5} in. of deflection due to the rigidity of both normal load washers. The load felt through this flexure is then:

$P = 0.95$ lb.

During tests the interactions in the balance are greater, as will be discussed in the data section, due to base and other component deflections.

By inspection, the drag case is the limiting factor and model-support weight.

$$f = Wn/2\Pi = 1/2\Pi \quad \frac{KL^3 + 6EI}{ML^3}$$

where $K = K_w + K_s$

Now since $6EI << KL^3$

$$f = 1/2\Pi \quad \frac{K_w + K_s}{M}$$

$f = 3000$ cps

$K_w = 6.67 \times 10^6$ lb/in.

$K_s = 0.943 \times 10^6$ lb/in.

Substituting:

$$M = 2.14 \times 10^{-2} \ \frac{\text{lb sec}^2}{\text{in.}}$$

$$W = (2.14 \times 10^{-2})(3.86 \times 10^2) = 8.26 \text{ in.}$$

The rotational inertia limit is obtained using the relationship

$$f = 1/2\Pi \quad \frac{2Kr^2}{J_o}$$

or $$J_o = \frac{2Kr^2}{4\Pi^2 f^2}$$

$r = 1.27$ in.

Substituting:

$$J_o = 6.92 \times 10^{-2} \text{ lb-in-sec}^2$$

Static calibration of Force Balance #199 was accomplished by hanging a weight pan and weights on a loading sleeve at various positions. The loading sleeve, Figure 45, is integrally connected to the balance saddle and is loaded in the negative and positive normal and axial directions as indicated in Figure 42. Calibration data for a 0-100 lb test and a 0-25 lb test are presented in Figures 46-57 and are self-explanatory.

To transfer the load sensor outputs into usable force data, it is necessary to establish relationships between outputs and applied loads with corrections for interactions.

The generalized relations are:

F_{ax} - axial load (lb.)

F_n - normal load (lb.)

F_A - aft load washer output (mv.)

F_f - forward load washer output (mv.)

A_f - axial load washer output (mv.)

C_{AX} - axial load washer calibration factor (mv/lb)

C_A - aft load washer calibration factor (mv/lb)

C_f - forward load washer calibration factor (mv/lb)

K_{AI} - ratio of interaction of drag on aft output

K_{fI} - ratio of interaction of drag on forward output

K_{NI} - ratio of interaction of normal on drag output

M_p - pitching moment (lb-in)

For the particular 0-100 lb. calibration data presented the equations are as follows:

$$F_n = \frac{F_A - 0.0232\ A_f}{9.0} + \frac{F_f + 0.0282\ A_f}{8.55}$$

$$F_{AX} = \frac{A_f}{7.38} - \frac{6.71 - 2.5\ X_L}{100} F_n$$

where X_L is the distance to a load point from a reference location; in this case a 1.10-inch diameter on the balance taper. The constants K_{AI} and K_{fI} are critically dependent upon load alignment during calibration.

A series of drop tests was performed on Balance 199, to determine load response, with and without the compensation system. The drop test was used to simulate a step load, or instantaneous load on the balance, and the response time was obtained by photographing the oscilloscope trace.

Each picture has three exposures. Two of the exposures are of the base and loaded lines. The third exposure is the response trace. The response trace was obtained by cutting a copper wire supporting the weight; the copper wire also being part of an external D.C. trigger circuit.

Figure 58 shows the uncompensated forward load washer response trace, the base, and loaded traces. With a scale factor of 2 millisec/cm the response appears to be about 1 millisec. Figure 59 shows the compensated and filtered response trace. With a time scale of 0.5 millisec/cm the response appears to be 2 millisec.

SUMMARY-DESIGN LIMITS

Outside Dia.	- 1.5 in.
Length	- 8.0 in.
Load Washer Spacing	- 2.54 in.
Design Loads:	
Normal	- 200 lb.
Axial	- 200 lb.
Recommended Usage:	
Normal	- 10 - 150 lb.
Drag	- 10 - 150 lb.
C.P. Location	- inside load centers

BALANCE DESIGN OBJECTIVES OF BALANCE 203

Force Balance #203 was developed as an answer to a need for a small diameter, low-load balance with the fast response necessary for shock tunnel application. The design was for a 1" outside diameter and a 1.5" load sensor spacing (Figure 60). Flexures are located as shown in Figures 61 and 62 and allow a smaller size than do flexures of a more common nature. Design loads were 40 lb. total lift and 20 lb. axial and were successfully met as discussed in a later section. A Kistler 901A load washer was chosen as the load sensing element because of its size and preload capability.

MODEL 901A LOAD WASHER

Sensitivity	20 pcb/lb.
Rigidity	15×10^{-8} in/lb
Size (I.D./O.D./Thk.)	0.26/0.55/0.31
Weight	0.3 oz.

As part of an effort to limit base deflection and localized bending in the load washer vicinity, a preload of 1000 lb. was used. The preloading element is a beryllium copper screw as shown in Figure 63. Linear extension and compression of the screw was attained by the necked-down shank. The stiffness of the screw is 6.1×10^5 lb/in as compared to 6.67×10^6 lb/in for the load washer.

Balance Base

As shown in Figures 61 and 62, the balance base is basically a semicircular segment. The various cut-out sections evolved from an effort to enclose the sensing elements in a base which was as stiff as possible while remaining within the design diameter of 1 inch. An estimate of base stiffness is obtained here by using a base as follows:

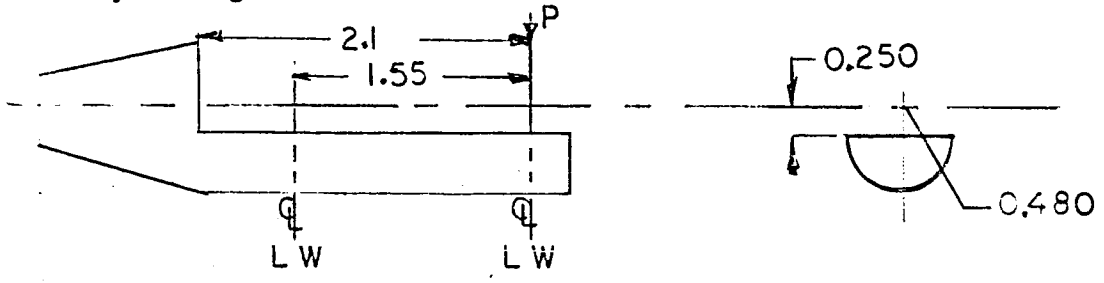

Assuming the worst condition of forward end loading and the following parameters:

$I = 8.99 \times 10^{-4}$ in^4

$L = 2.1$ in.

$E = 2.9 \times 10^7$ lb/in^2 (17-4 PH)

$P = 40$

Deflection is

$$y = \frac{PL^3}{3EI}$$

$$= 0.0047 \text{ in.}$$

Spring stiffness:

$$K_b = \frac{P}{y} = 8{,}420 \text{ lb/in}$$

The stiffness is not as high as desired, but is limited by balance size requirements.

Axial Flexure

The 4 axial flexures are shown in Figure 62 in the normal positions and are weak in the drag direction while being strong in the lift direction. Under a 20 lb. axial force, the axial load washer allows a deflection d_{AX}, and the lift flexures (Figure 62) allow an elongation, d_{AF}. The sum $d_{AX} + d_{AF}$ is then the interaction seen by the axial flexures.

The axial deflection d_{AX} is

$$d_{AX} = \frac{20 \text{ lb.}}{6.67 \times 10^6 \text{ lb/in}} = 3 \times 10^{-6} \text{ in}$$

The lift flexure elongation is:

$$d_{AF} = \frac{PL}{AE}$$

Where P = 10 lb for each flexure

$A = 1 \times 10^{-3}$ in^2 area of lift flexure

$d_{AF} = 8.62 \times 10^{-5}$ in.

Total deflection then is 5.86×10^{-5} in.

Drag flexure section properties are:

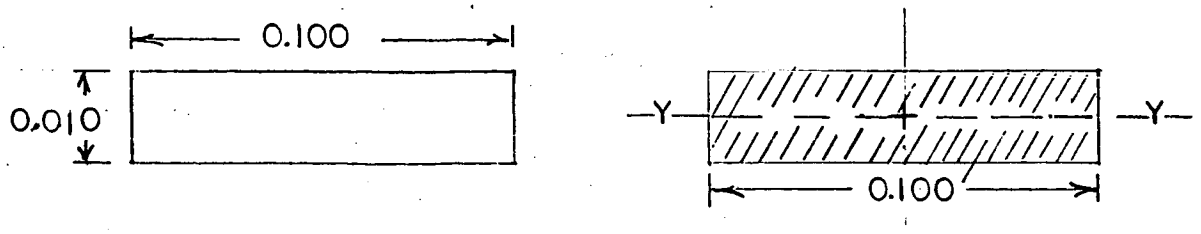

$$I_{yy} = 8.33 \times 10^{-9} \text{ in}^4$$

Using the equation for a beam built-in at both ends

$$P = \frac{12\ EIy}{L^3}$$

which gives an interaction force through all four flexures of 0.712 lb. which is 3.5% of the total axial load of 20 lb.

Normal Flexures

Using a method similar to that presented above, the interaction through the lift flexures became 0.34% of the normal load of 40 lb.

Actual interactions during calibration were larger due to excessive base deflection and deflections of other balance components.

A series of tests was conducted to determine the balance response to a step input with and without the filter and compensation circuit. Weights were suspended on the loading sleeve (Figure 65) with a copper wire which was part of a simple triggering circuit. The response without filtering is better than 0.5 milliseconds and with a 350 cps filter it is about 2 milliseconds.

Static calibration was accomplished by suspending various weights from the balance loading sleeve at varying load points which are numbered from the aft end. Figures 66 to 70 are plots of a 0-40 lb calibration as described. Figures 71 to 74 are of a 0-6 lb low load calibration. To transfer the load sensor outputs into usable force data it is necessary to establish relationships between sensor outputs and applied loads with corrections for interactions.

The generalized equations are:

F_{AX}	axial load (lb)
F_N	normal load (lb)
F_A	aft load washer output (mv)
F_f	forward load washer output (mv)
A_f	axial load washer output (mv)
C_{AX}	axial load washer calibration factor (mv/lb)
C_A	aft load washer calibration factor (mv/lb)
C_f	forward load washer calibration factor (mv/lb)
K_{AI}	ratio of interaction of drag on aft output
K_{fI}	ratio of interaction of drag on forward output
K_{NI}	ratio of interaction of normal on drag output
M_p	pitching moment (lb-in)

For the 0-40 lb calibration data presented, the following constants and equations were determined.

$$K_{AI} = 0.0483$$

$$K_{fI} = -0.0266$$

$$K_{NI} = 0.046\ X_L - 0.1085$$

$$C_A = 16.4\ \text{mv/lb}$$

$$C_f = 15.4\ \text{mv/lb}$$

$$C_{AX} = 16.5\ \text{mv/lb}$$

Where X_L is the load center distance from a reference point. The reference in this case was chosen as the forward end of Balance #203 sting-taper. The distance to the aft load washer is 1.60 in. The relationships upon substitution are:

$$F_N = \frac{F_A - 0.0483A_f}{16.4} + \frac{F_f + 0.0266A_f}{15.4}$$

$$F_{AX} = \frac{A_f}{16.5} - F_N(0.046\ X_L - 0.1085)$$

The interaction constants K_{AI} and K_{fI} were found to be critically dependent upon axial load alignment during calibration. The data reduction method for the low-load (0-6 lb) calibration is approached in the same manner.

Summary of Design

Outside Diameter - 1.0 in.

Length - 6.19 in.

Load Washer Spacing - 1.5 in.

Recommended Loads:

Normal - 0.40 lb.
Axial - 0-40 lb.

C.P. Location - between load washer centers

FIGURES

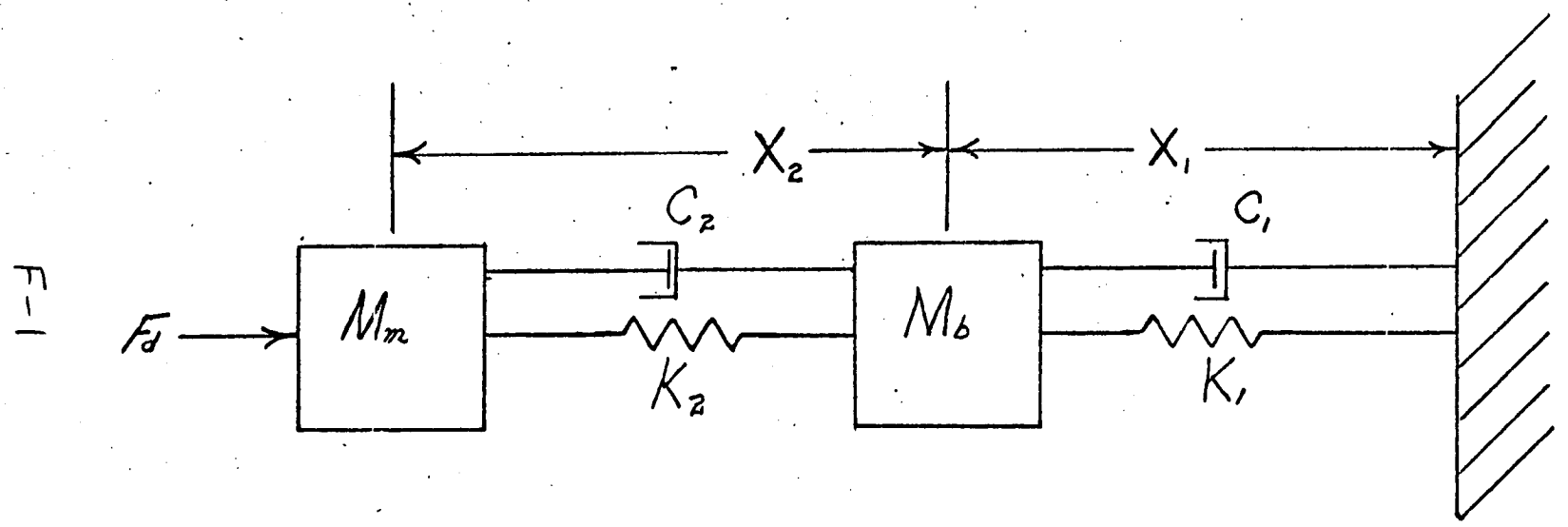

Figure 1. Mechanical Model - Force Balance System

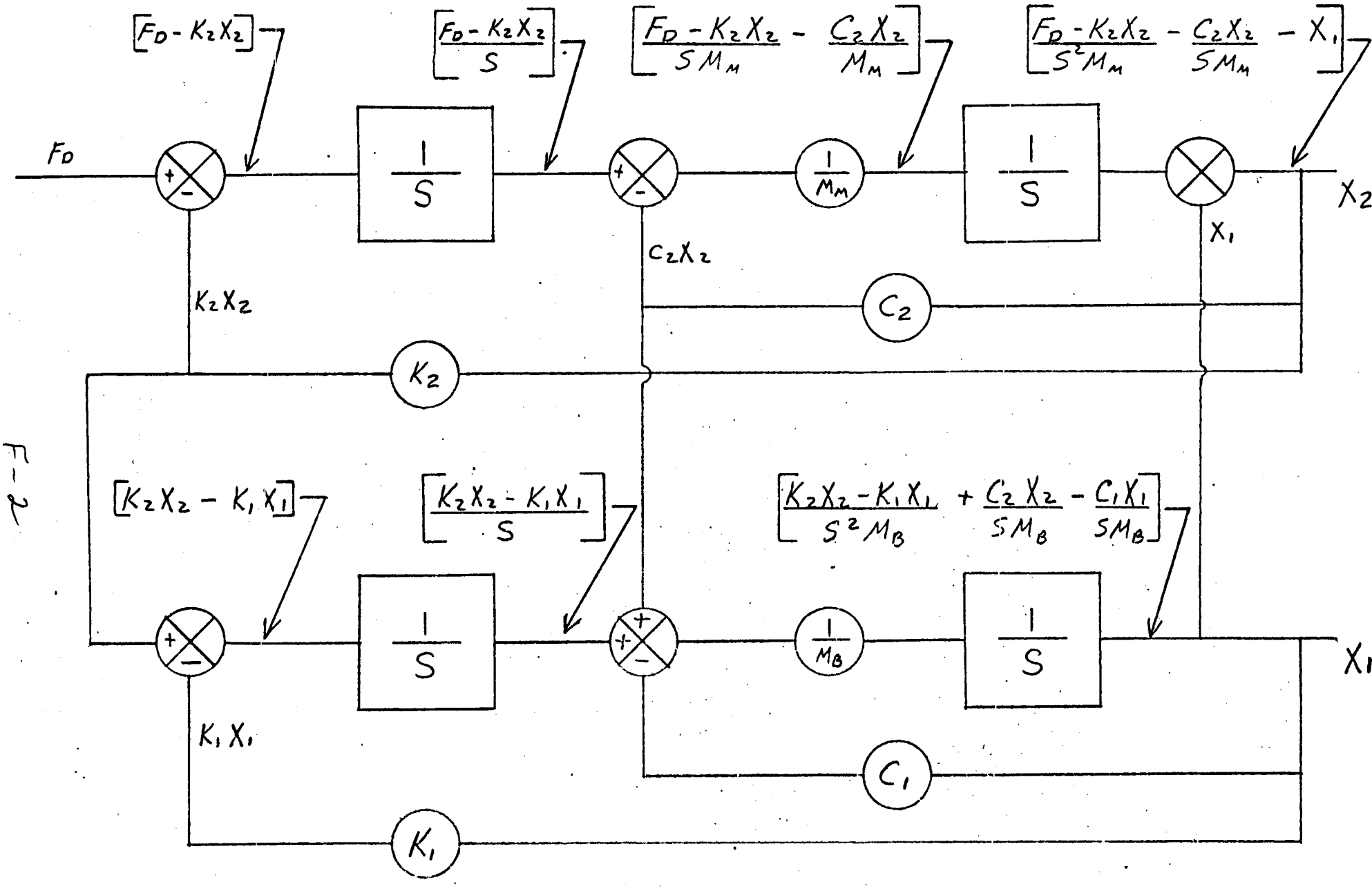

Figure 2. Force Balance System Block Diagram

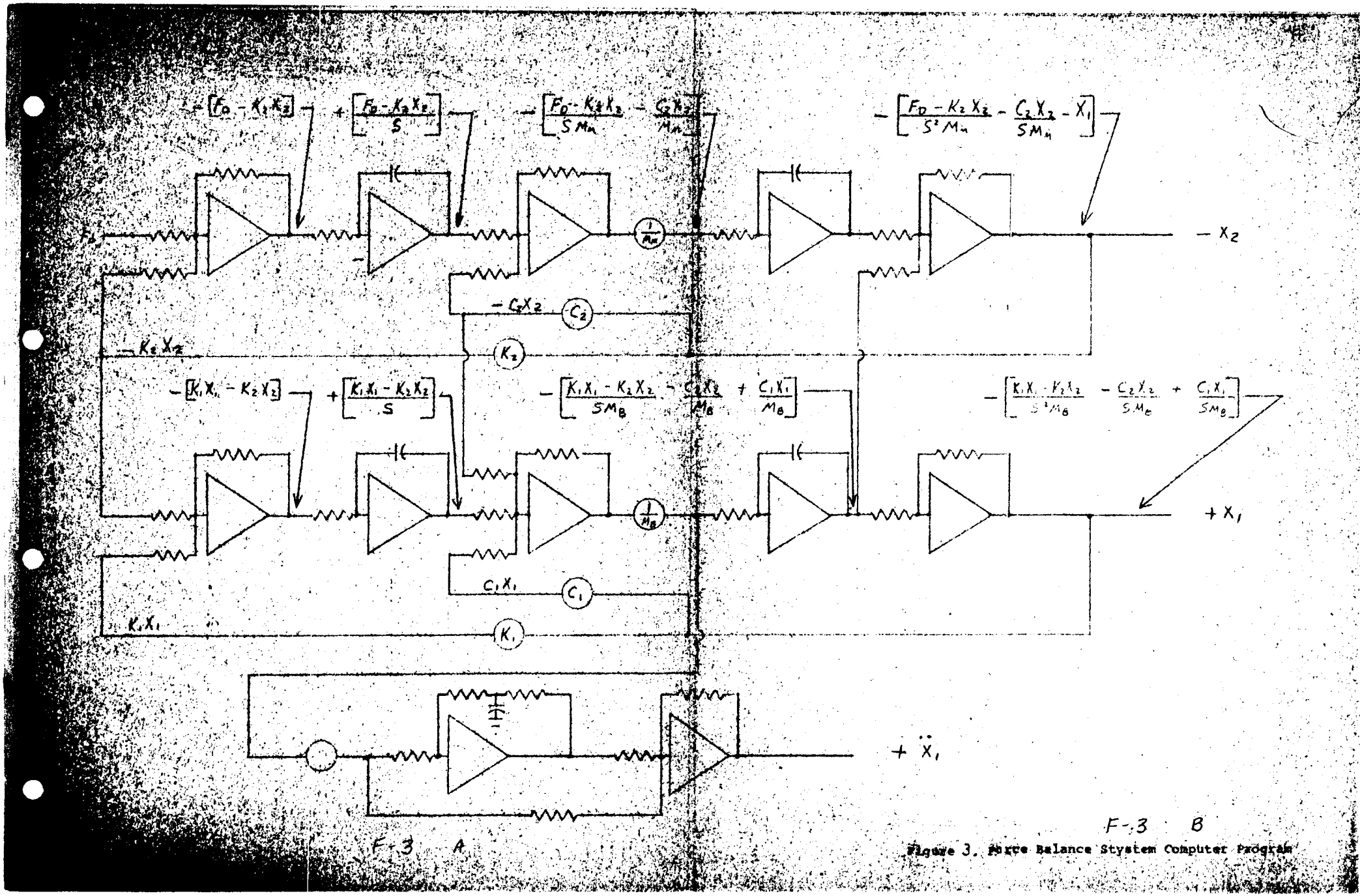

Figure 3. Force Balance System Computer Program

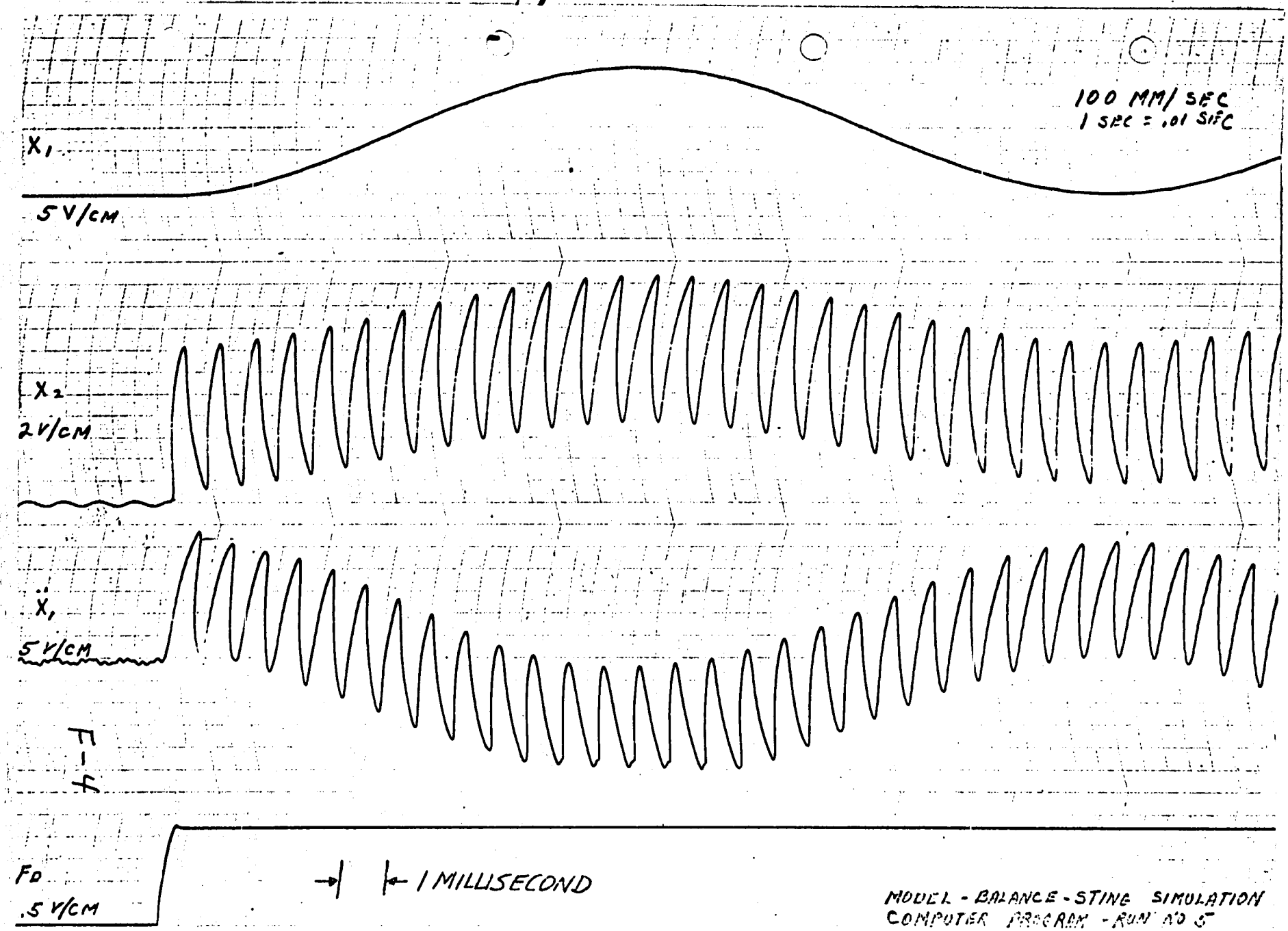

MODEL - BALANCE - STING SIMULATION
COMPUTER PROGRAM - RUN NO 3

FIG 4

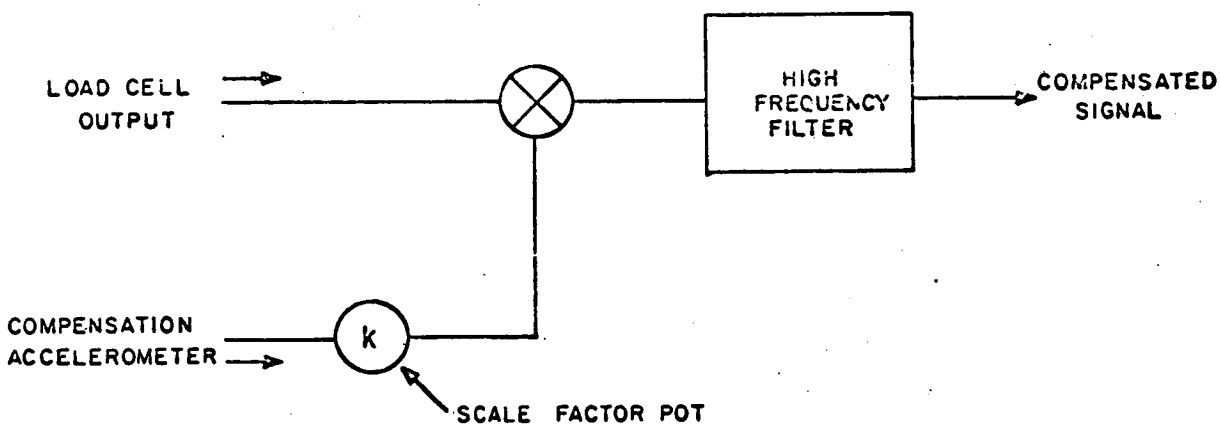

A. COMPENSATION SCHEME NO. 1

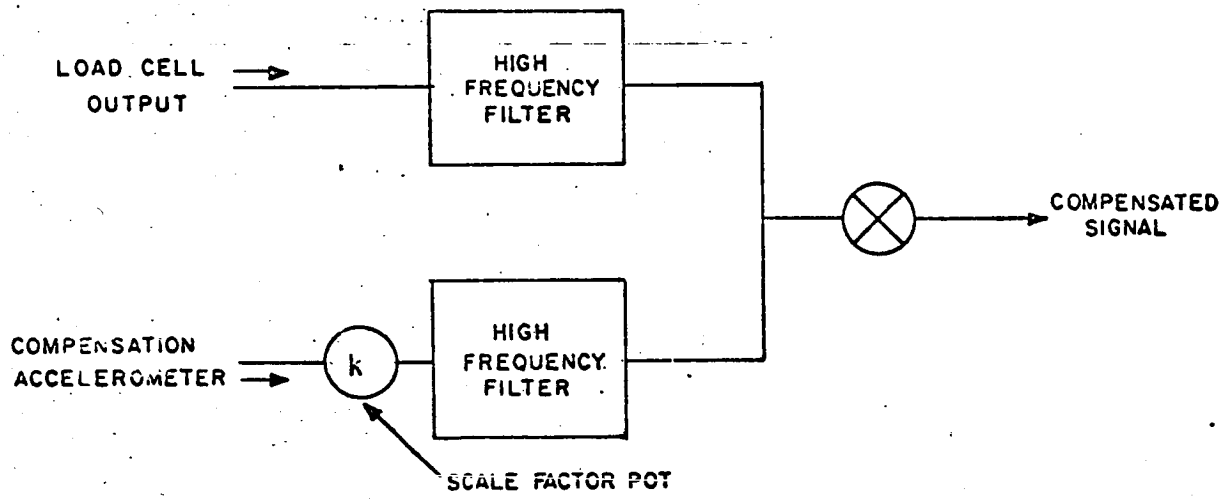

B. COMPENSATION SCHEME NO. 2

FIG NO. 5

F-5

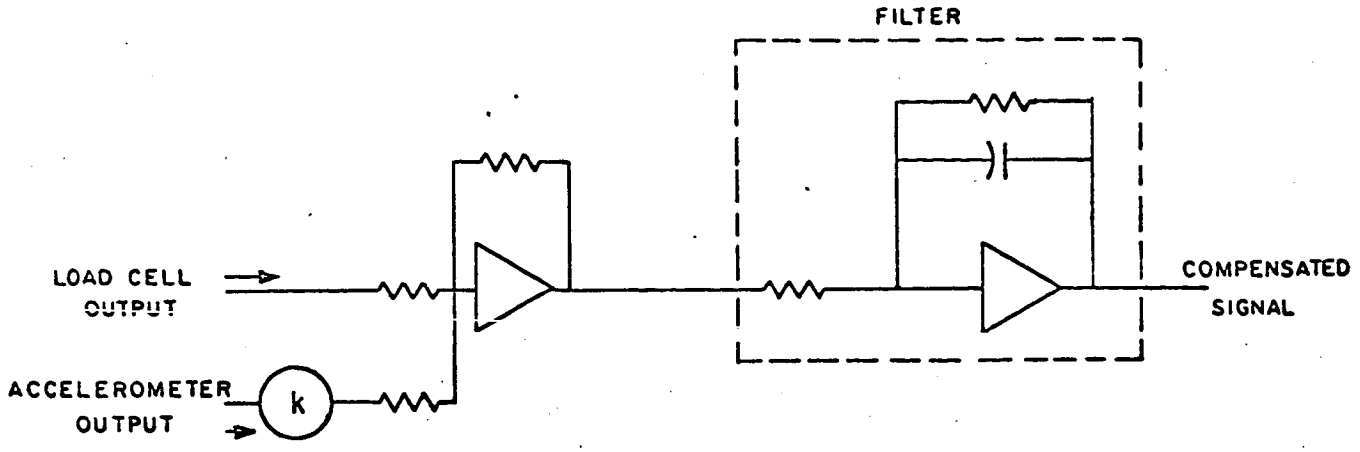

A. COMPUTER PROGRAM SCHEME NO. 1

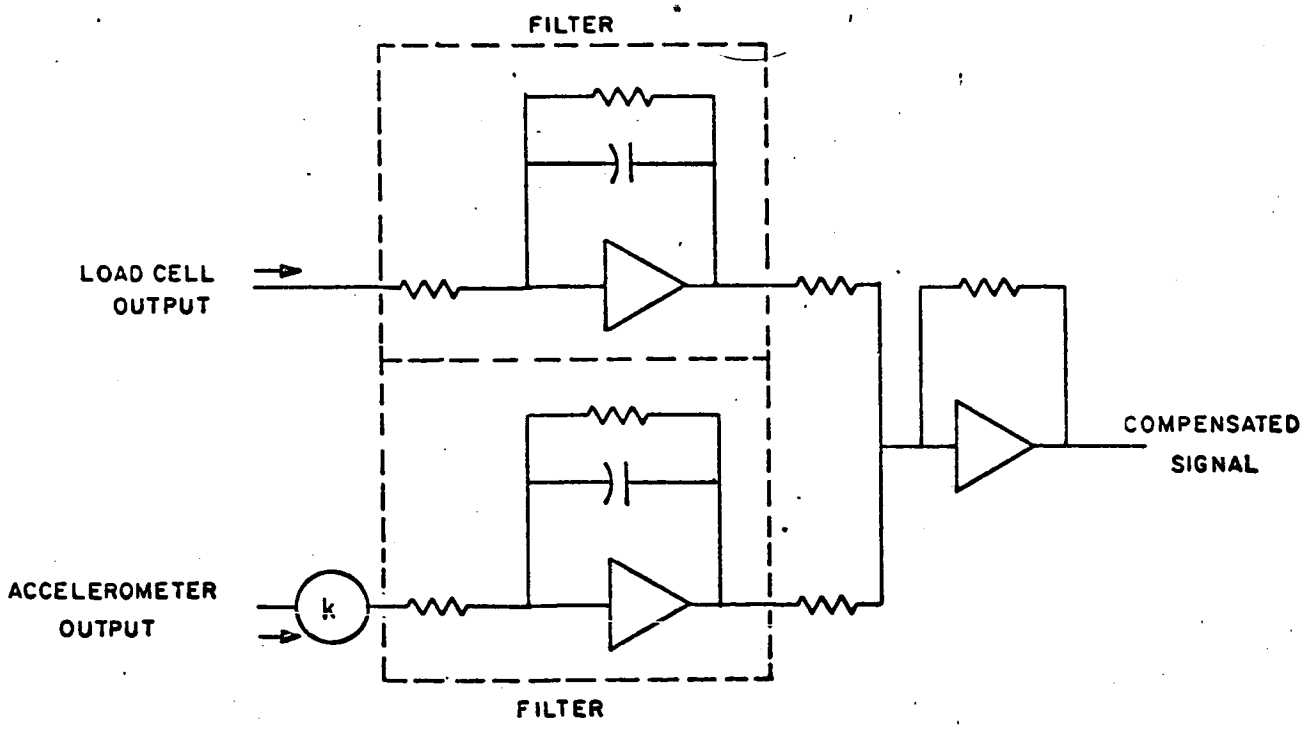

B. COMPUTER PROGRAM SCHEME NO. 2

FIG. NO. 6

F-6

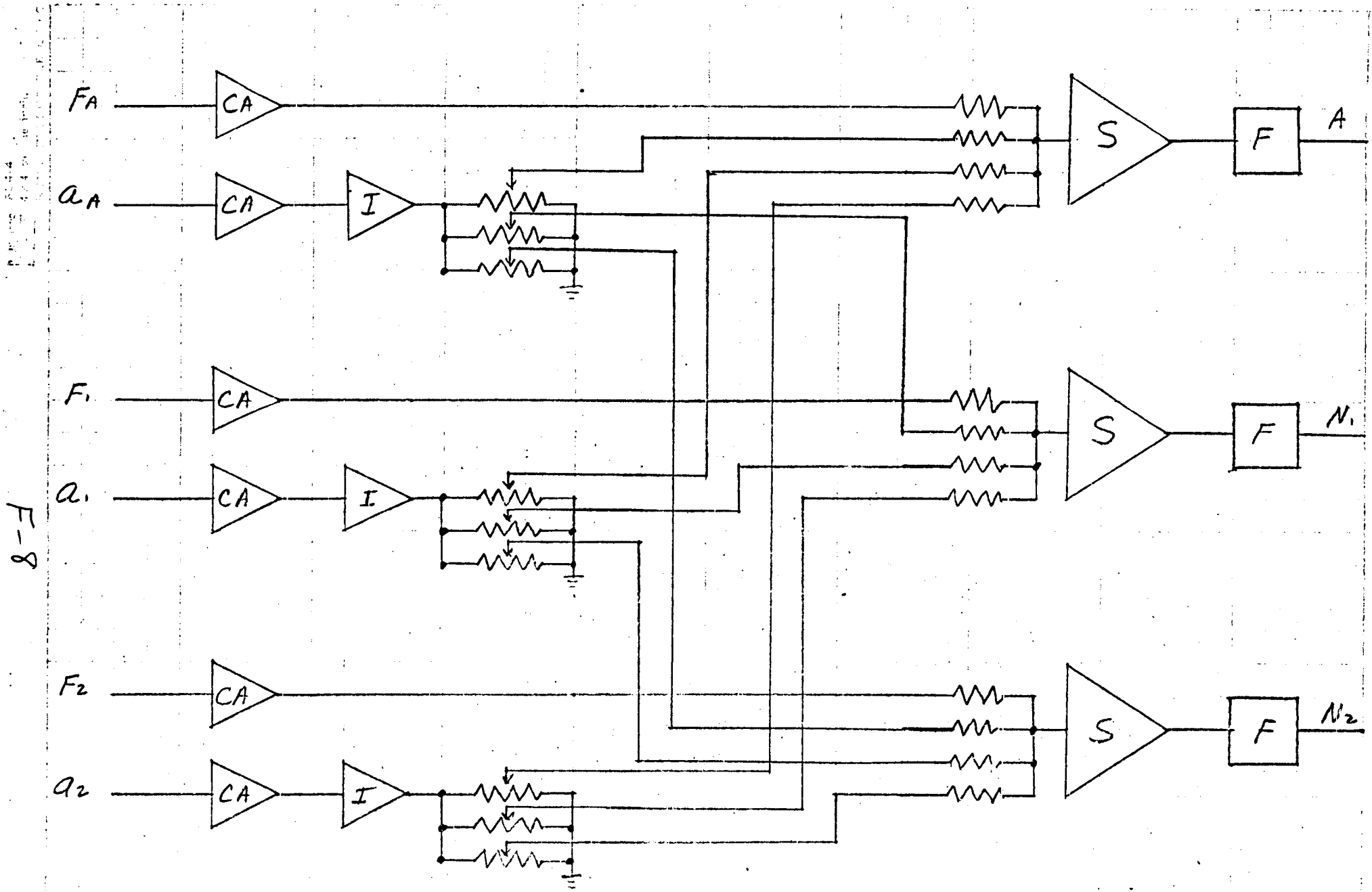

COMPENSATION NETWORK

FIG. 8

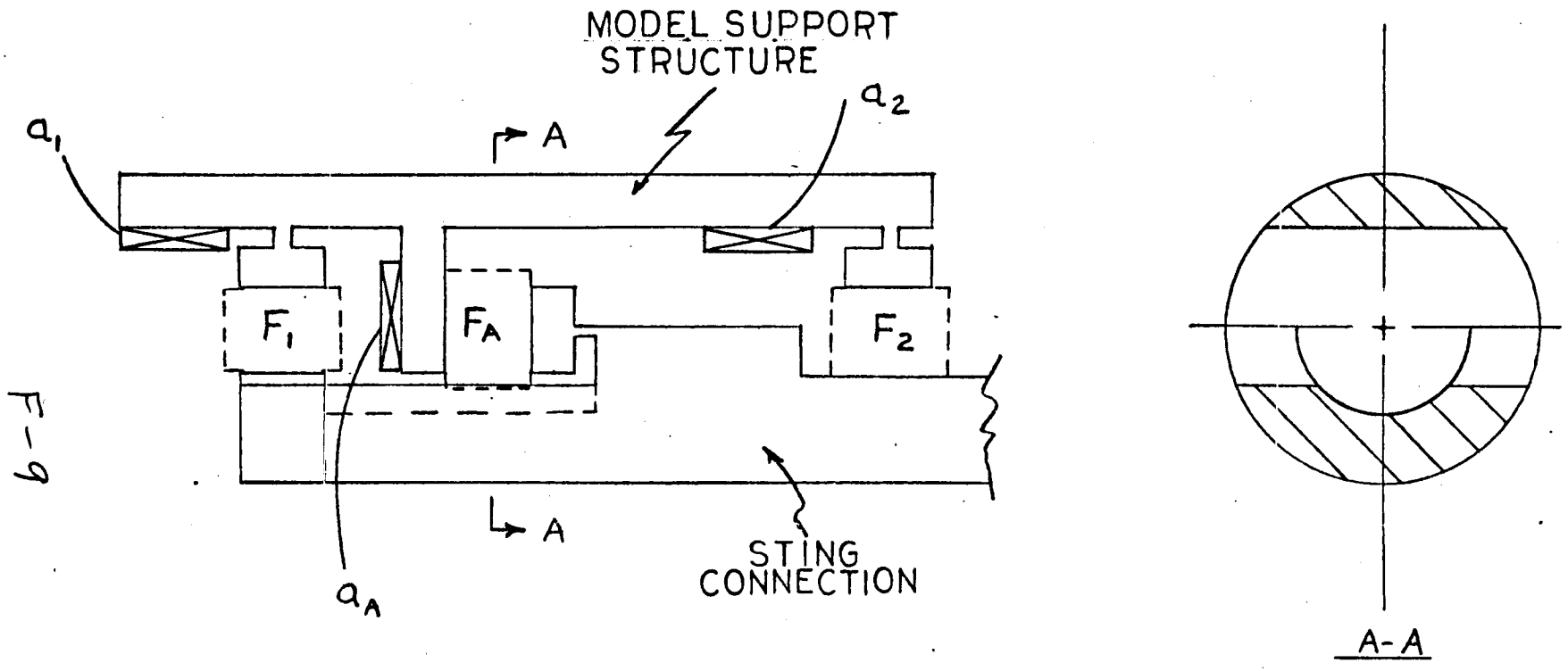

F-9

3 LOAD CELL FORCE BALANCE

FIG. 9

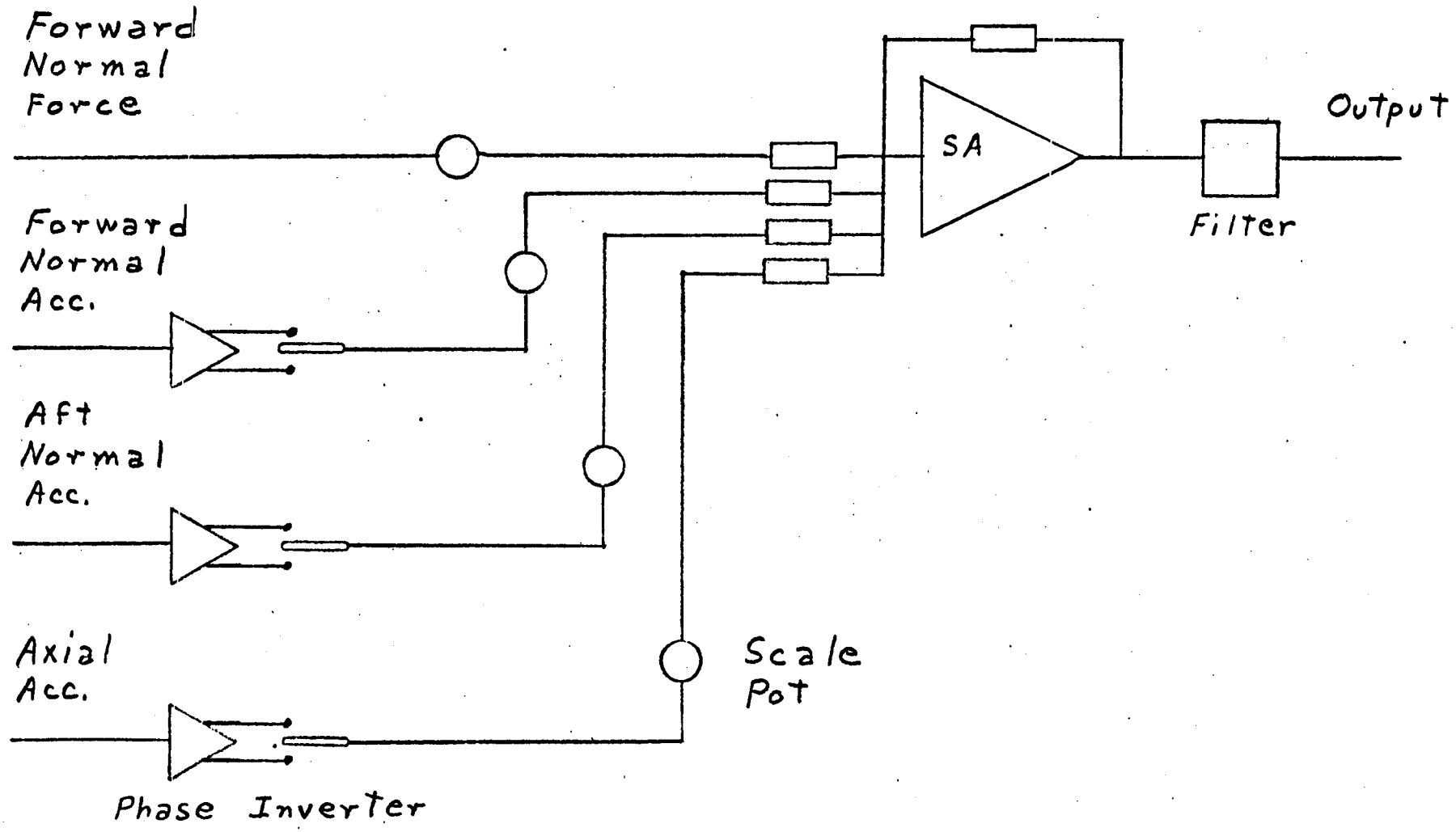

F-10

Block Diagram - Forward Compensation Channel

Figure 10

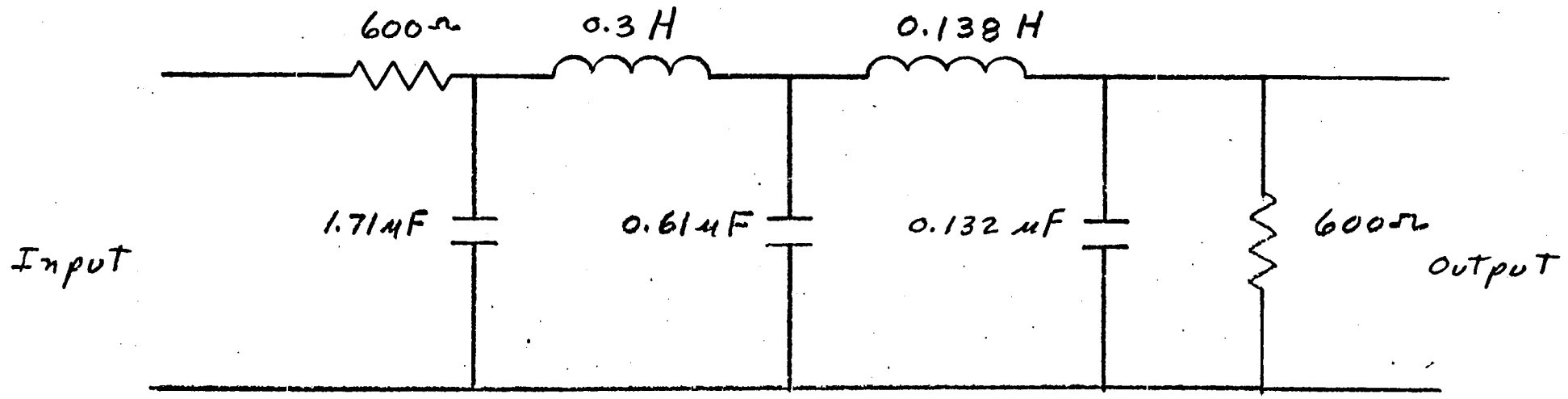

F-11

Linear-Phase Low-Pass Filter

Figure 11

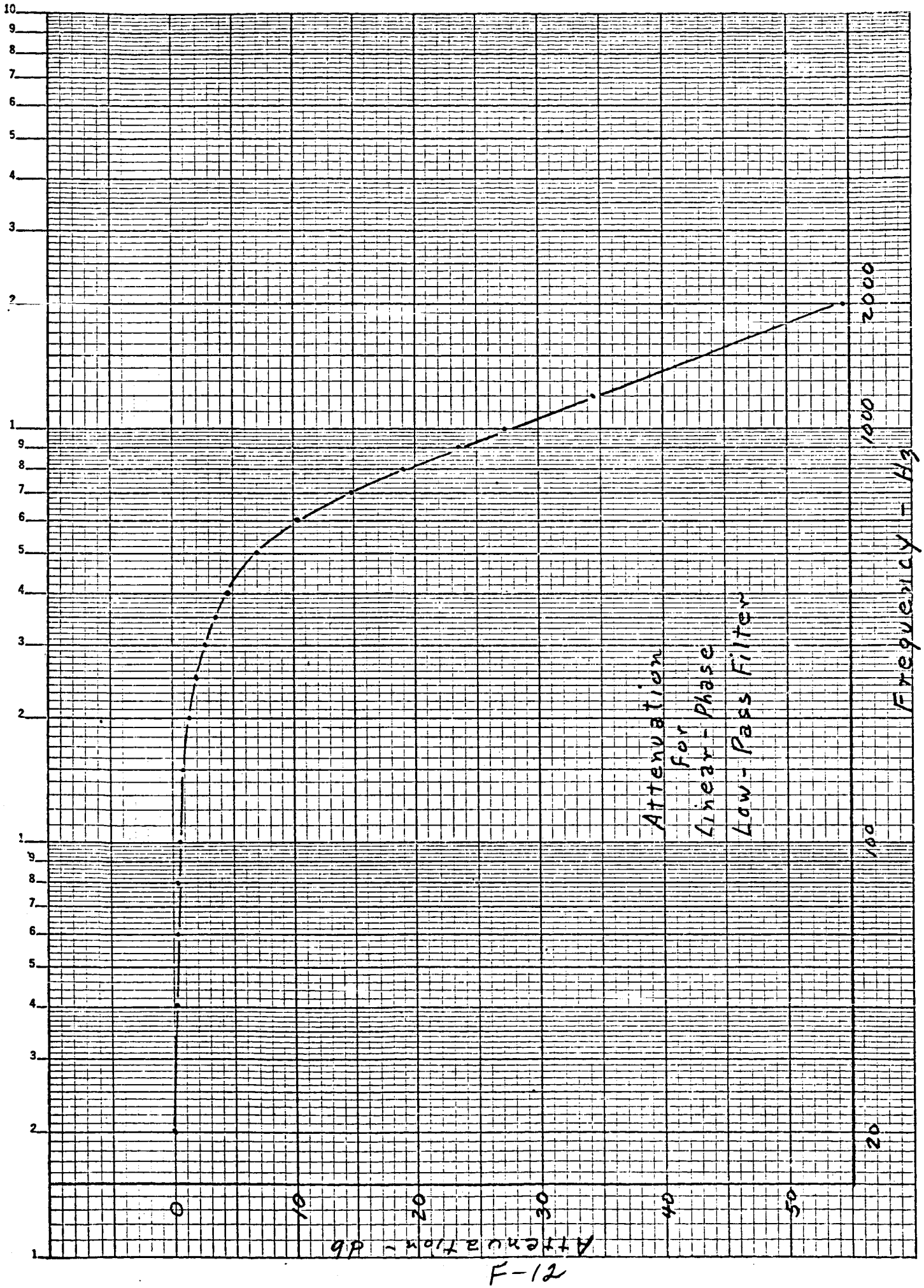

Figure 12

F-12

SEMI-LOGARITHM 359-71G
KEUFFEL & ESSER CO. MADE IN U.S.A.
5 CYCLES X 70 DIVISIONS

K&E 5 X 5 TO THE CENTI ER 359-15G
KEUFFEL & ESSER CO. MADE IN U.S.A.

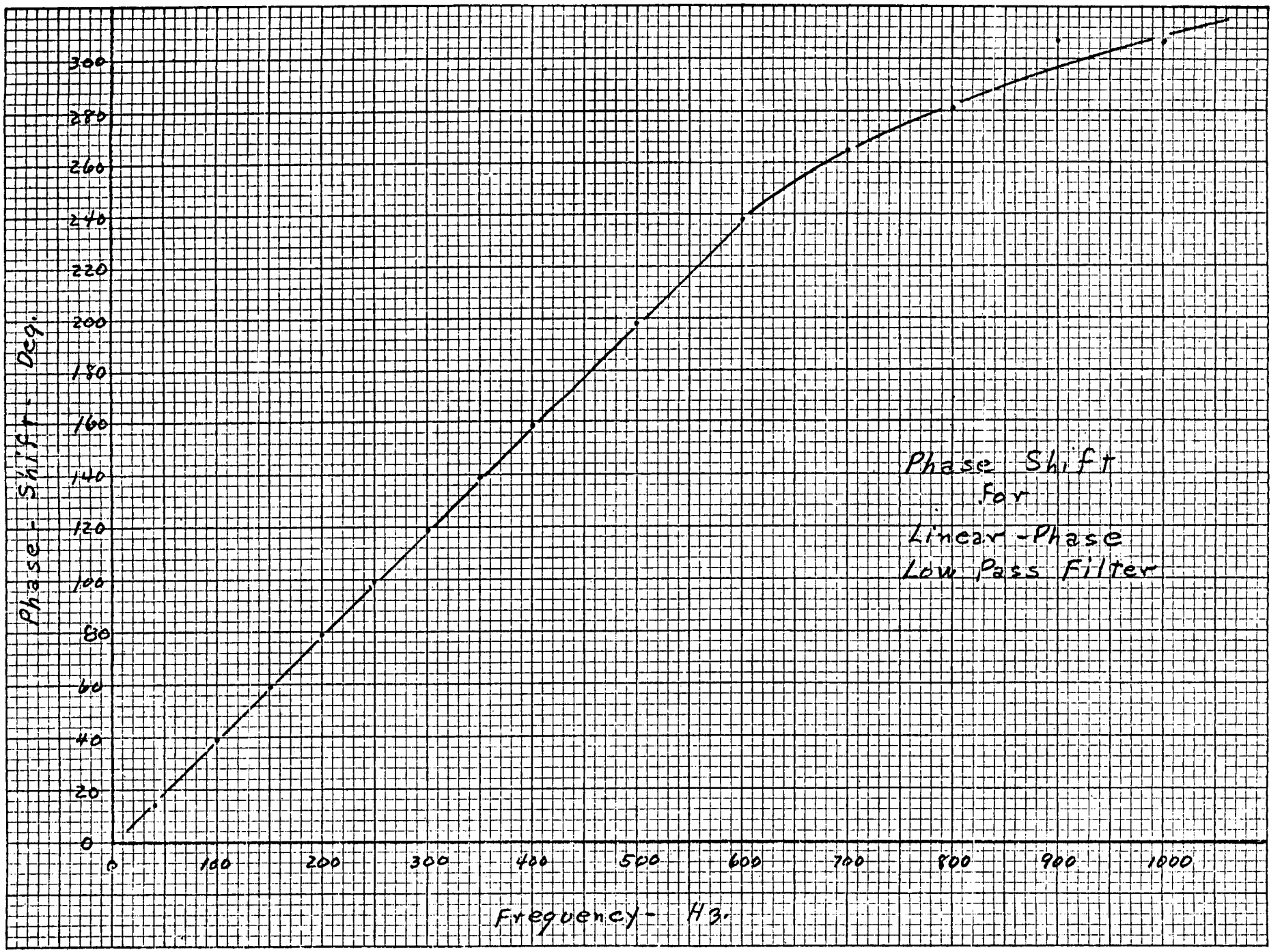

F-13

F-14 A

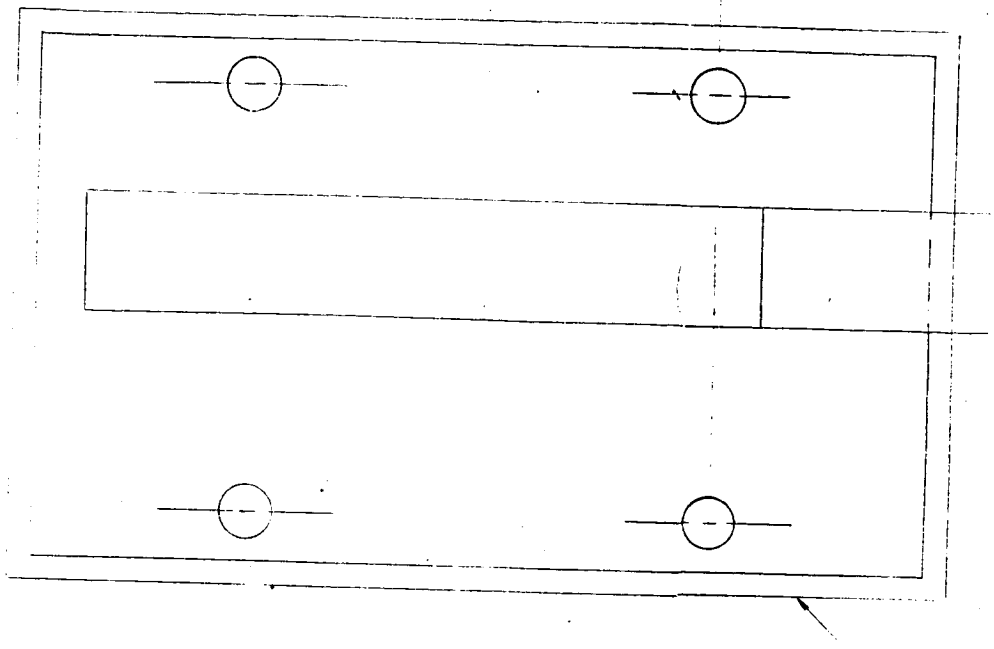

SLIDE 14B

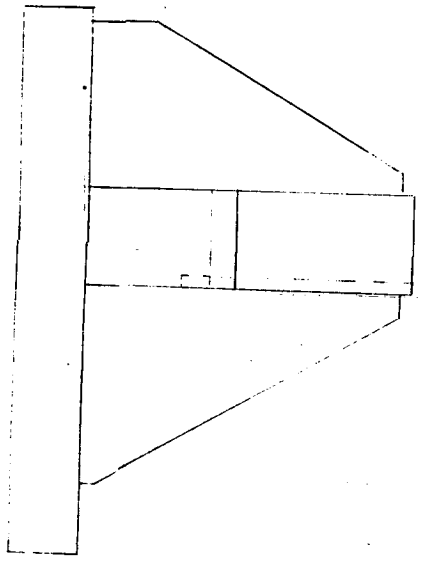

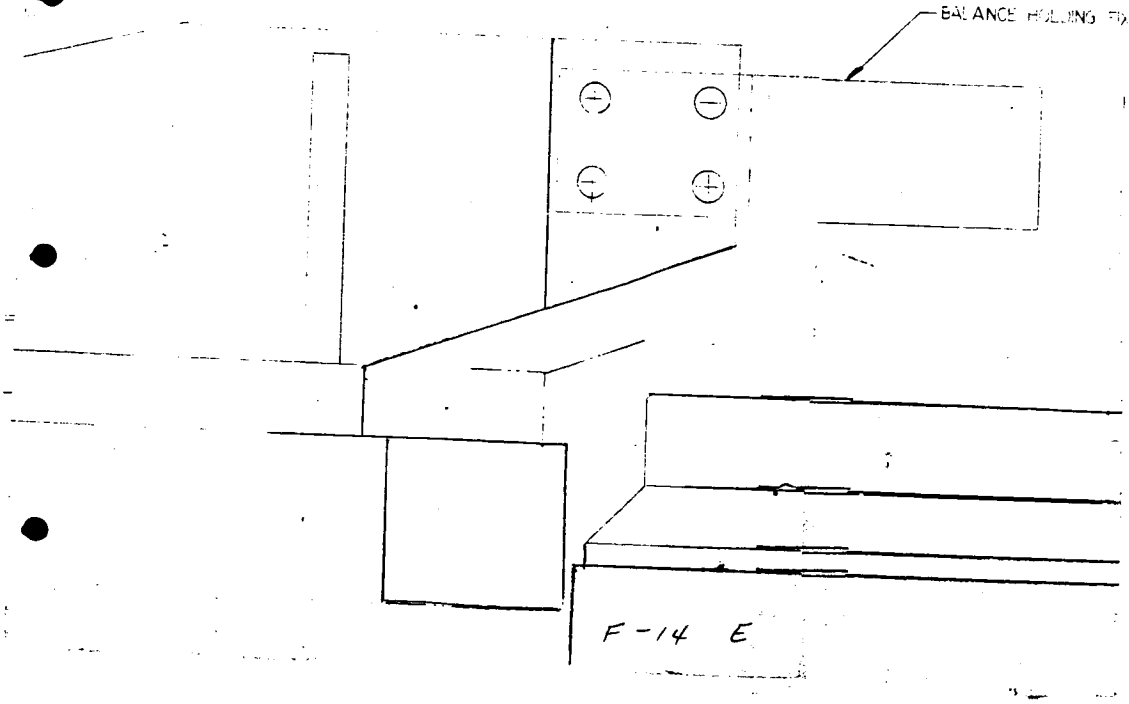

F-14 E

F-14 B

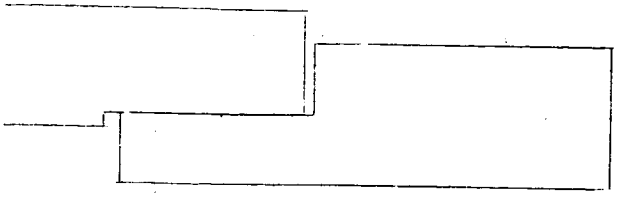

F-14 C

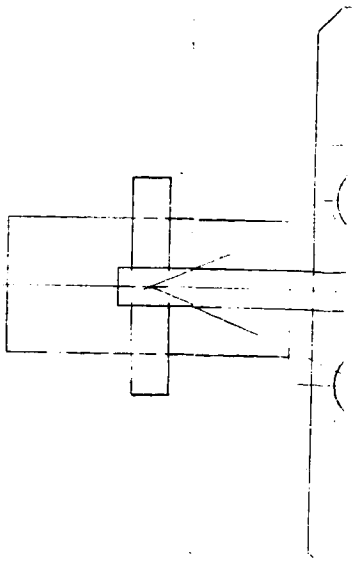

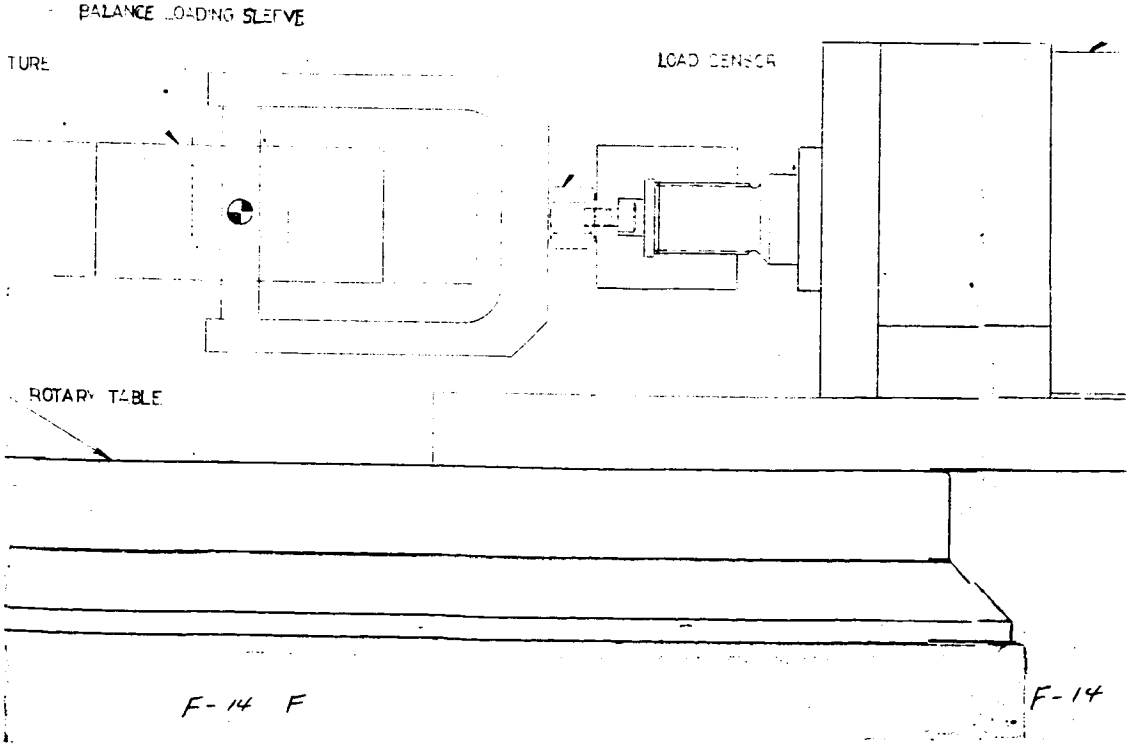

F-14 F

F-14

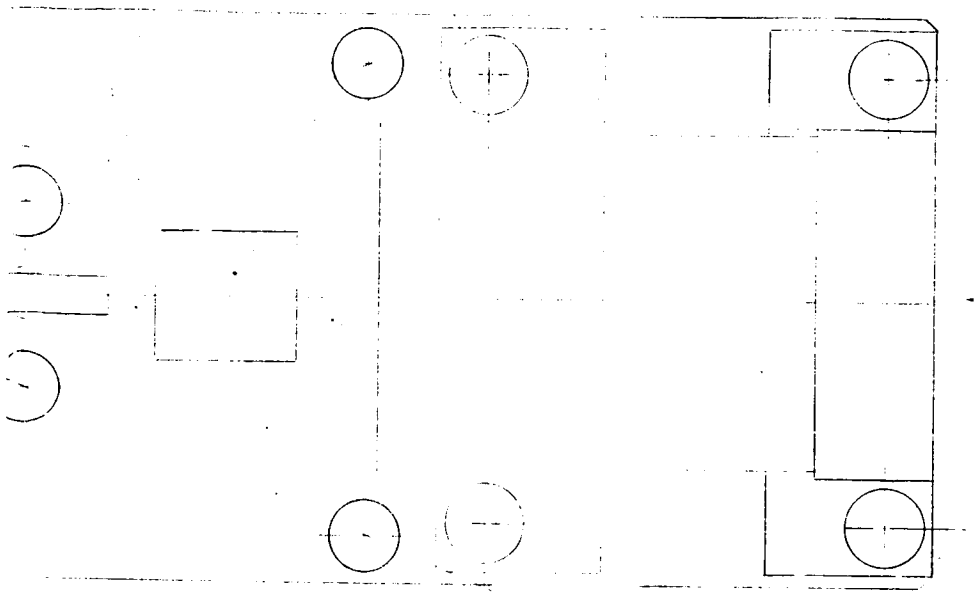

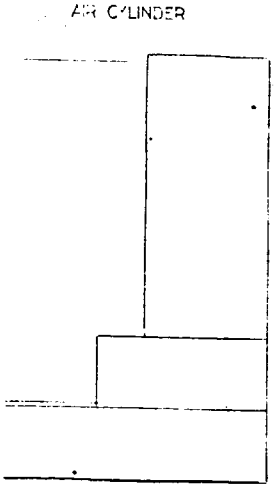

FORCE BALANCE
STATIC LOADING SYSTEM

FIG. 14

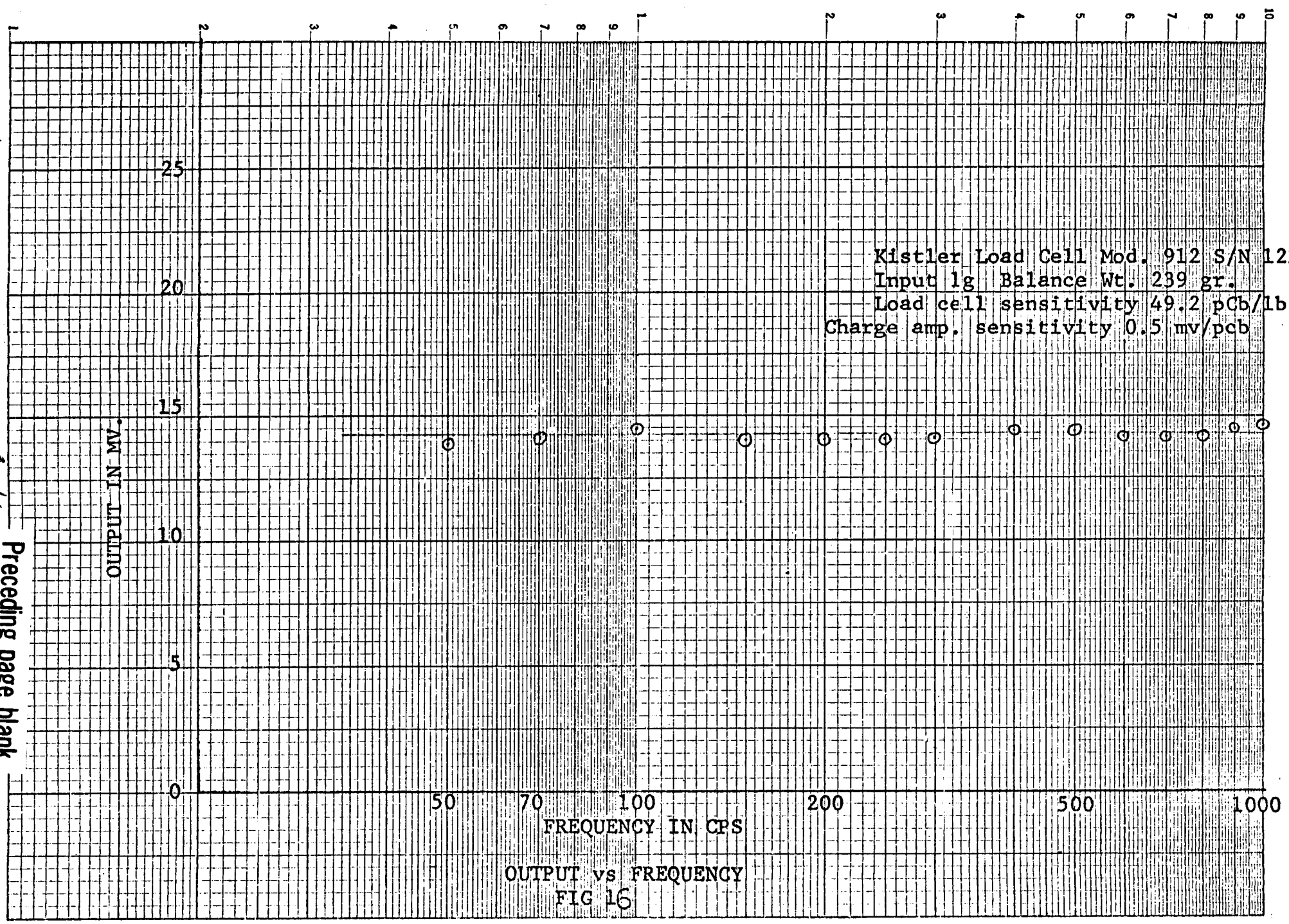

OUTPUT vs FREQUENCY
FIG 16

F-16

Preceding page blank

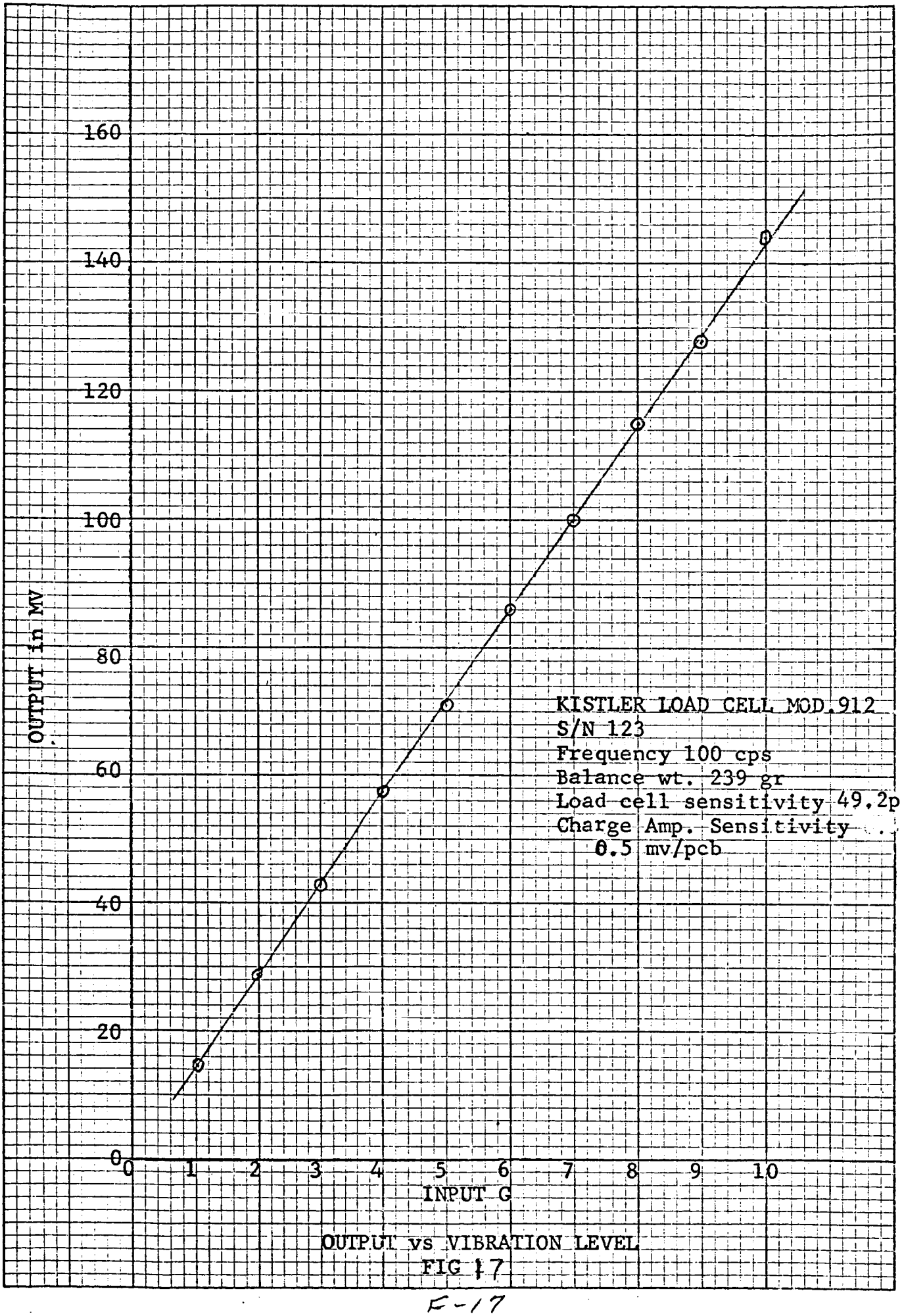

OUTPUT vs VIBRATION LEVEL

FIG 17

359-5DG
MADE IN U.S.A.
10 X 10 TO THE I
KEUFFEL & ESSER CO

FORCE BALANCE DESIGN #1

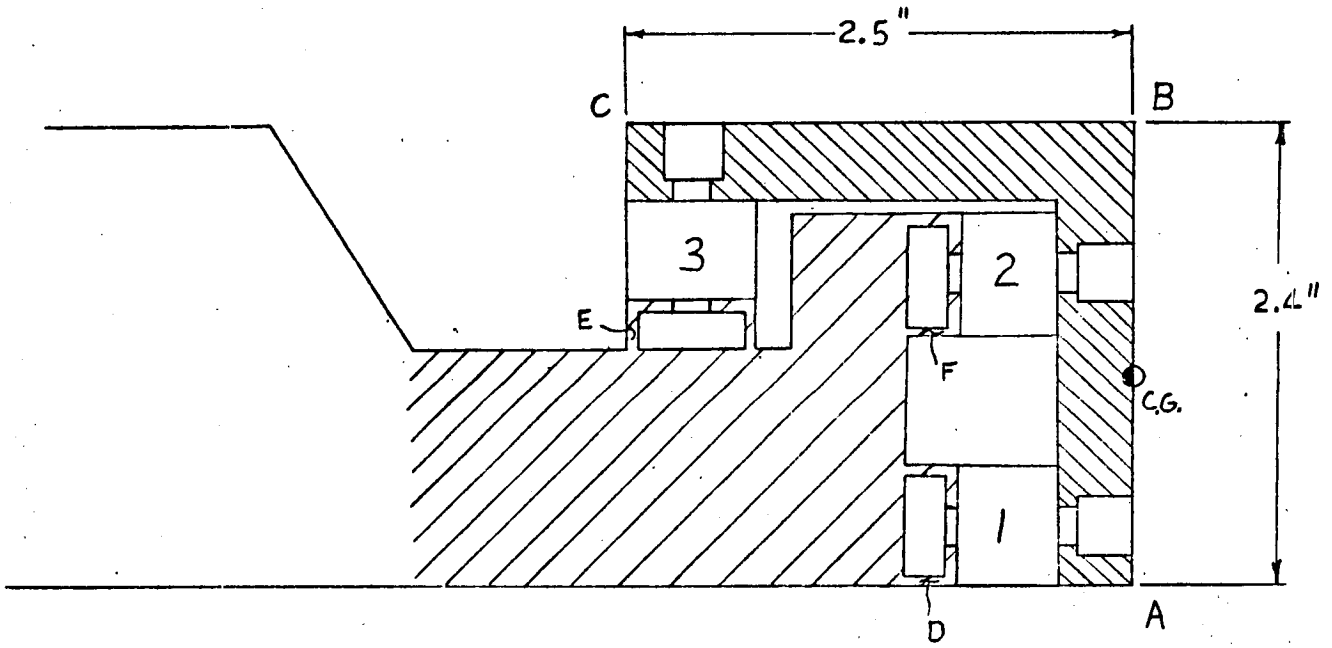

Fig. 18

STING

LOAD FRAME

FORCE BALANCE DESIGN # 2

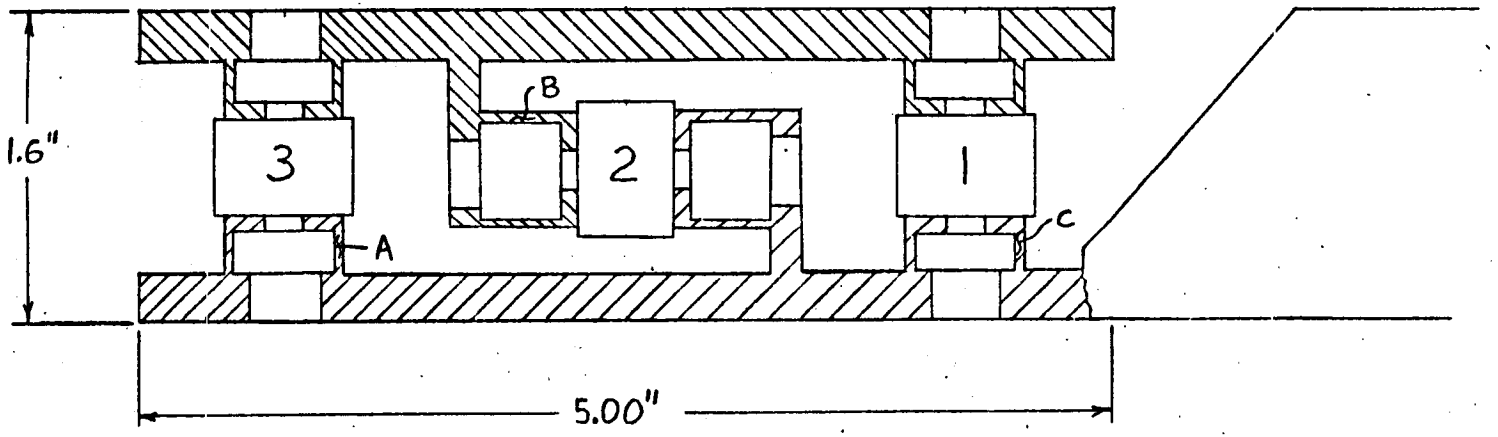

Fig. 19

STING

LOAD FRAME

LOADING DIAGRAM FOR
PHASE II TESTS

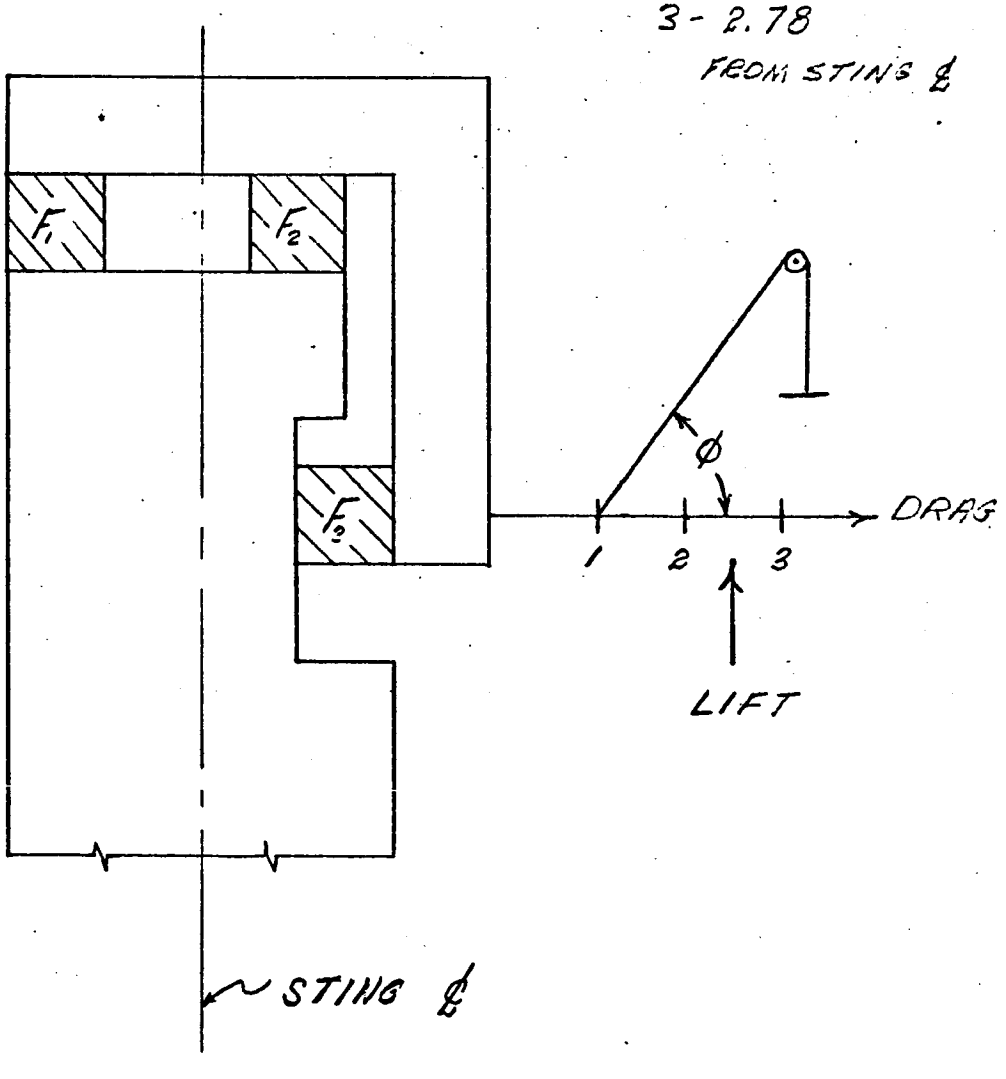

FIGURE 20

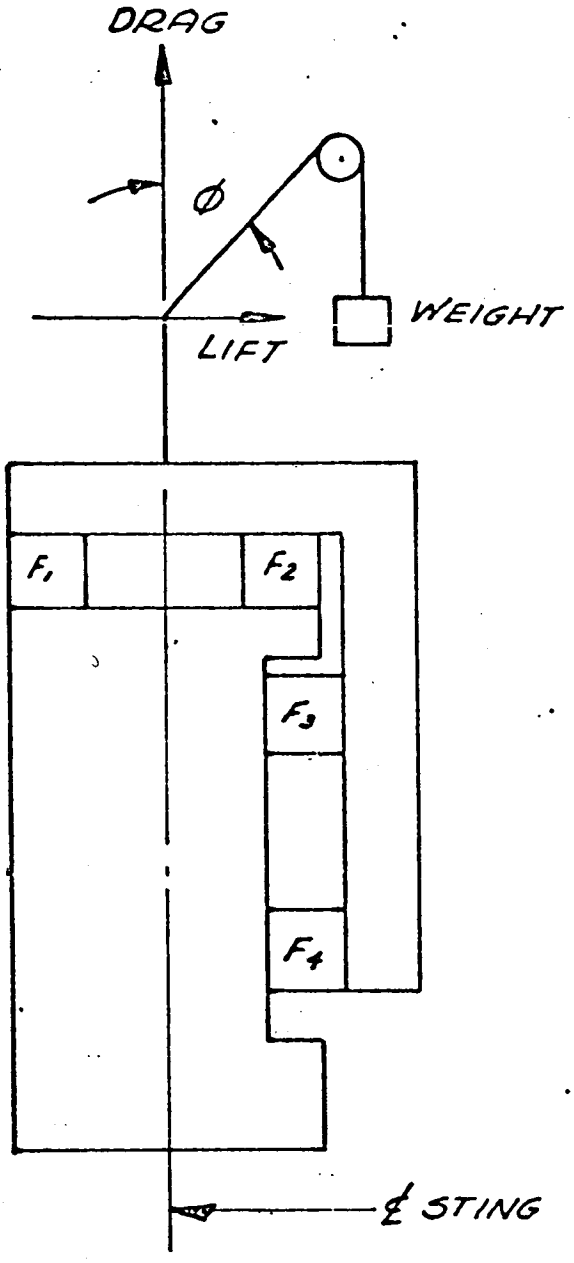

LOADING DIAGRAM FOR
PHASE I TESTS

FIG. 21

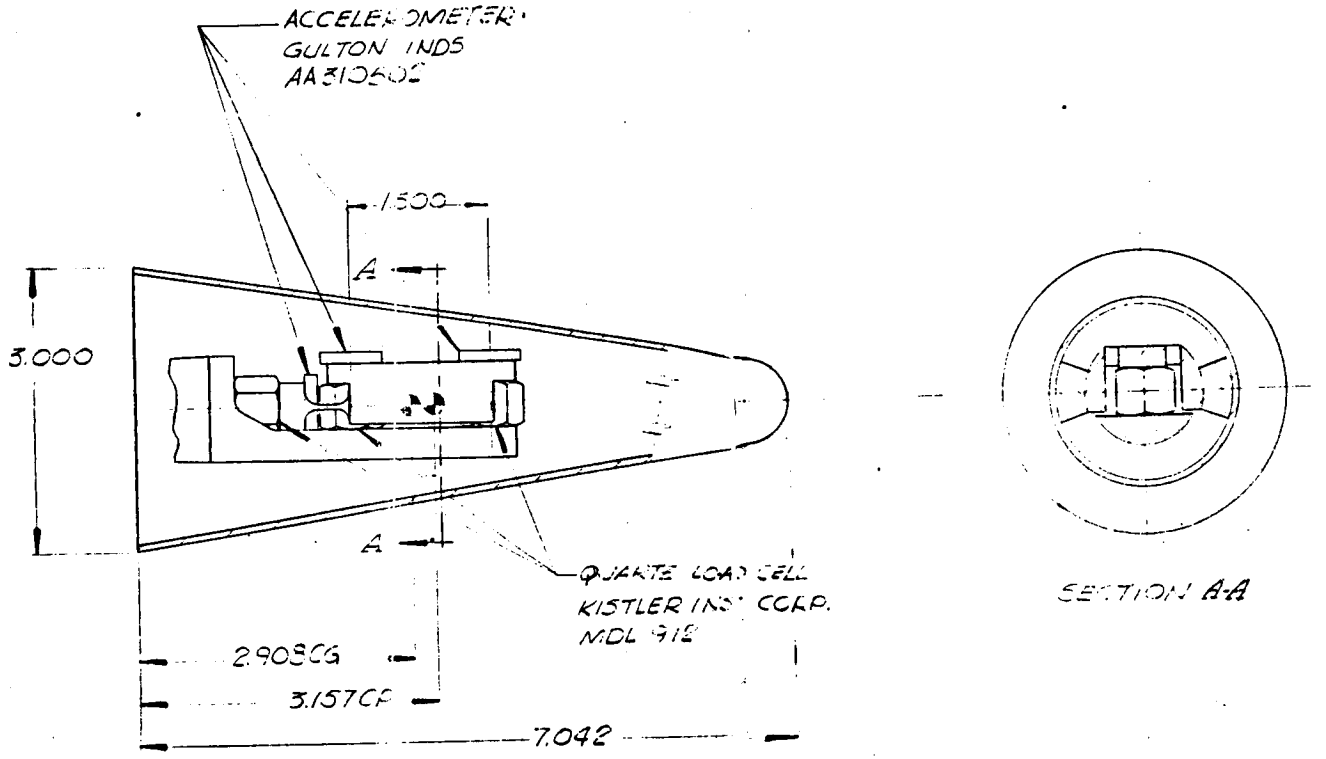

SECTION A-A

NEXT ASSY. / USED ON / APPLICATION	UNLESS OTHERWISE SPECIFIED: DIMENSIONS ARE IN INCHES; TOLERANCE ON FRACTIONS ±1/64; DECIMALS ±.004; ANGLES ±1°; MATERIAL; FINAL PROTECTIVE FINISH	CONTRACT; APPROVED DATE; DRAWN 29 JAN DATE; CHECKED DATE; PROJ. ENG. DATE	FORCE BALANCE MODEL ASSY. TUNNEL MODEL NO 1	SCALE 1/1; UNIT WT.	Astro-Space LABORATORIES INC, A SUBSIDIARY OF DEVICO INSTRUMENT CORPORATION, HUNTSVILLE ALABAMA; FIG. 22

F-22 A

F-22-B

NAVSHIPS FORM 482-3 (AUGUST 1960)

NOTICE.—WHEN GOVERNMENT DRAWINGS, SPECIFICATIONS, OR OTHER DATA ARE USED FOR ANY PURPOSE OTHER THAN IN CONNECTION WITH A DEFINITELY RELATED GOVERNMENT PROCUREMENT OPERATION, THE UNITED STATES GOVERNMENT THEREBY INCURS NO RESPONSIBILITY NOR ANY OBLIGATION WHATSOEVER; AND THE FACT THAT THE GOVERNMENT MAY HAVE FORMULATED, FURNISHED, OR IN ANY WAY SUPPLIED THE SAID DRAWINGS, SPECIFICATIONS OR OTHER DATA IS NOT TO BE REGARDED BY IMPLICATION OR OTHERWISE AS IN ANY MANNER LICENSING THE HOLDER OR ANY OTHER PERSON OR CORPORATION, OR CONVEYING ANY RIGHTS OR PERMISSION TO MANUFACTURE, USE, OR SELL ANY PATENTED INVENTION THAT MAY IN ANY WAY BE RELATED THERETO.

F-23 A

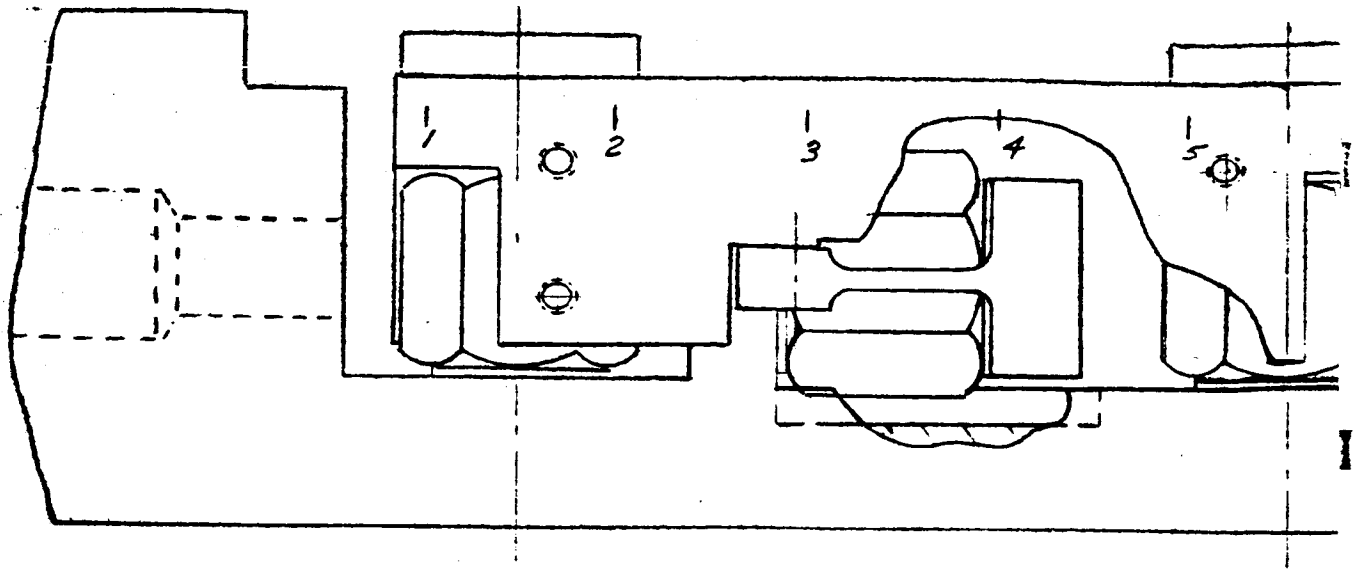

VIEW D-D

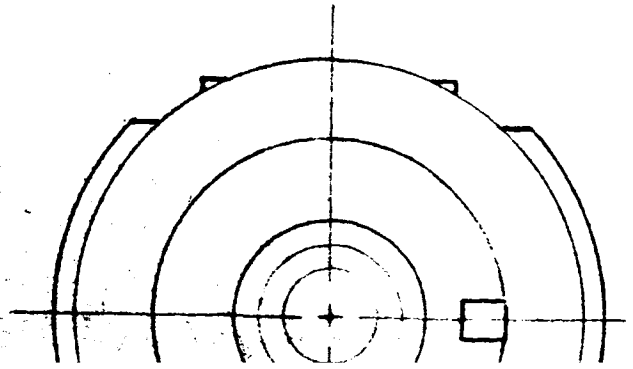

1.1003
1.0997
DIA.

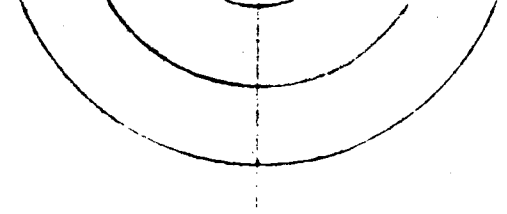

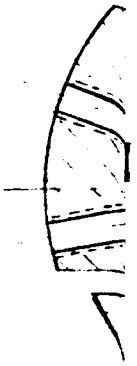

F- 23 E

F-23 B

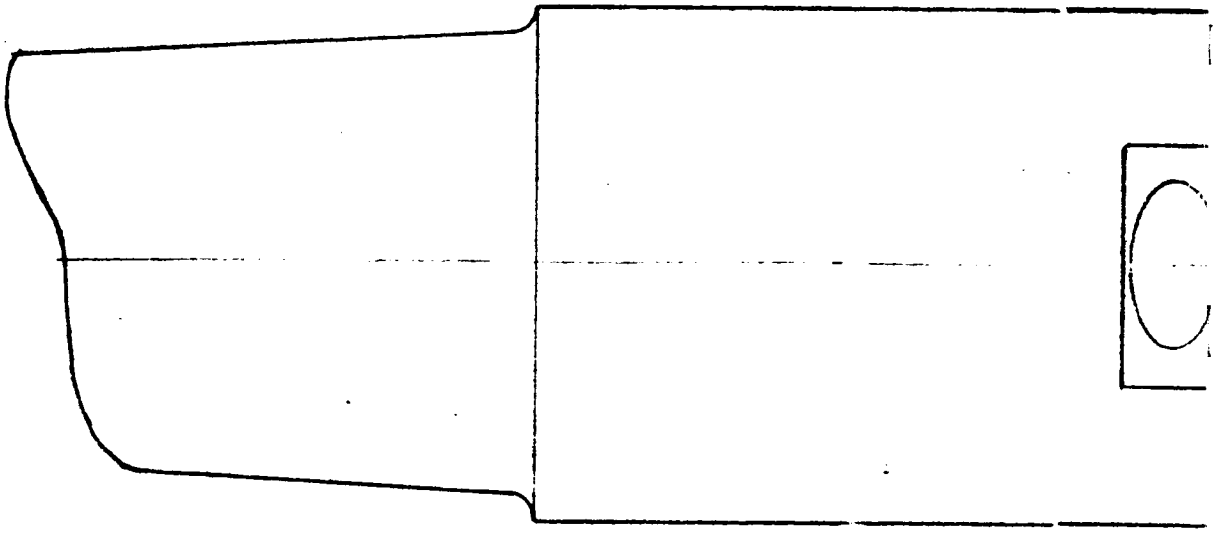

1" TAPER / 12"
TO MATCH TAPER
RUG GAGE 80M

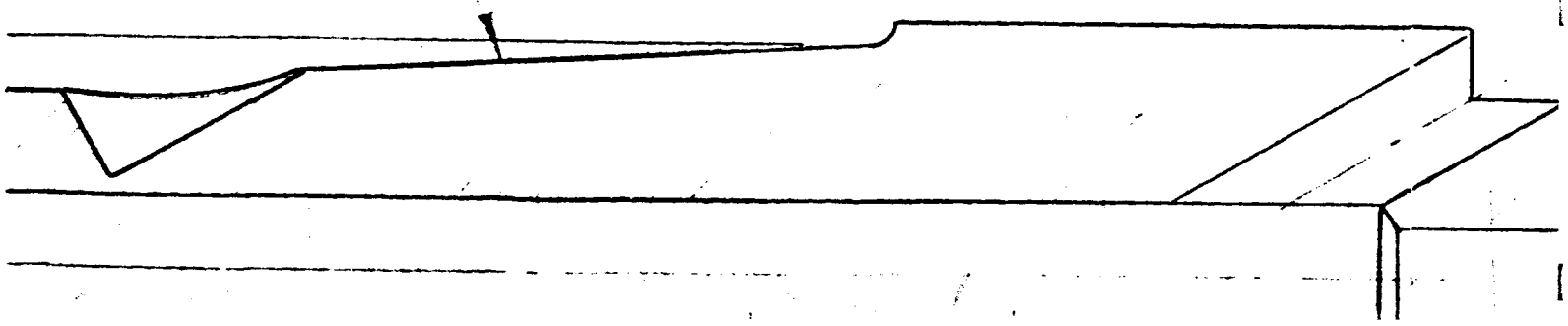

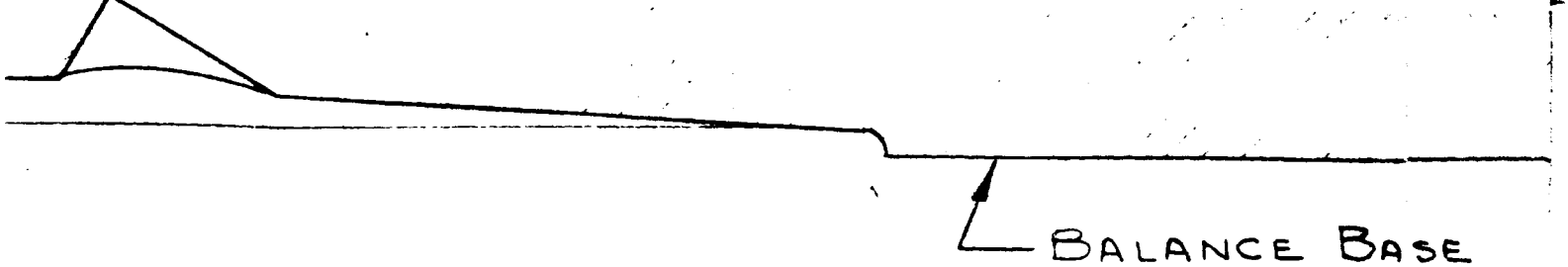

SECTION A-A

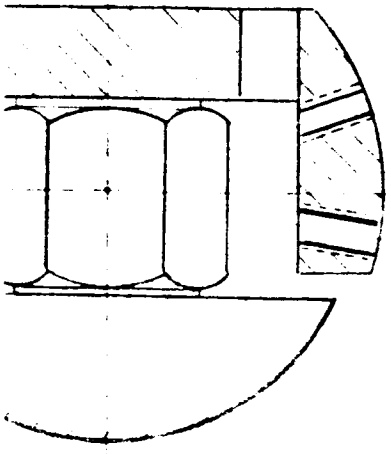

TION B-B

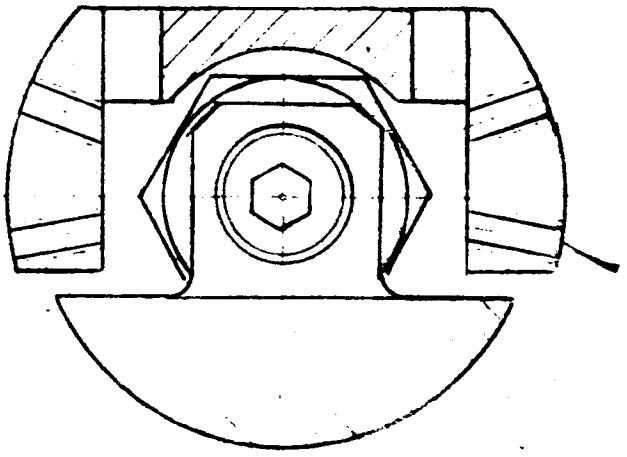

SECTION C-C

F-23 C

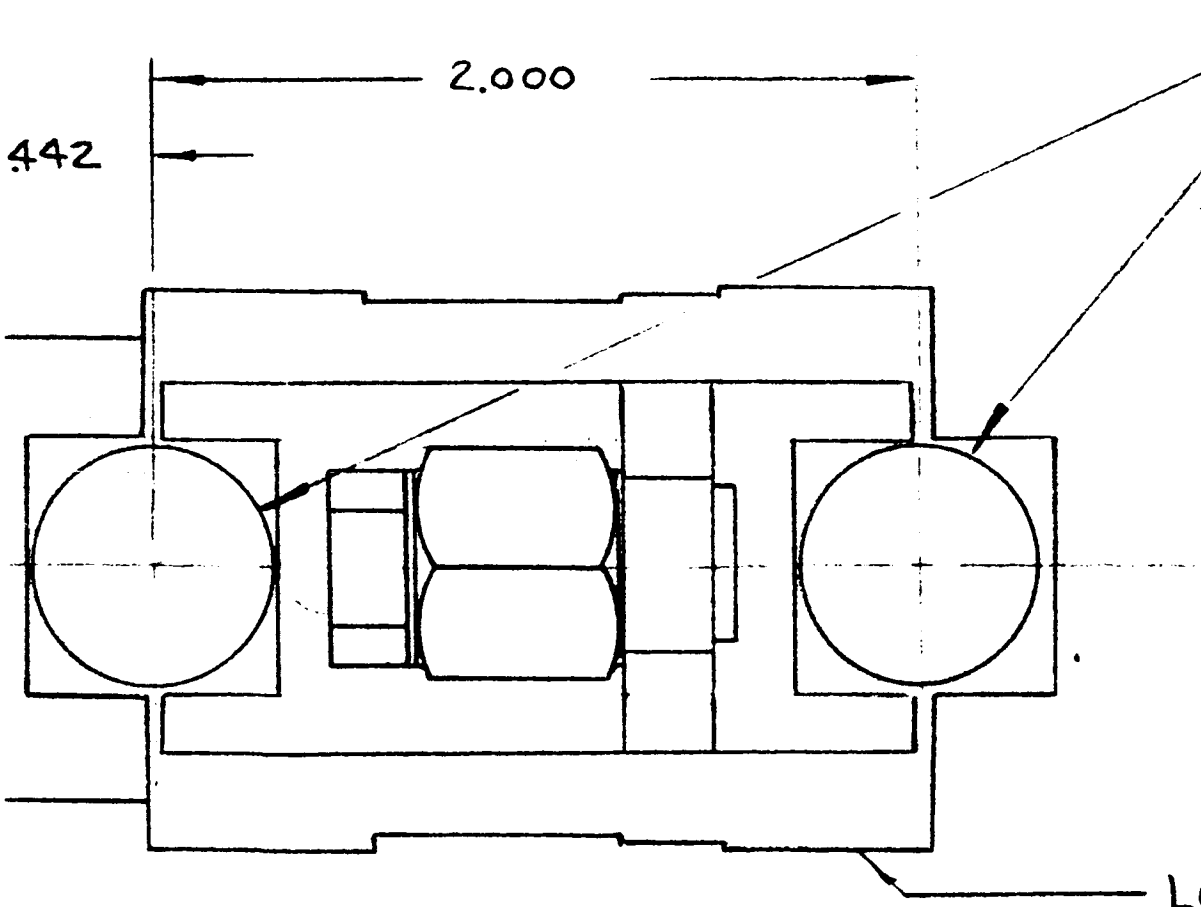
2.000
.442
ACCE
GLEN
2
LOAD FRAME
80M31618
D
C
B
QUARTZ L
KISTLER M
2 REQ'D

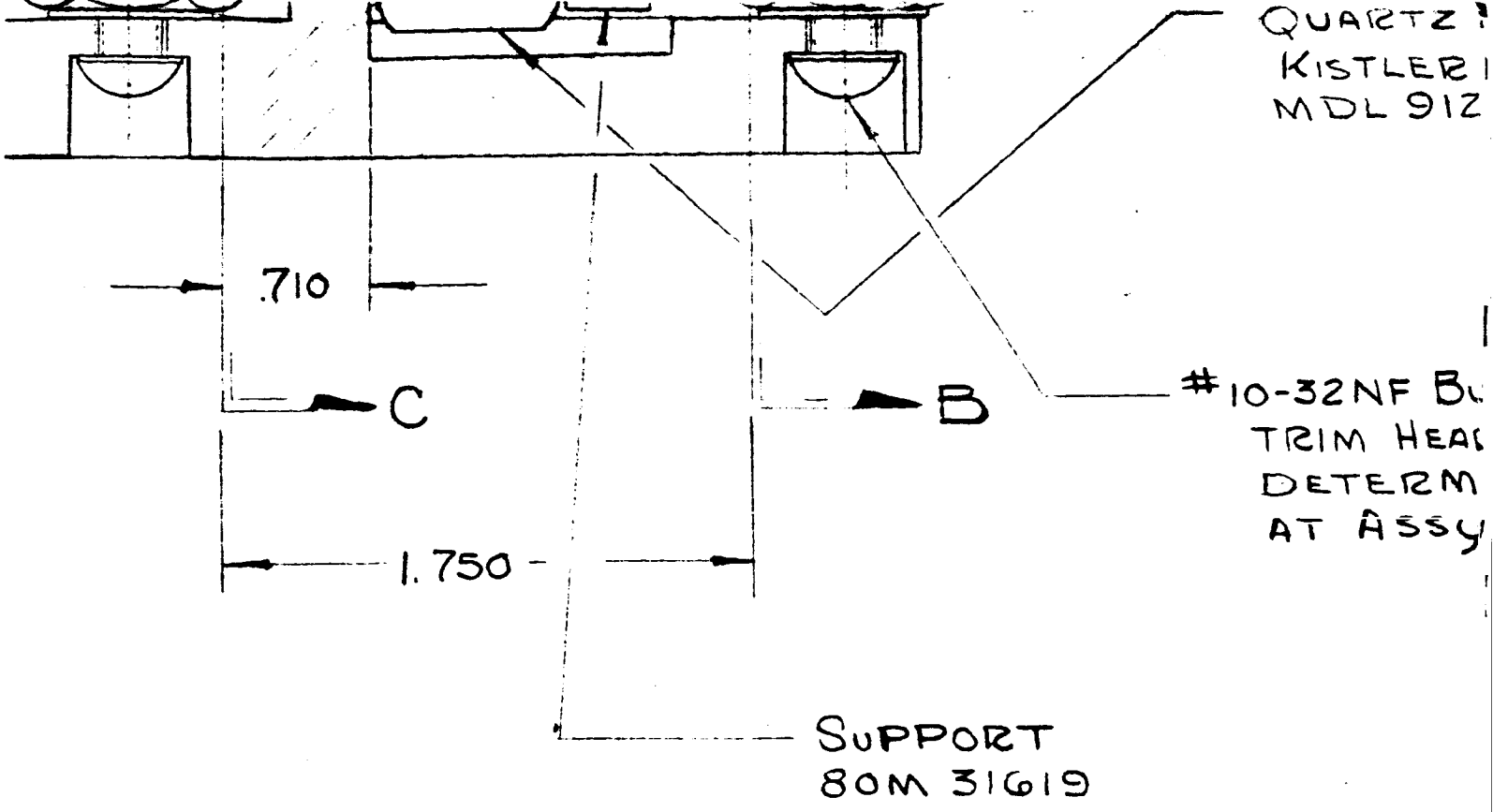

— #4-40 NC-2 TAP THRU
MATE WITH ADAPTER
80M31657
8 HOLES.

F-23 G

SEE ENGINEERING RECORDS	
NEXT ASSY	USED ON
APPLICATION	

UNLESS OTHERWISE SPECIFIED

DIMENSIONS ARE IN INCHES

TOLERANCES ON
FRACTIONS DECIMALS ANGLES

MATERIAL

HEAT TREATMENT

FINAL PROTECTIVE FINISH

:T No.	M F	REVISIONS				
		ZONE	SYM	DESCRIPTION	DATE	APPROVAL

F-23 D

EROMETER
ITE MDL AA 310502
2EQ'D

D CELL
L. 912

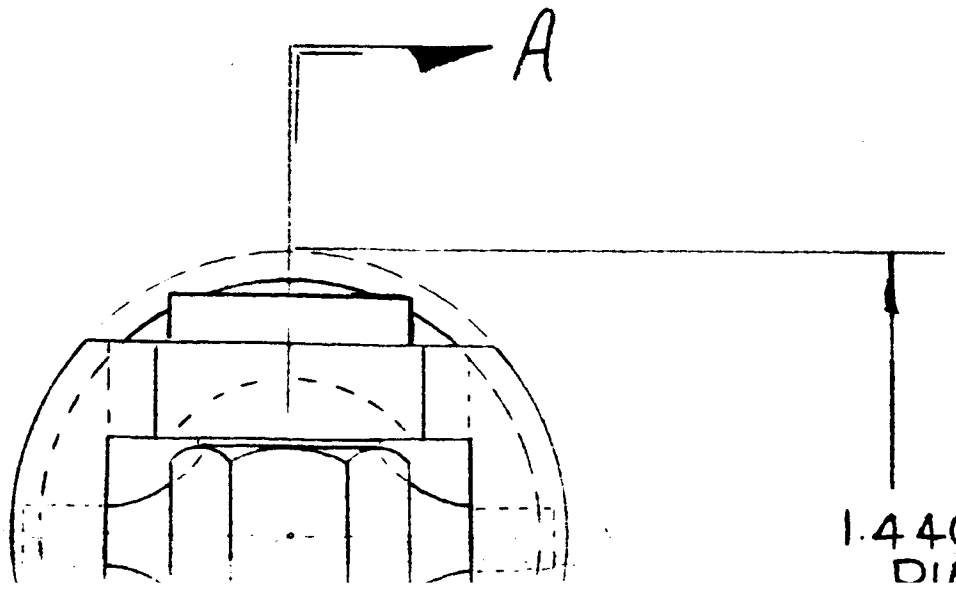

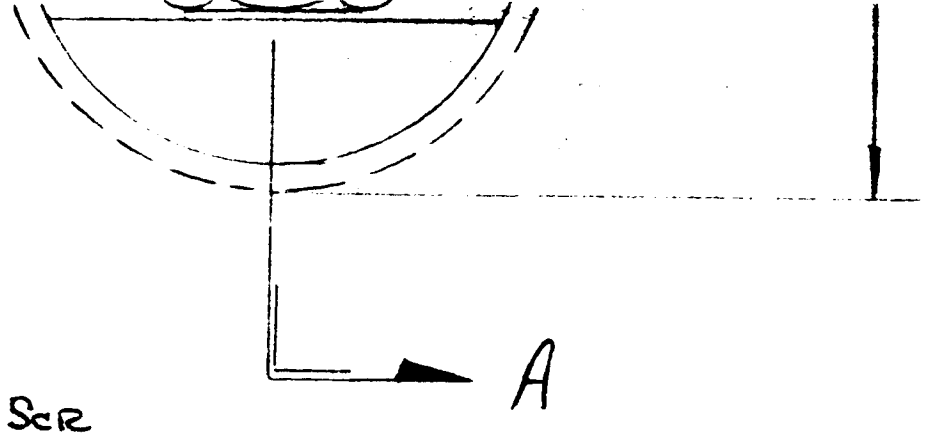

OAD CELL

M102

TTON HD. SOC SCR
TO .340 ± 010 DIA.
NE MAX. LENGTH

F-23 H

IGINAL DATE DRAWING			DISTR CODE
BRADSHAW	CHECKER	TUNNEL BALANCE 198	GEORGE C. MARSHALL SPACE FLIGHT CENTER NATIONAL AERONAUTICS AND SPACE ADMINISTRATION HUNTSVILLE, ALABAMA
CKER	STRESS		
INEER	ENGINEER		
MITTED			
ROVED		WEIGHT CHECKER / DATE / CODE	DWG SIZE D — 80M41605
DIRECTOR		SCALE 2/1 / UNIT WEIGHT	SHEET 1 OF 1

FIG 23

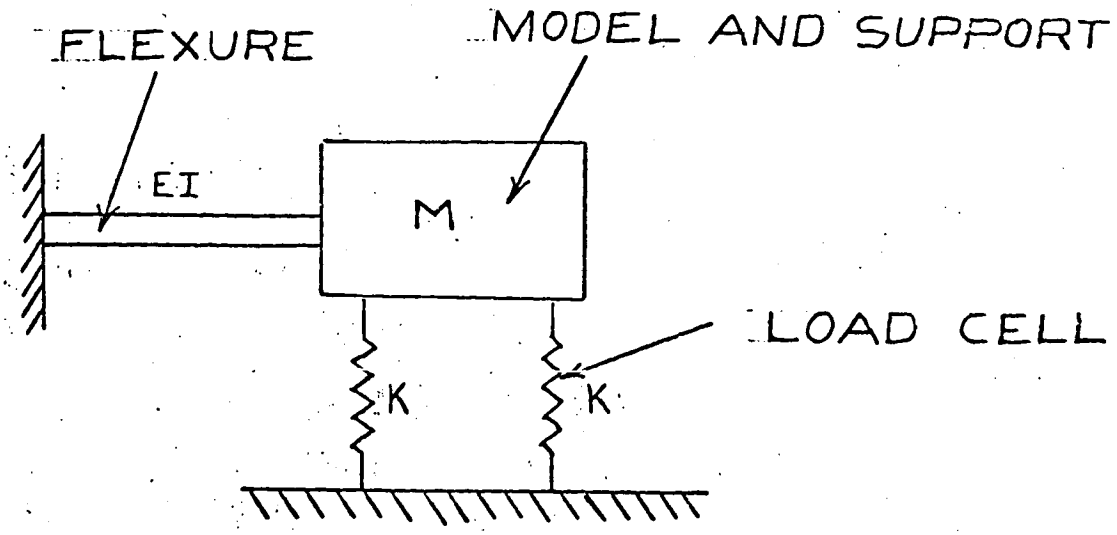

SYSTEM

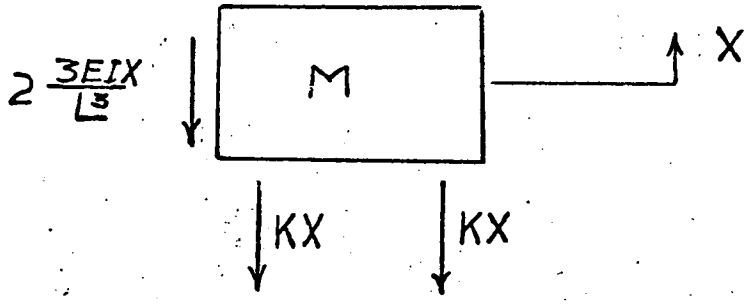

FREE BODY

D.E.

$$M\ddot{X} + 2KX + 2\frac{3EI}{L^3}X = 0$$

LIFT DYNAMICS

FIG. 24

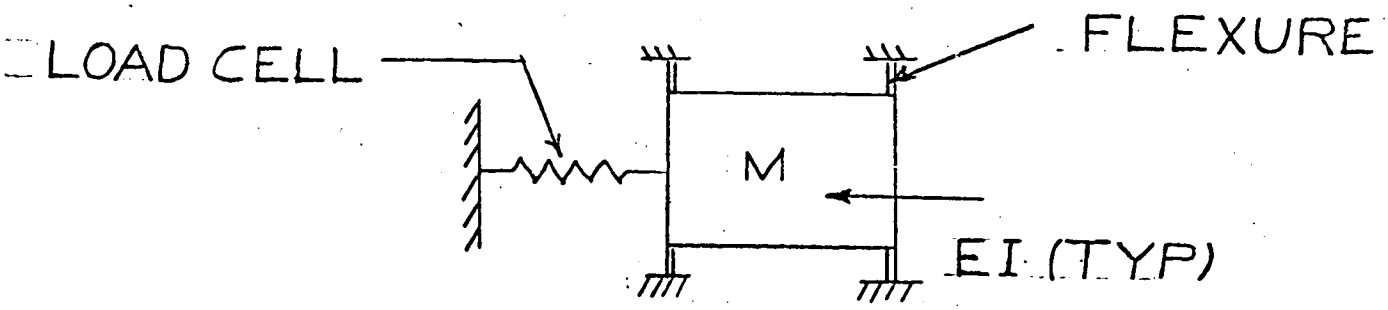

SYSTEM

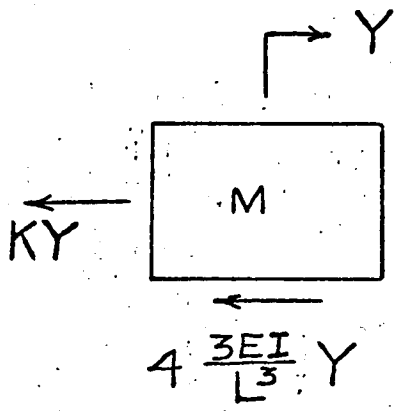

FREE - BODY

D.E.

$$M\ddot{Y} + KY + 4\frac{3EI}{L^3}Y = 0$$

DRAG DYNAMICS

FIG. 25

F-25

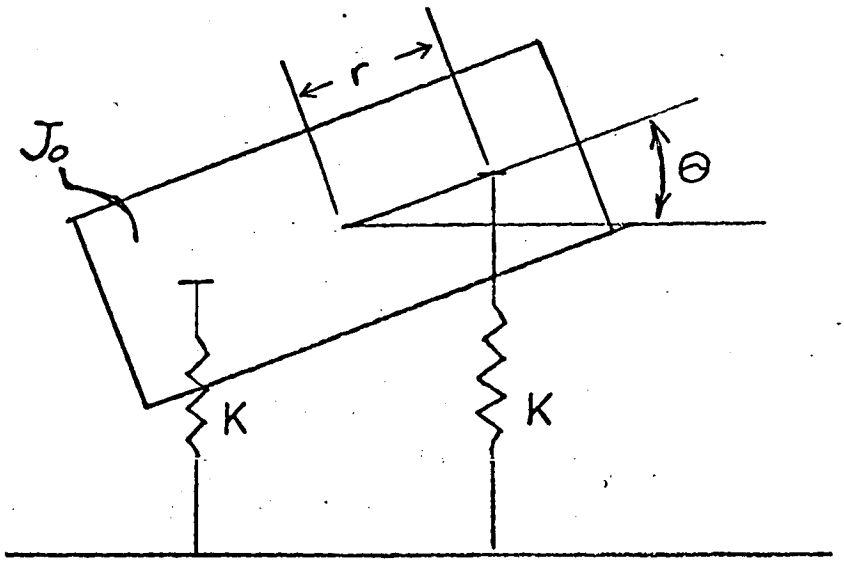

D.E.

$$J_o\ddot{\theta} + 2Kr^2\theta = 0$$

ROTATIONAL DYNAMICS

FIG. 26

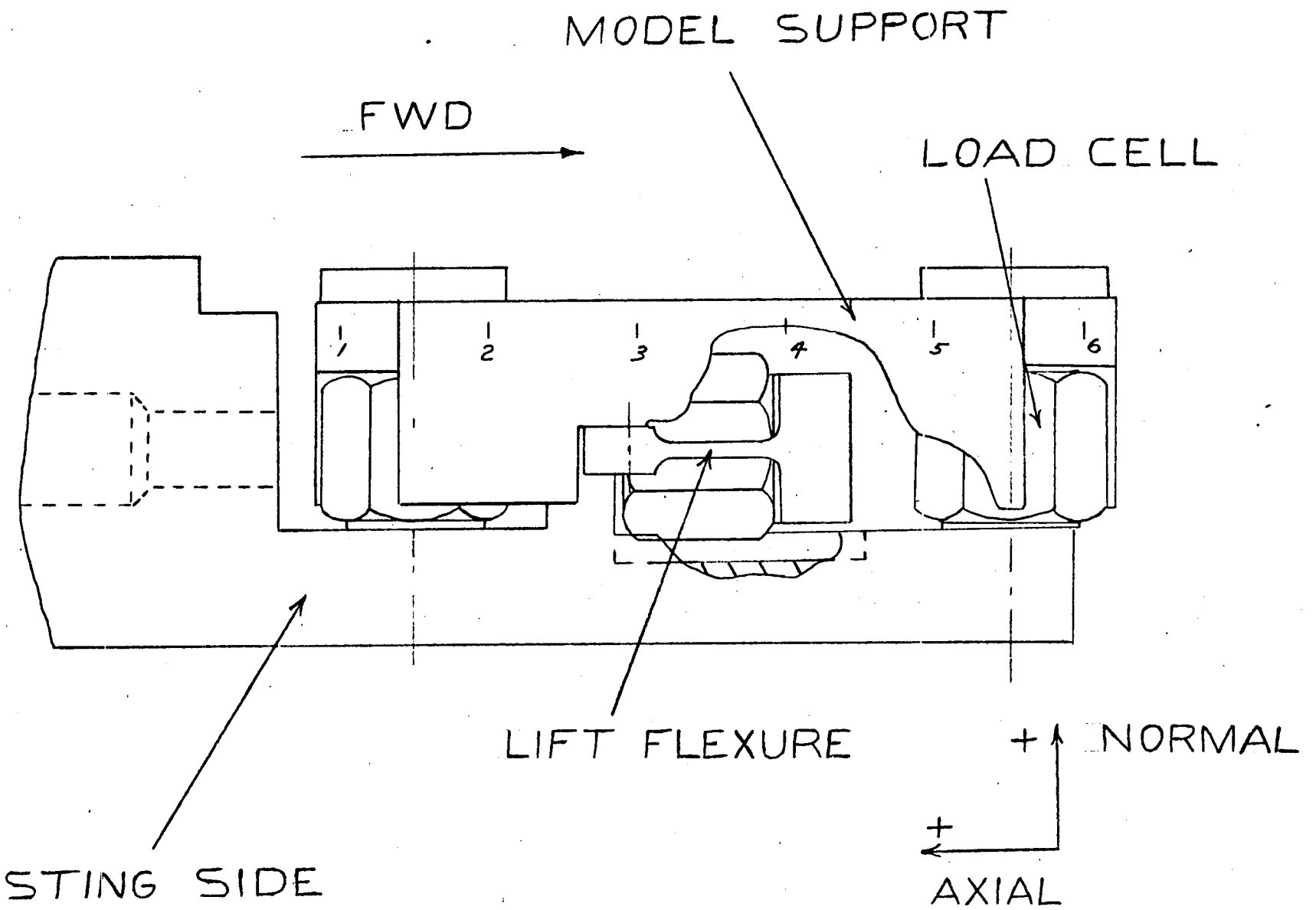

F-27

BALANCE No. 198

FIGURE 27

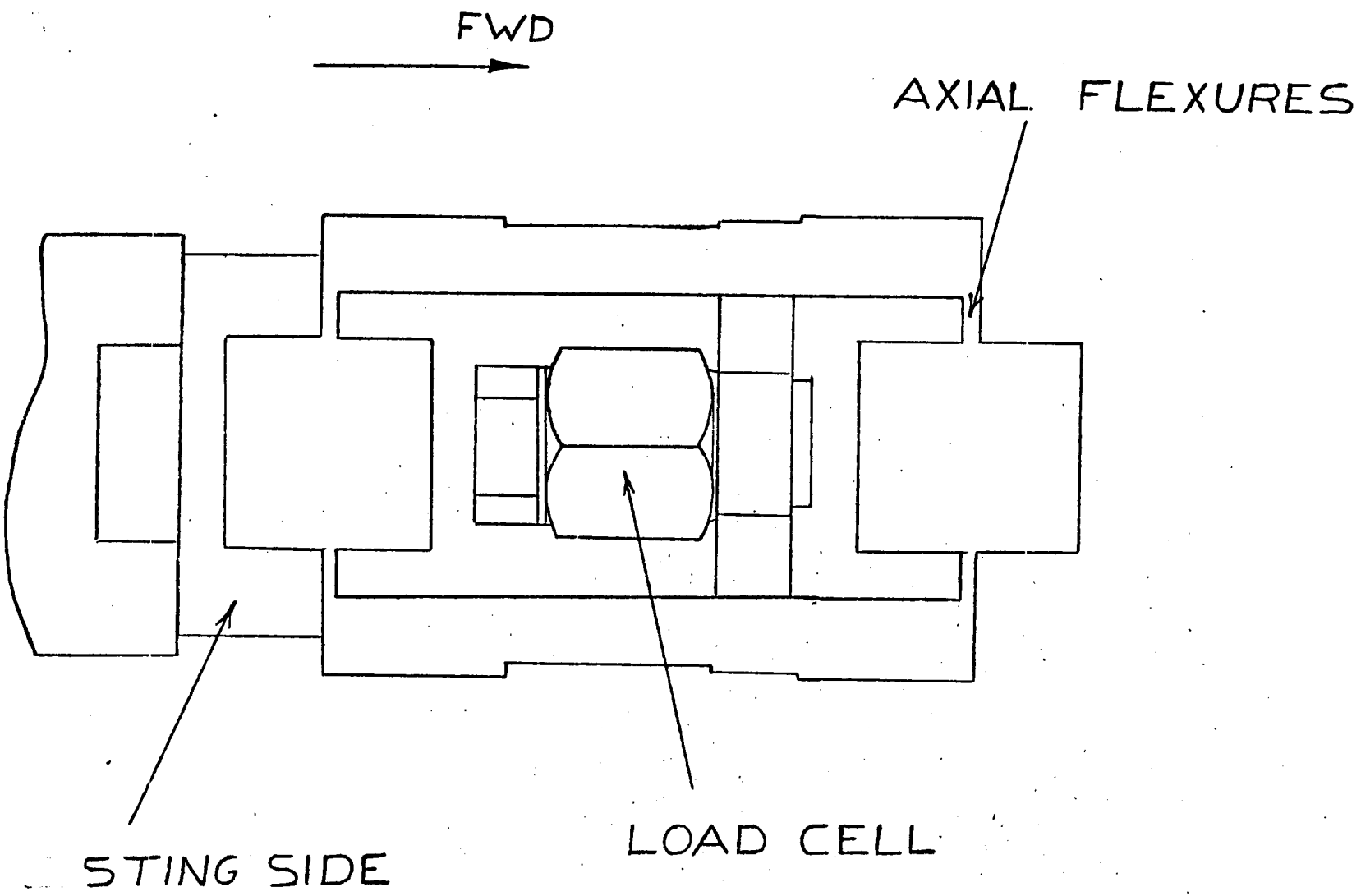

F-28

BALANCE No. 198

Figure 28

ELECTRO INSTRUMENTS, INC.
SAN DIEGO, CALIFORNIA
NO. R200-10
MADE IN U.S.A.

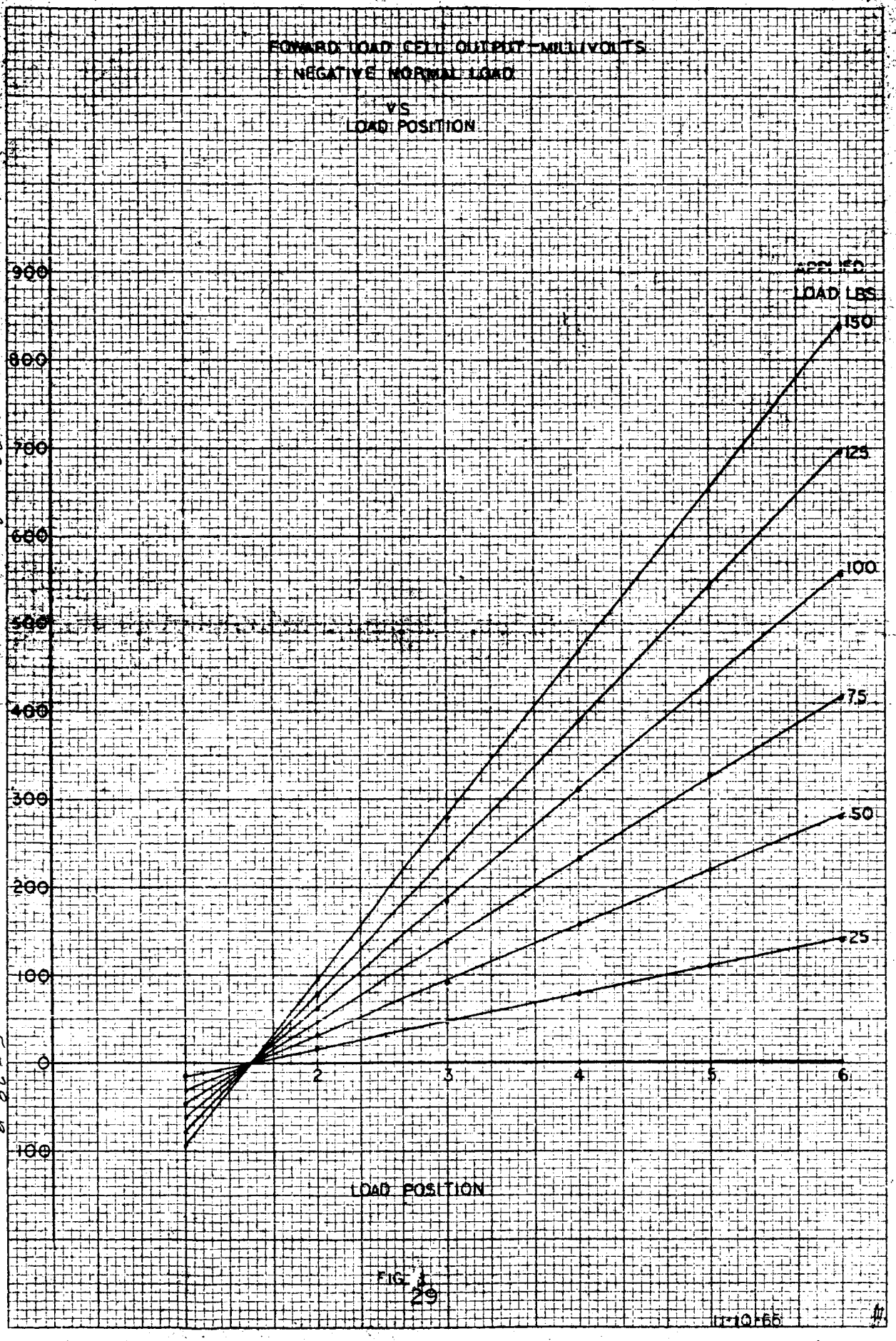

F-29 A

F-29 B

FIG. 29

11-10-65

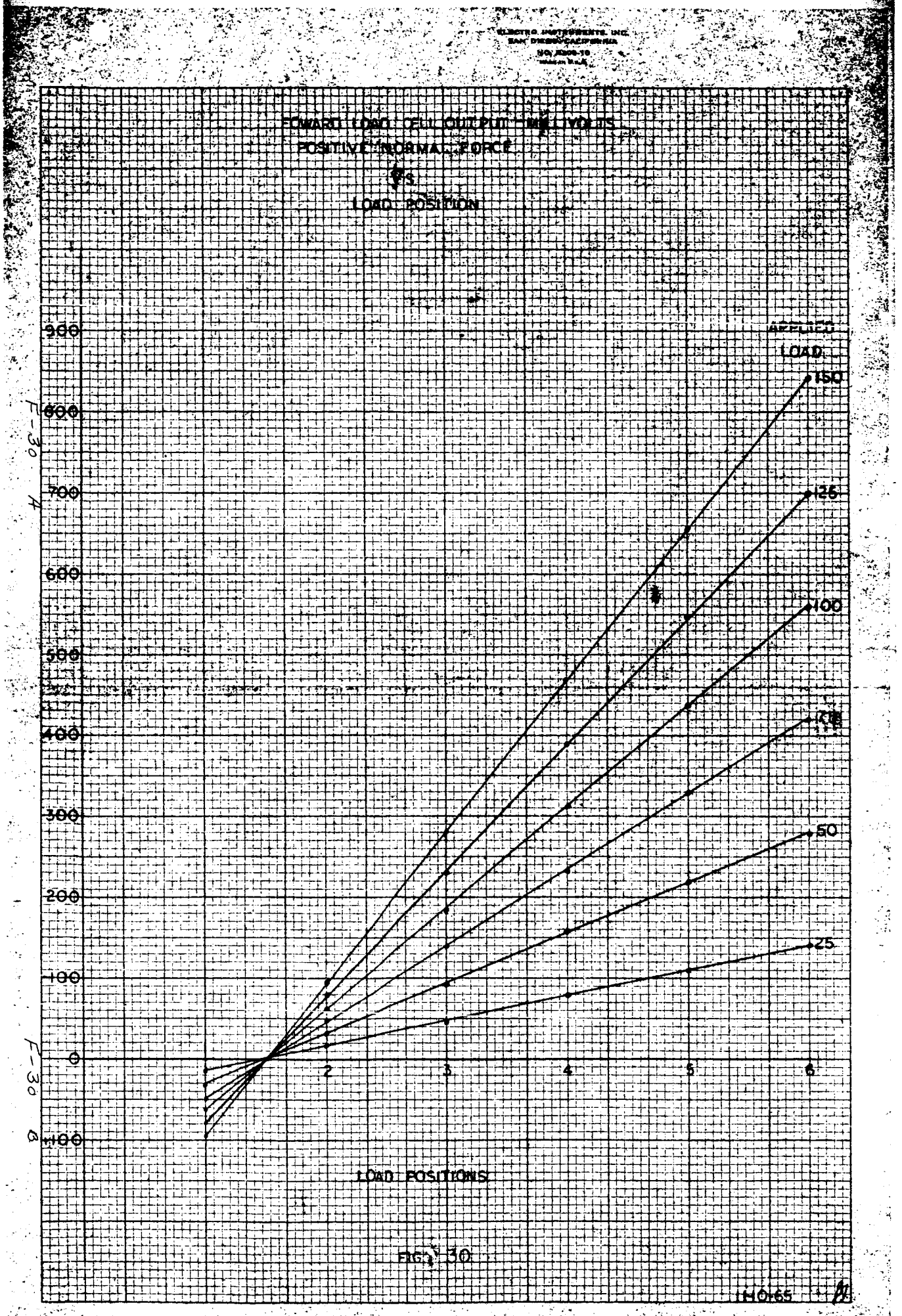
FORWARD LOAD CELL OUTPUT - MILLIVOLTS
POSITIVE NORMAL FORCE
VS.
LOAD POSITION
APPLIED LOAD
150
125
100
75
50
25
900
800
700
600
500
400
300
200
100
0
100
2
3
4
5
6
LOAD POSITIONS
F-30 A
F-30 B
FIG. 30
NO. 65

ELECTRO INSTRUMENTS, INC.
SAN DIEGO, CALIFORNIA
NO. R509-16
MADE IN U.S.A.

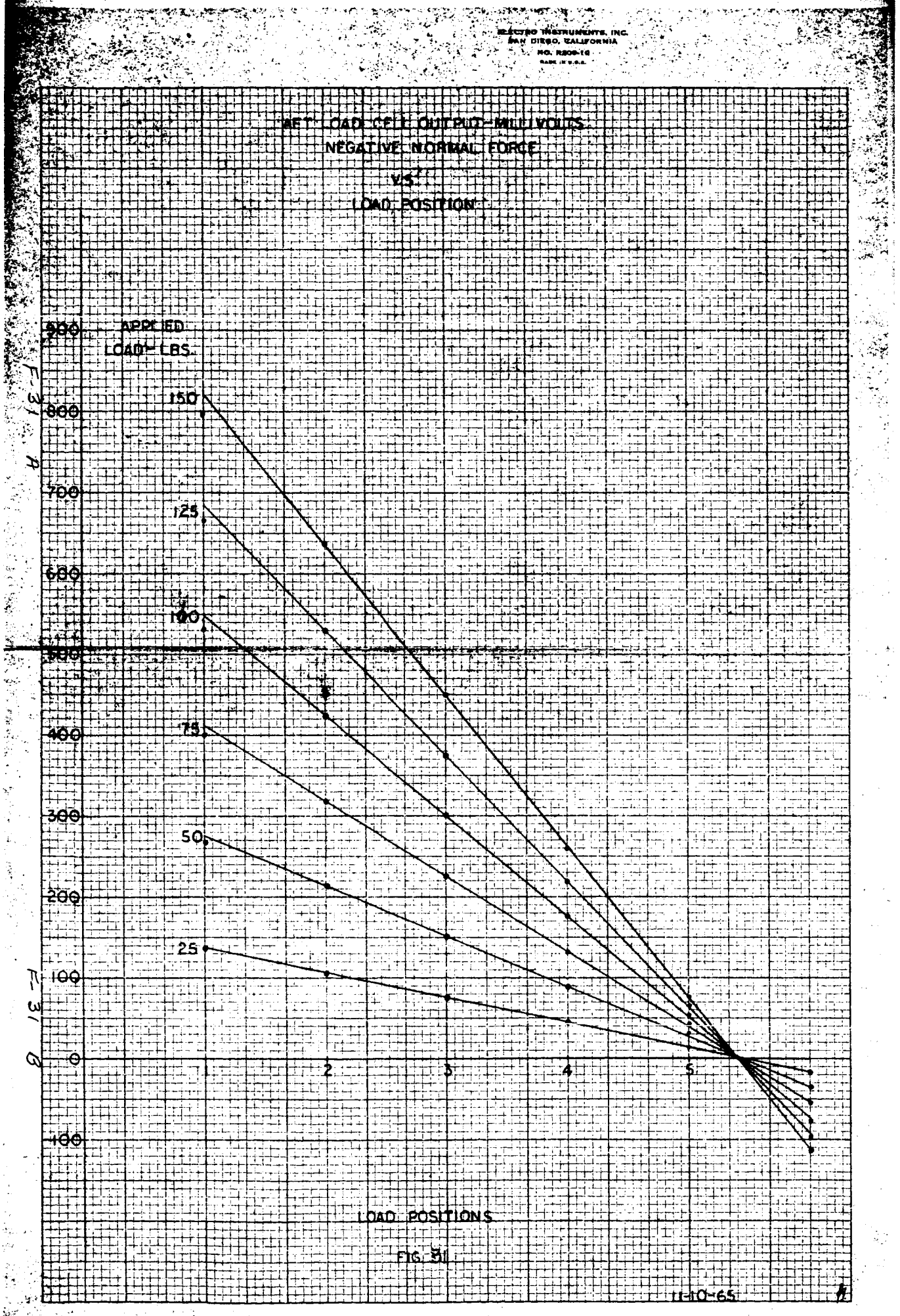

ELECTRO INSTRUMENTS, INC.
SAN DIEGO, CALIFORNIA
NO. R500-10
MADE IN U.S.A.

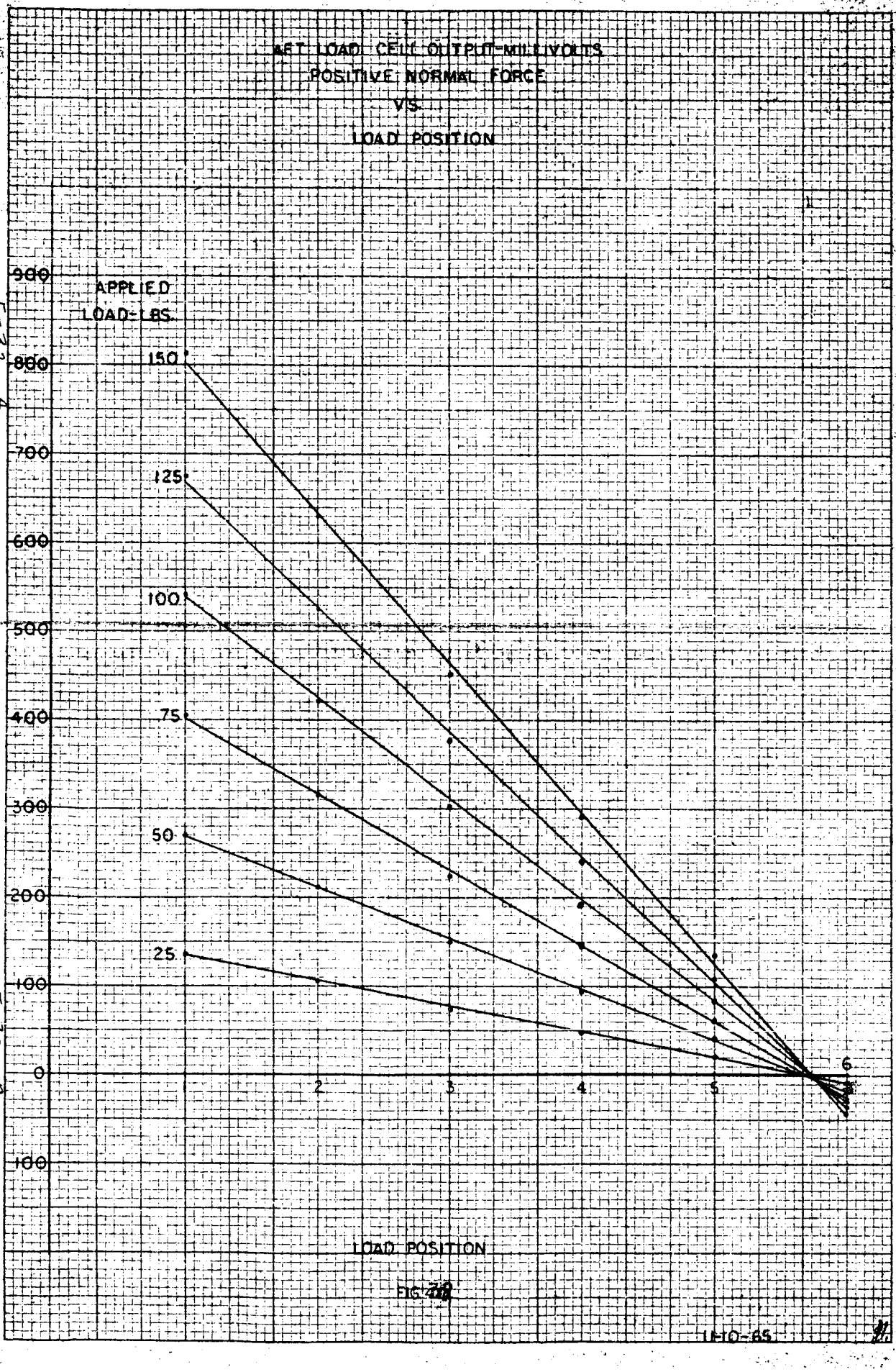

F-32 A

F-32 B

FIG 32

11-10-65

ELECTRO INSTRUMENTS, INC.
SAN DIEGO, CALIFORNIA
NO. R200-10

NET LOAD CELL OUTPUT-MILLIVOLTS
POSITIVE NORMAL FORCE
VS
LOAD POSITION

APPLIED LOAD LBS.

150
125
100
75
50
25

900
800
700
600
500
400
300
200
100
0
-100

2
3
4
5
6

LOAD POSITIONS

FIG 5D

F-33 A

F-33 B

1-10-65

ELECTRO INSTRUMENTS, INC.
SAN DIEGO, CALIFORNIA
NO. 5888-10Y
MADE IN U.S.A.

AXIAL LOAD CELL OUTPUT-MILLIVOLTS
VS.
APPLIED LOAD

330
300
270
240
210
180
150
120
90
60
30

10 20 30 40 50 60 70 80

APPLIED LOAD-LBS.

FIG. #4

11-10-65

F-34

F-34

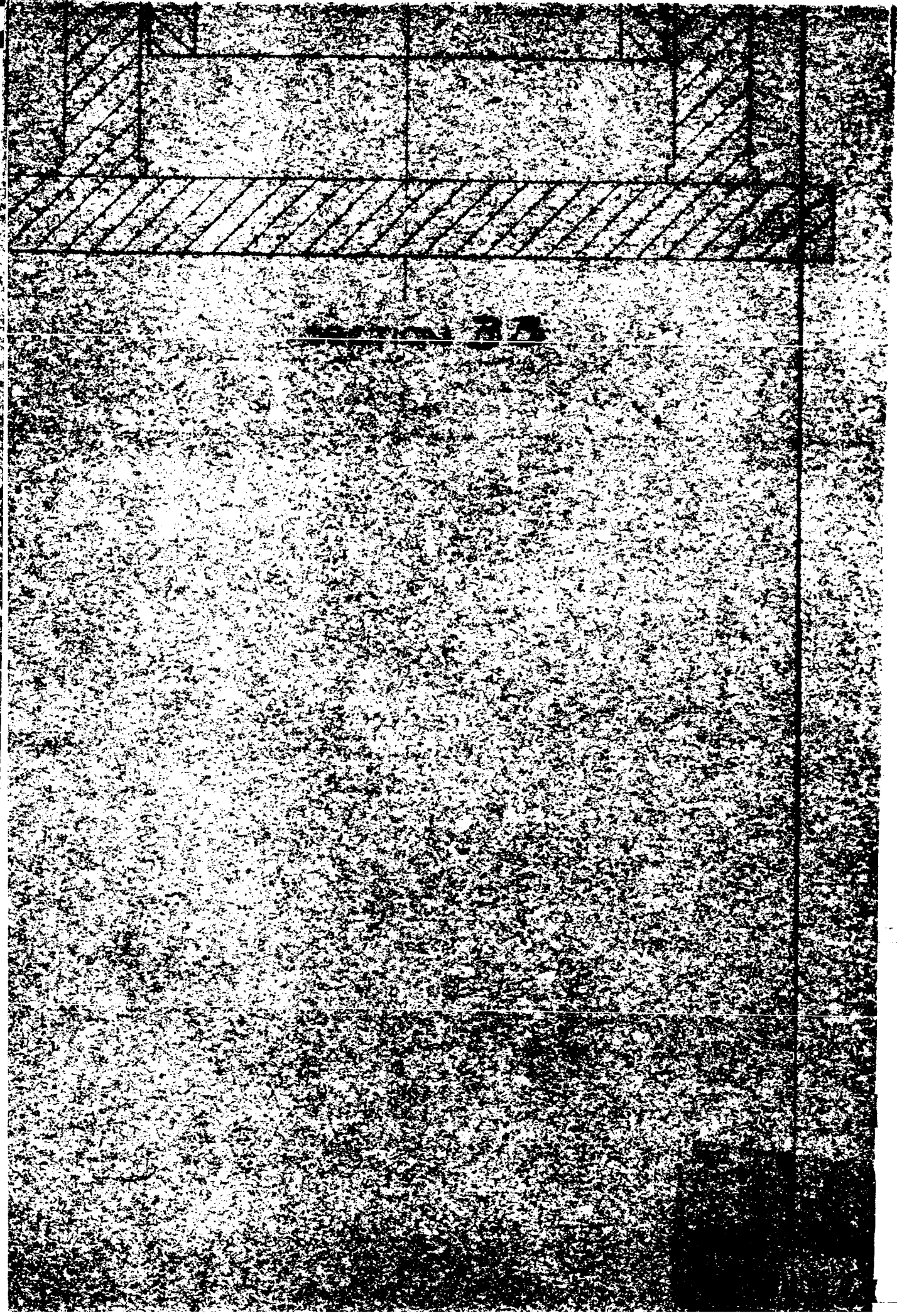

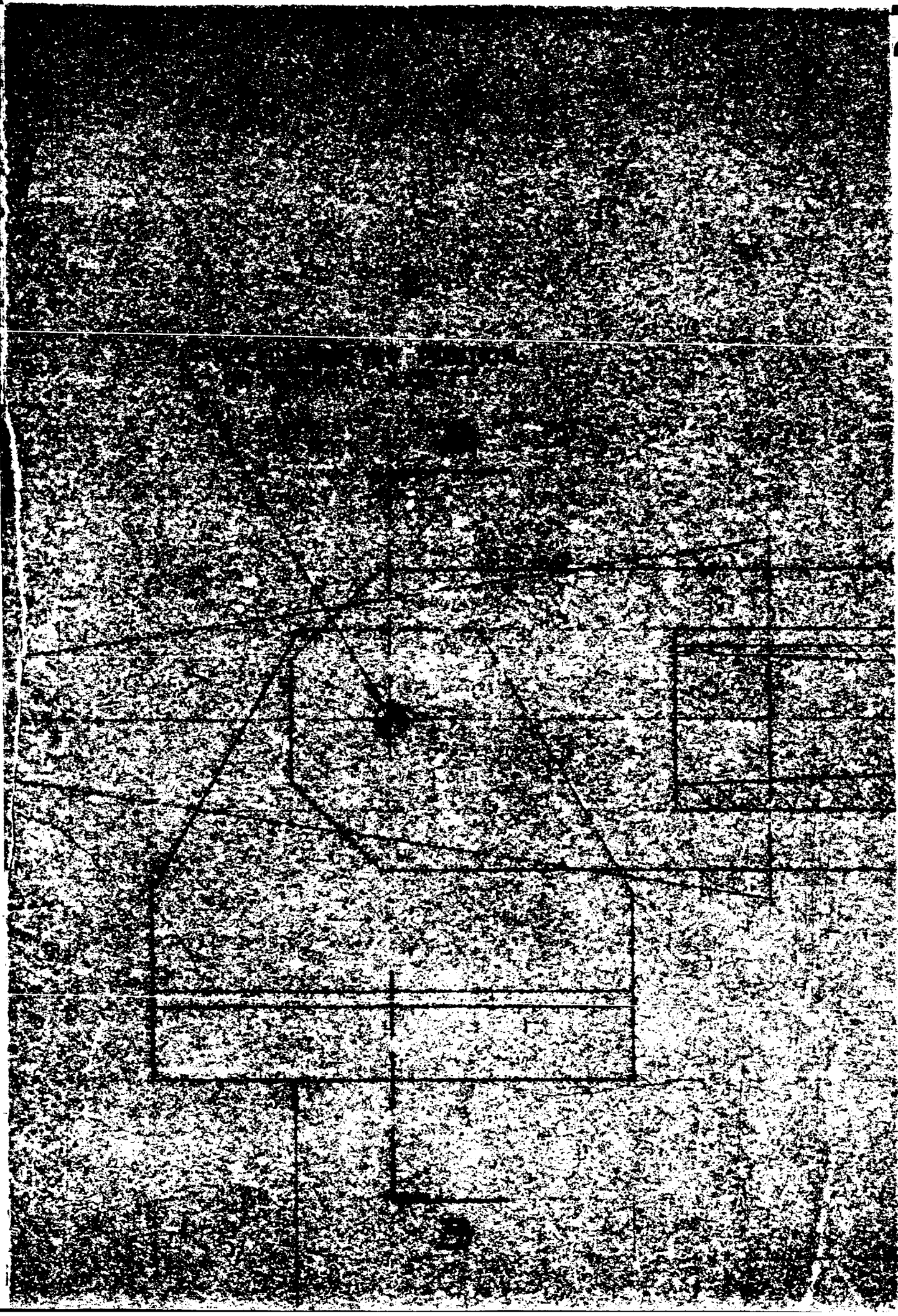

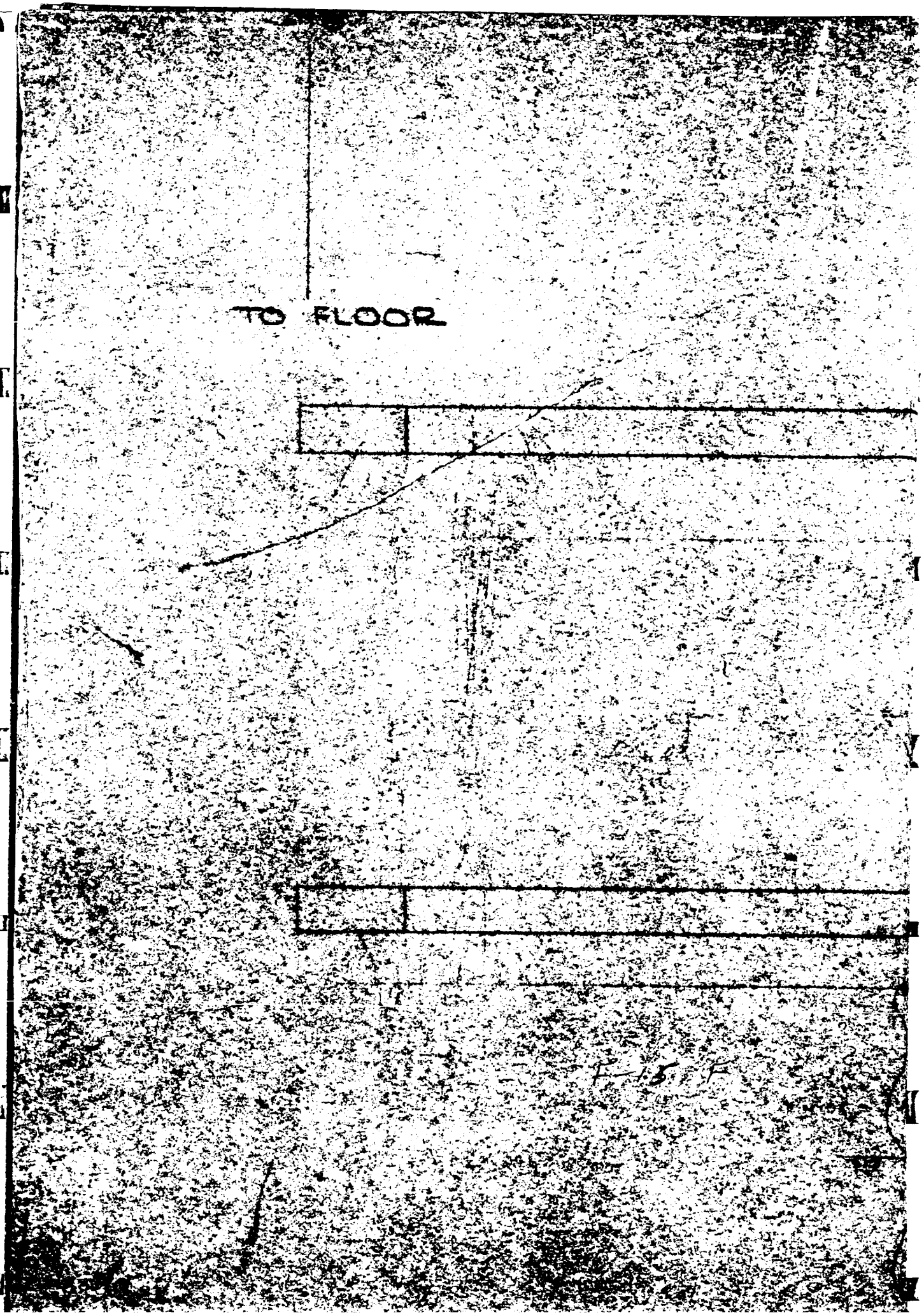
TO FLOOR

MODEL

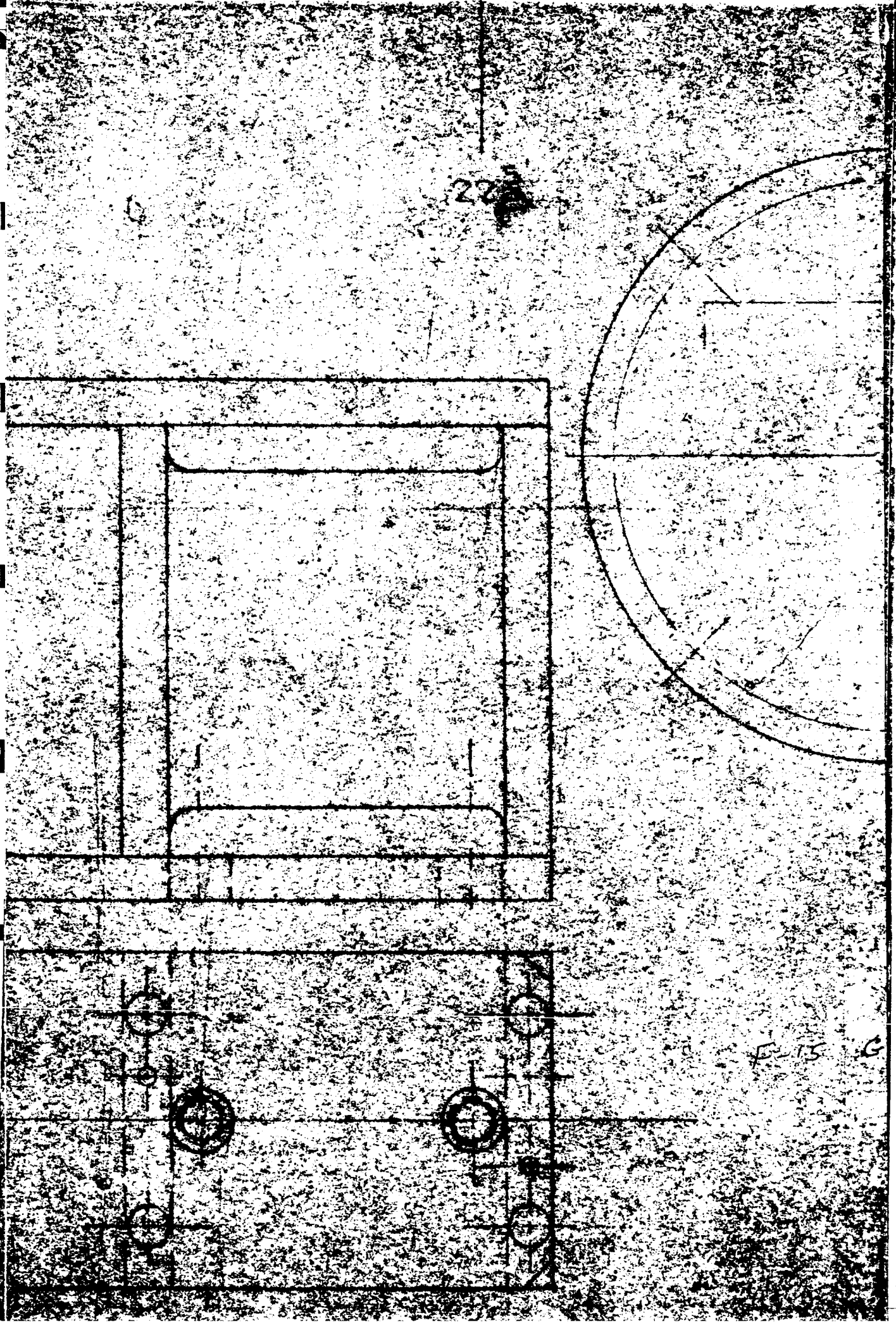
22
F-13 G

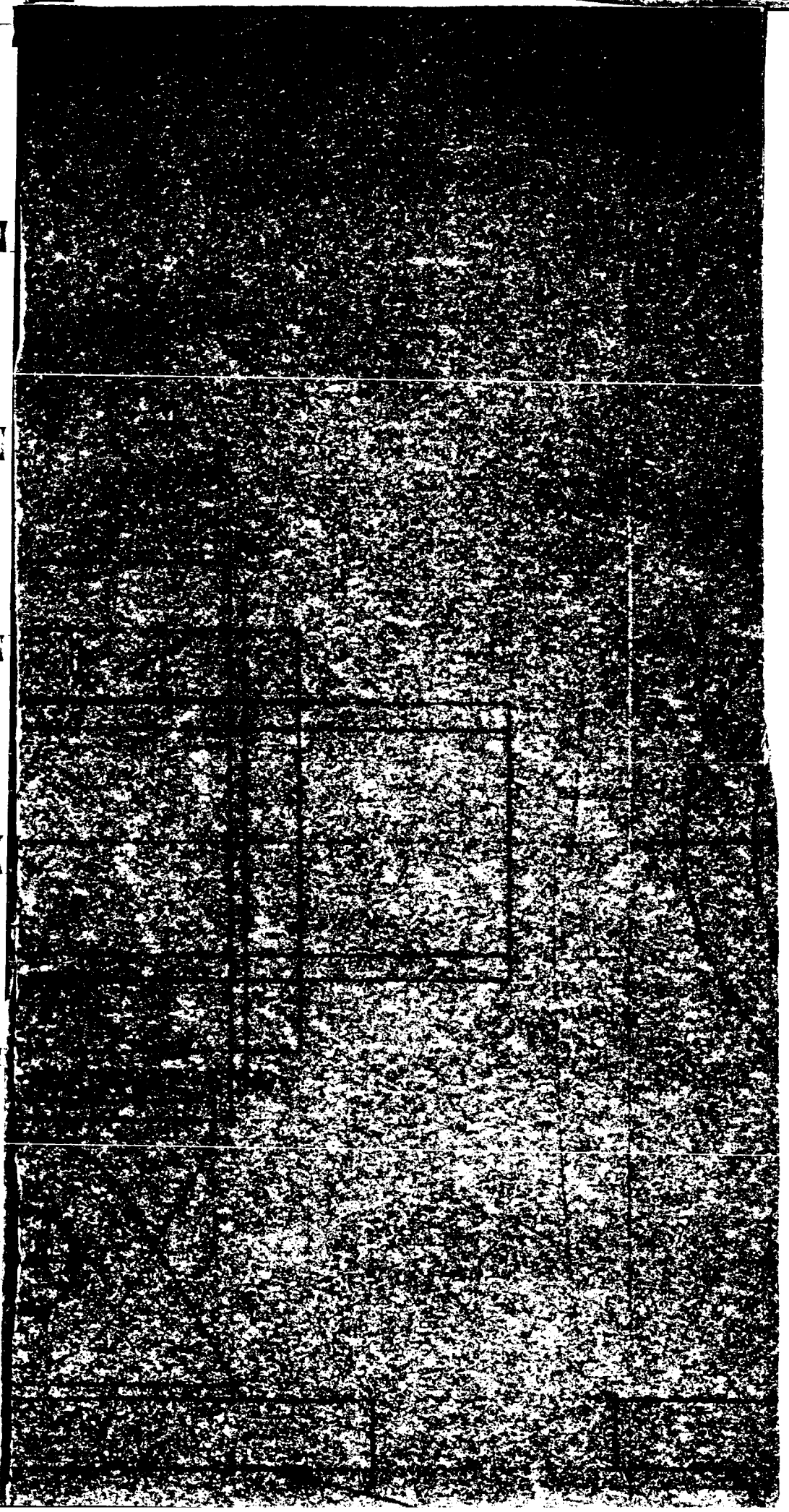

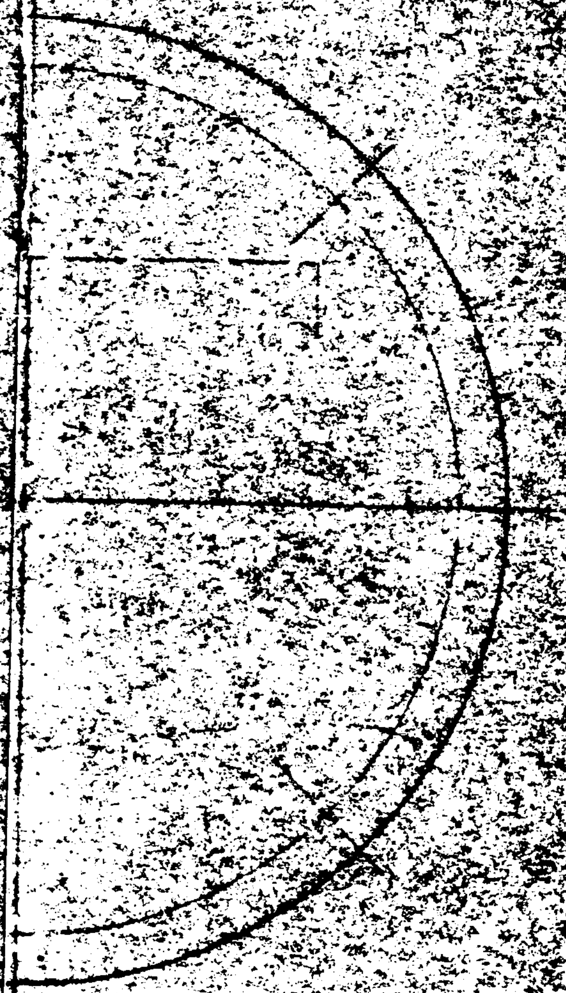

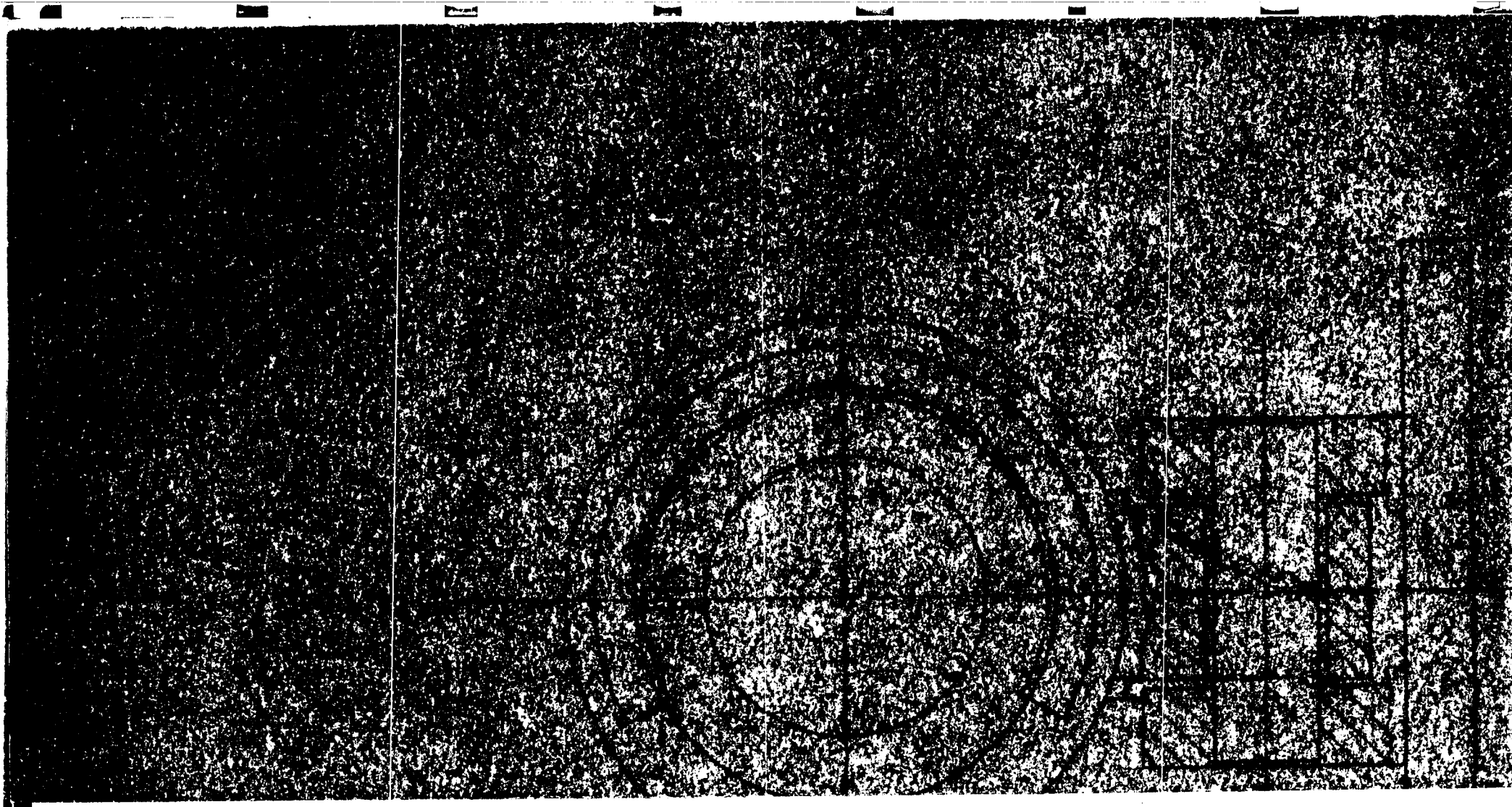

VIBRATION MOTION

VIBRATION FIXTURE

FIG. 25

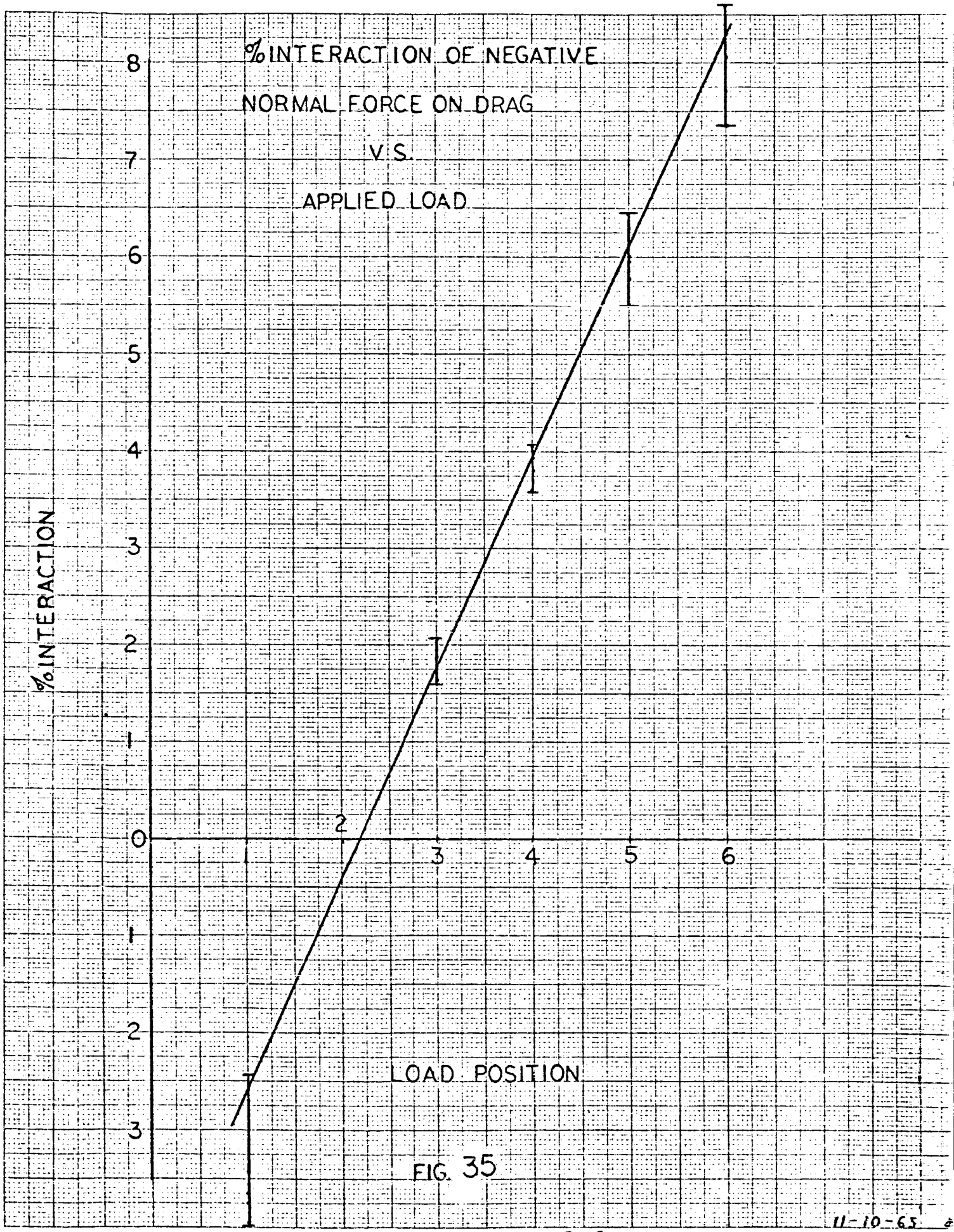

FIG. 35

11-10-65

F-35

CLEARPRINT PAPER CO. NO. C39X. MILLIMETERS. 200 BY 250 DIVISIONS
CLEARPRINT CHARTS
PRINTED IN U.S.A. ON CLEARPRINT TECHNICAL PAPER NO. 1015

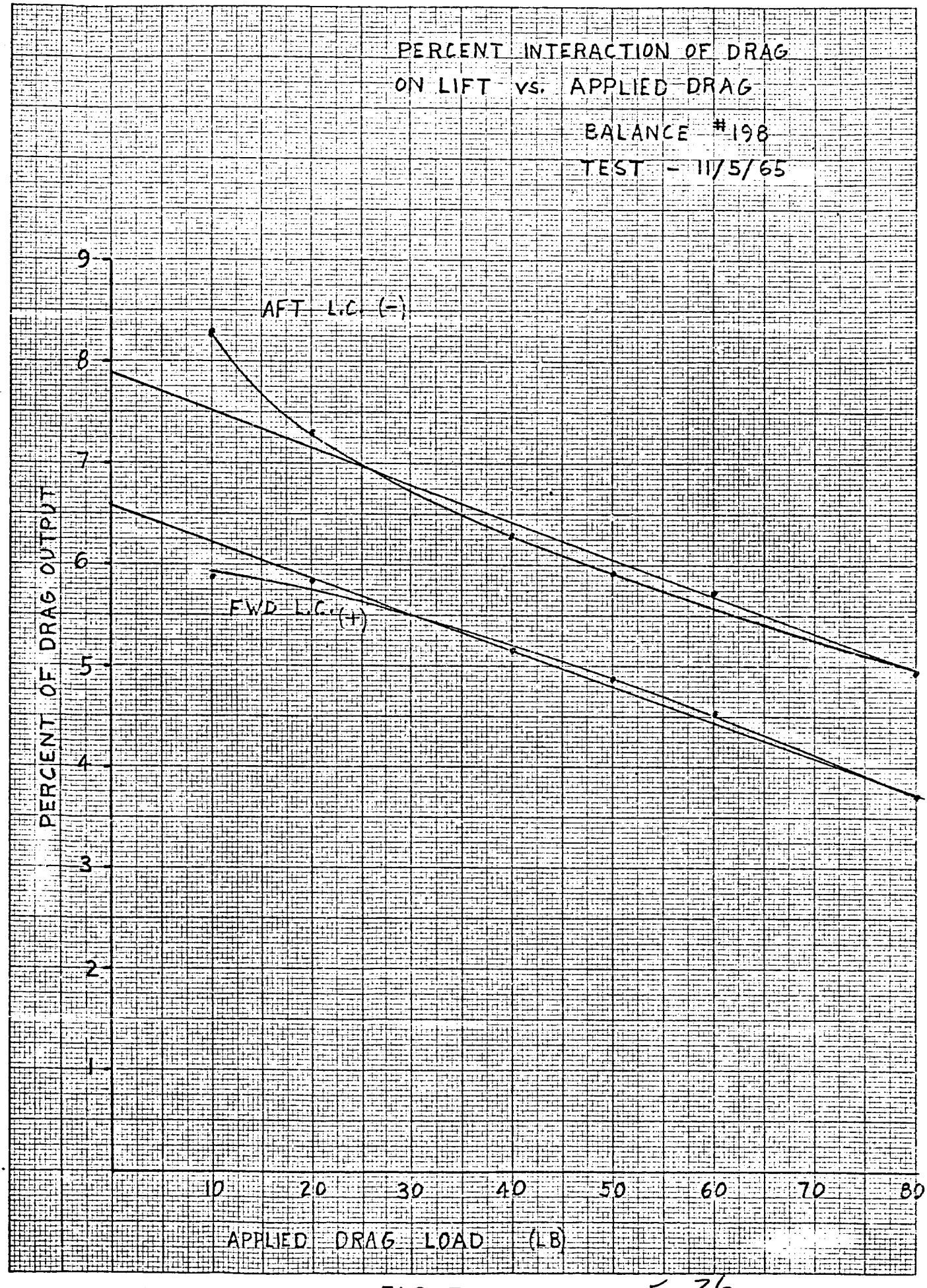

FIG. 36

F-36

10 X 10 TO THE CEN ETER 46 1512
18 X 25 CM. MADE IN U.S.A.
KEUFFEL & ESSER CO.

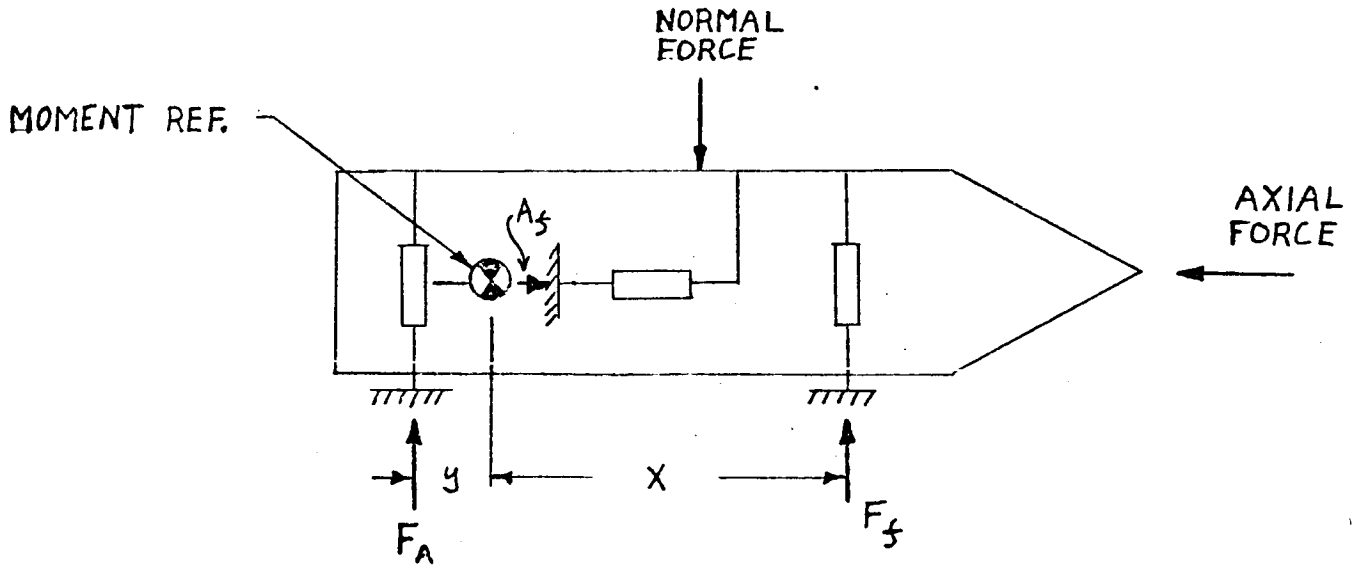

FORCE AND MOMENT EQUATIONS:

$$F_{AX} = \frac{A_f}{C_{AX}} - K_{NI} F_N \qquad (1)$$

$$F_N = \frac{F_A - K_{AI} A_f}{C_A} + \frac{F_f - K_{fI} A_f}{C_f} \qquad (2)$$

$$M_P = \left[\frac{F_A - K_{AI} A_f}{C_A}\right] y - \left[\frac{F_f - K_{fI} A_f}{C_f}\right] x \qquad (3)$$

NOTATION IS DESCRIBED IN THE TEXT.

Figure 37

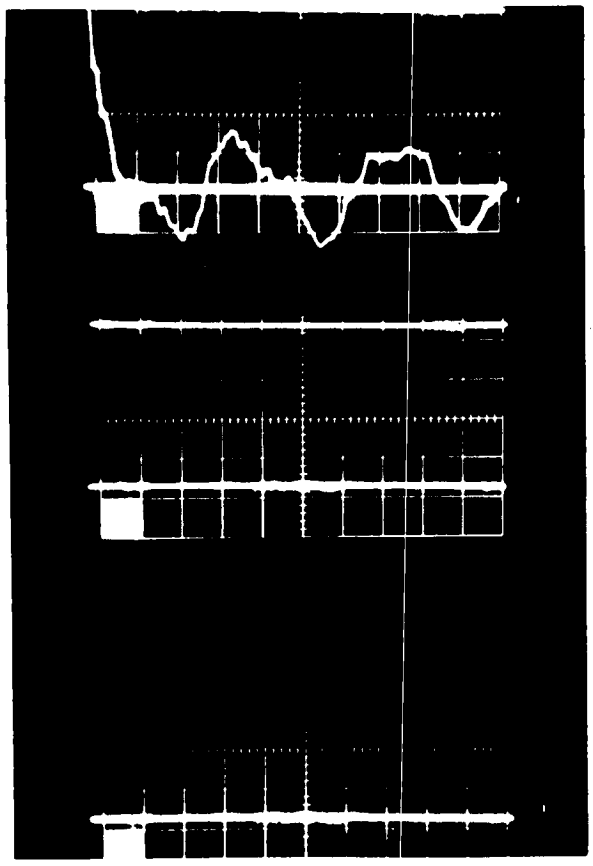

a.

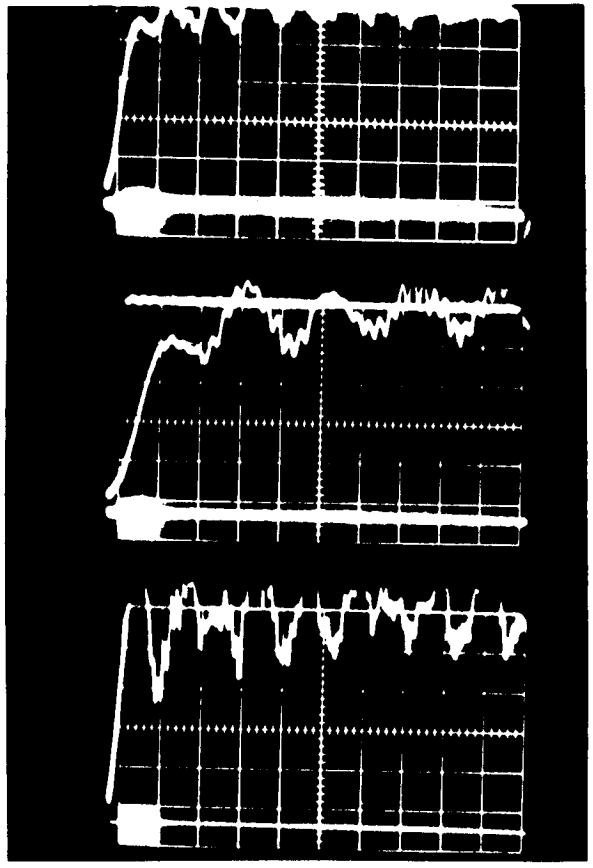

b.

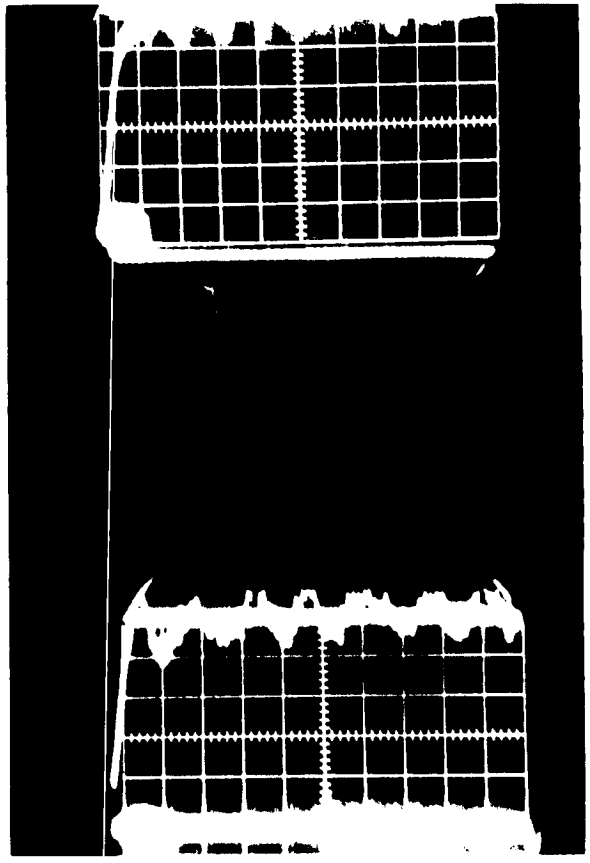

c.

Figure 38 - a,b,& c - Balance 198

quartz force transducers

Small size, high capacity and high rigidity characterize quartz load cells, load washers and force links. Specifications for Series 900 load washers and Series 930 force links are those of Models 902 and 932, respectively, except for specific differences tabulated below main chart.

TYPICAL MODELS	912  HIGH SENSITIVITY	912H  IMPACT FORCE	902  LOAD WASHER	932  FORCE LINK
Range, compression ..... to lbs.	5000	5000	8000	4000
Range, tension ..... to lbs.	500	500	(to preload)	2000
Resolution ..... lb.	0.002	0.002	0.01	0.01
Overload ..... %	20	20	10	10
Sensitivity (nominal) ..... pCb/lb.	50	50	10	10
Frequency response (flat within ±5%) .. near DC to	10KC	10KC	8KC	5KC
Resonant frequency (nominal) (no load) ..... KC	70	70	50	35
Rigidity ..... in./lb.	20×10^{-8}	20×10^{-8}	6×10^{-8}	12×10^{-8}
Rise time ..... μ sec.	10	10	15	20
Linearity ..... %	1	1	1	1
Repeatability and hysteresis ..... %	0.5	0.5	0.5	0.5
Eccentric loading error* ..... %	4	4	4	5
Capacitance (nominal) ..... pf	60	60	90	90
Insulation resistance (minimum) ..... ohms	10^{13}	10^{13}	10^{12}	10^{12}
Temperature sensitivity ..... %/°F	0.01	0.01	0.01	0.01
Temperature range ..... °F	−400/ +500	−400/ +500	−400/ +500	−320/ +500
Side force (maximum) ..... lbs.	100	100	20% range	20% range
Shock and vibration ..... g's	10,000	10,000	10,000	5,000
Cable connector, side coaxial, teflon insulation	10-32	10-32	10-32	10-32
Mounting holes, 10-32 thread, internal ..... in.	1/8	1/8	—	3/8-24
Mounting studs, 10-32 Be-Cu (supplied) ..... in.	0.28	0.28	—	—
Case materials ..... S. S.	416, 17-4ph	416, 17-4ph	S. S.	S. S.
Size (load washer ID x OD x Thk) ..... in.	.62hex x .5	.62hex x .5	.41 x .87 x .39	.87 x 1.62
Weight (approximate) ..... oz.	0.6	0.7	0.7	3.3
Price ..... $	290.00	300.00	240.00	280.00

Max. sensitivity change, load applied one side (halfway between inner and outer edges of supporting surface).

LOAD WASHERS, MODEL	901	903	904	905	906	907
Range ..... lbs.	3500	12,000	20,000	30,000	45,000	90,000
Rigidity ..... in./lb.	15×10^{-8}	4×10^{-8}	2.5×10^{-8}	1.5×10^{-8}	1×10^{-8}	$.5 \times 10^{-8}$
Size (ID/OD/Thk) ... in.	.26/.55/.39	.51/1.1/.43	.67/1.34/.47	.83/1.58/.51	1.04/2.05/.59	1.6/2.96/.67
Weight ..... oz.	0.3	1.3	2	3	6	12
Price ..... $	240.00	280.00	320.00	380.00	480.00	580.00

FORCE LINKS, MODEL	931	933	934	935	936	937
Range, tension ..... lbs.	1000	4000	7000	10,000	15,000	25,000
Range, compression . lbs.	1500	6000	10,000	15,000	25,000	45,000
Rigidity ..... in./lb.	30×10^{-8}	9×10^{-8}	7×10^{-8}	5.5×10^{-8}	4×10^{-8}	2.5×10^{-8}
Size (OD x Height) ... in.	.55 x 1.25	1.1 x 2	1.34 x 2.5	1.58 x 3	2.05 x 3.5	2.96 x 4.25
Mounting thread ..... NF	1/4-28	1/2-20	5/8-18	3/4-16	1-14	1 1/4-12
Weight ..... oz.	1.1	7	13	25	50	100
Price ..... $	280.00	340.00	380.00	460.00	580.00	680.00

KISTLER INSTRUMENT CORPORATION: 8989 SHERIDAN DR., CLARENCE, N.Y. 14031

KISTLER

advanced dynamic instrumentation

F-39

160165

FIG 39

PRELIMINARY SHOULDER SCREW

BAL # 199

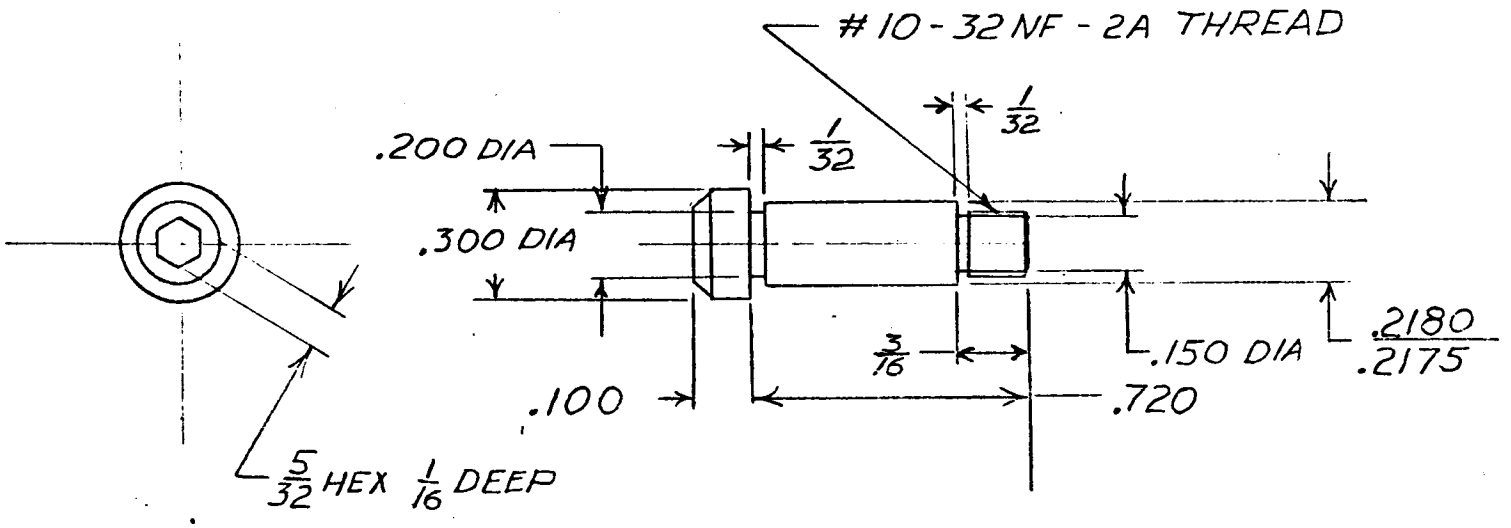

FIG 40

F-40

F-41 B

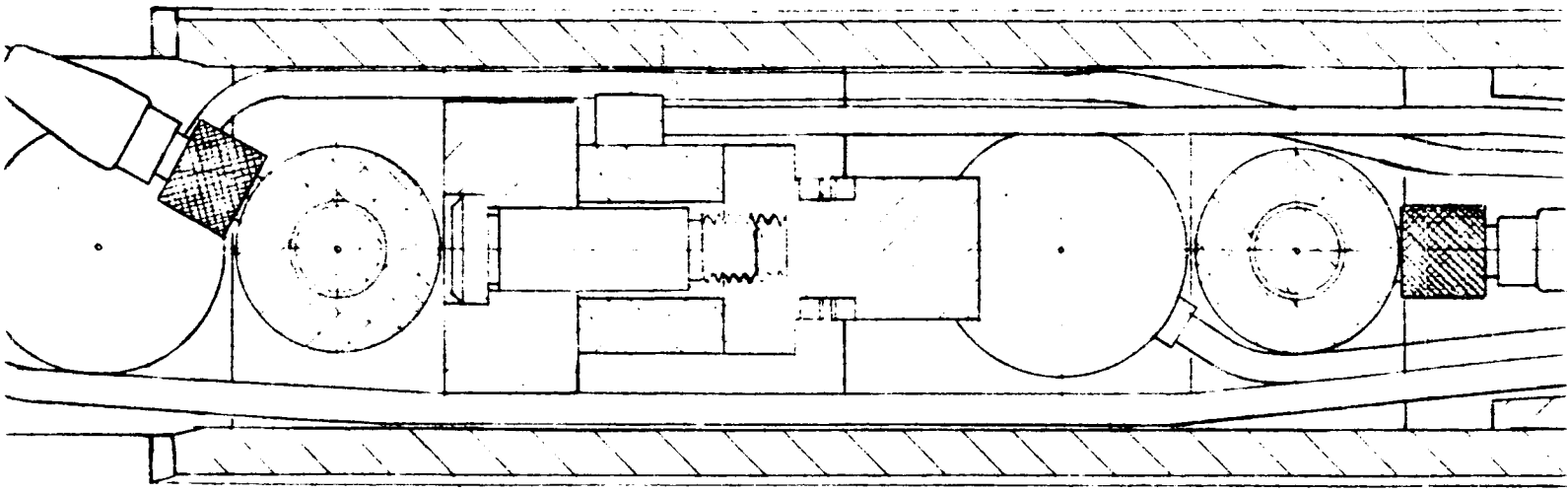

SECTION A-A

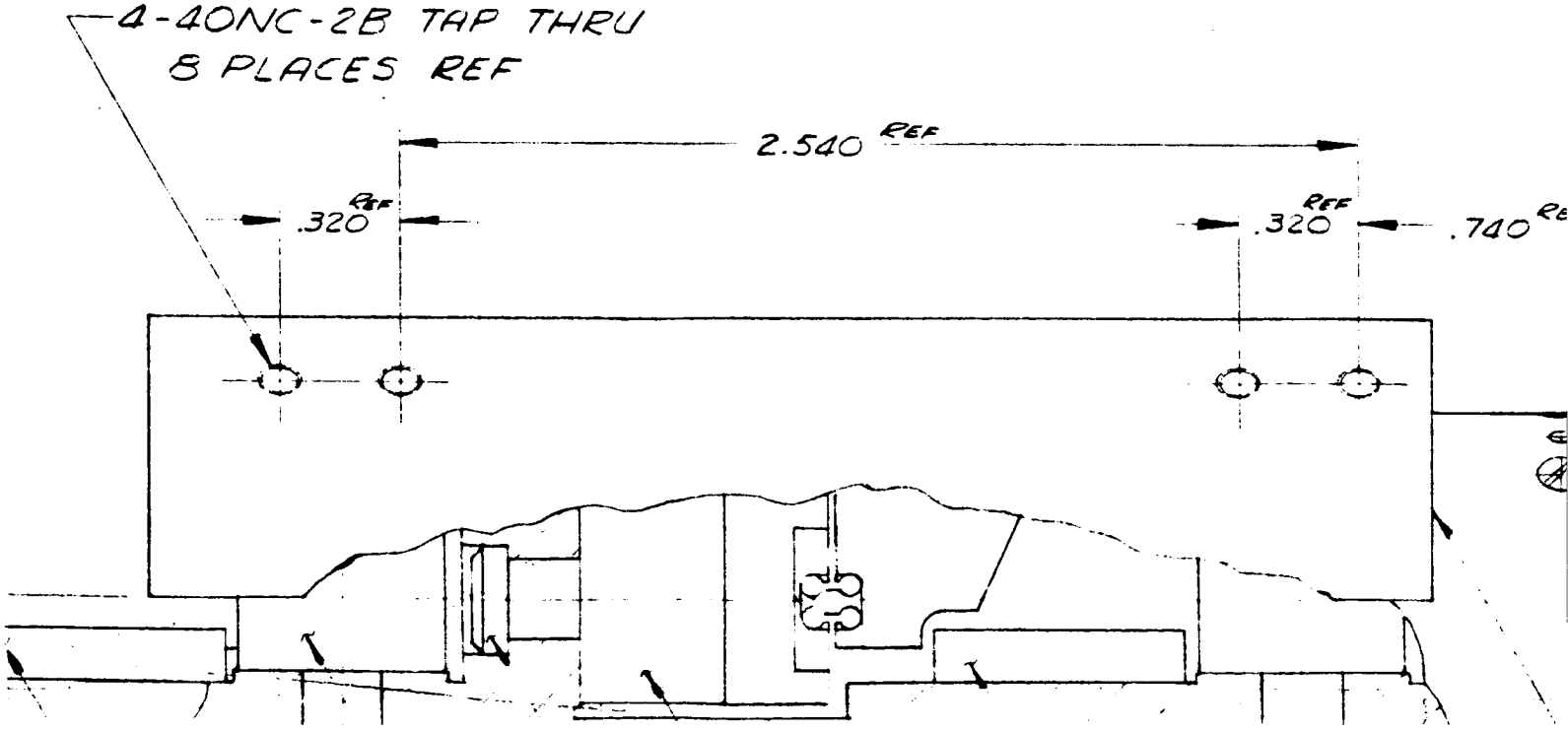

NOTES

<1> PURCHASED FROM GULTON IN.
METUCHEN, NEW JERSEY

<2> PURCHASED FROM KISTLER IN:
8989 SHERIDAN DR. CLARENCE

<3> PURCHASED FROM MICRODOT,
5960 W. BOWCROFT ST, LOS AN.

4-

F-41 B

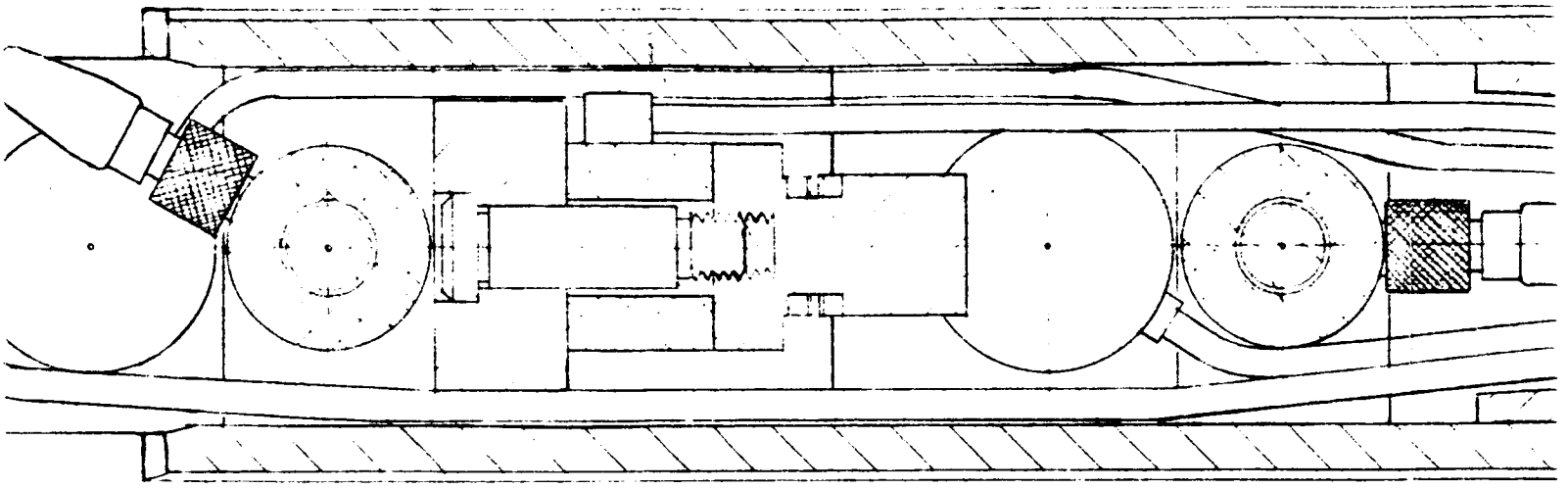

SECTION A-A

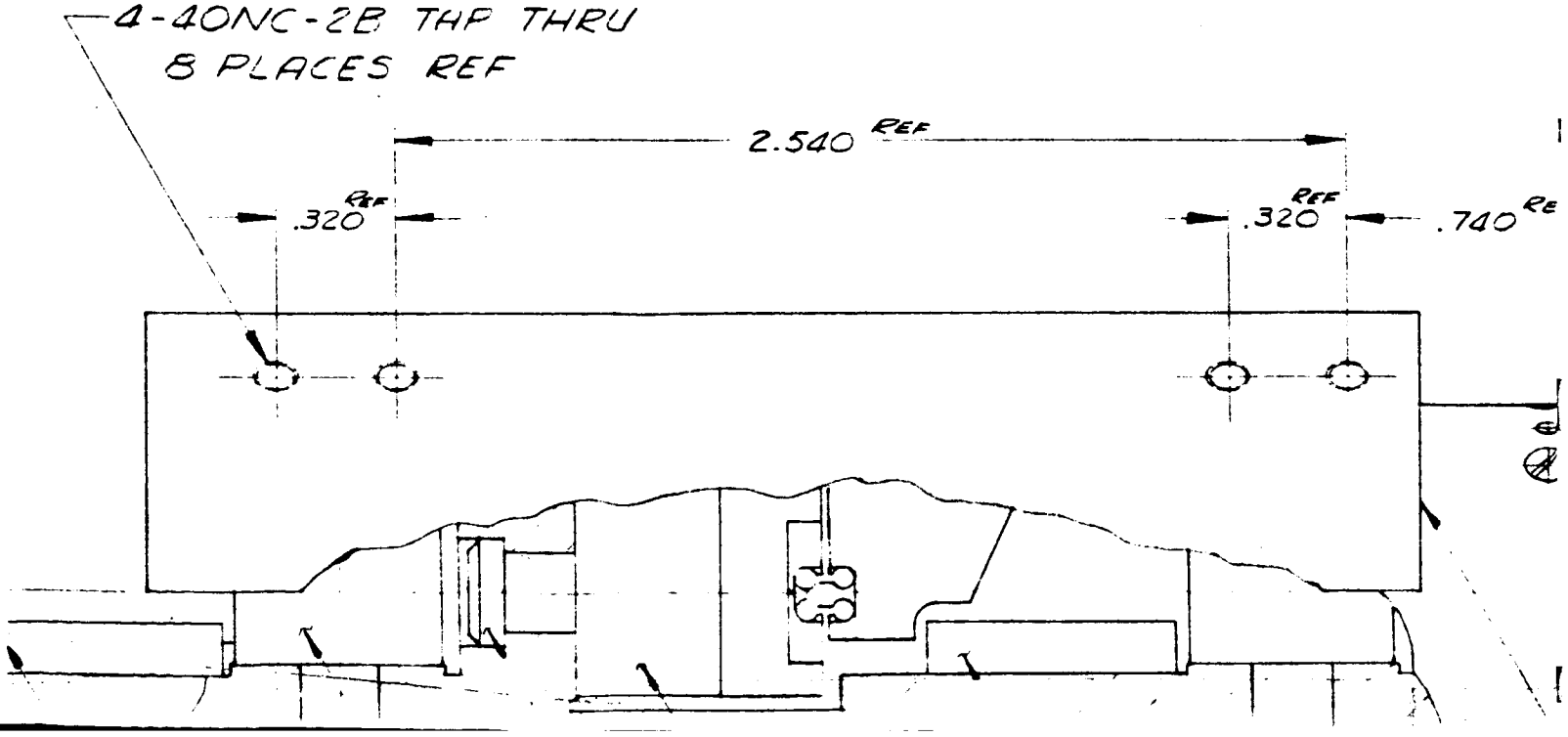

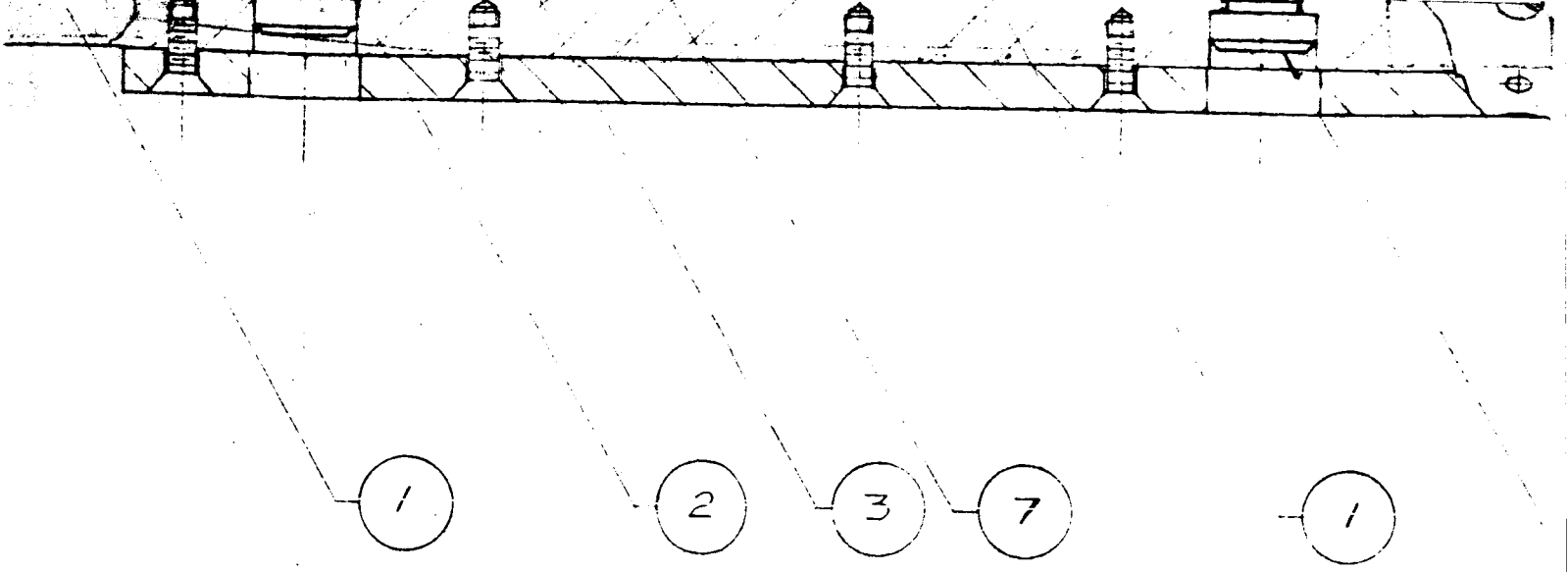

USTRIES, INC.

TRUMENT CORP.
N. Y.

YC.
TLES, CAL.

F-41 C

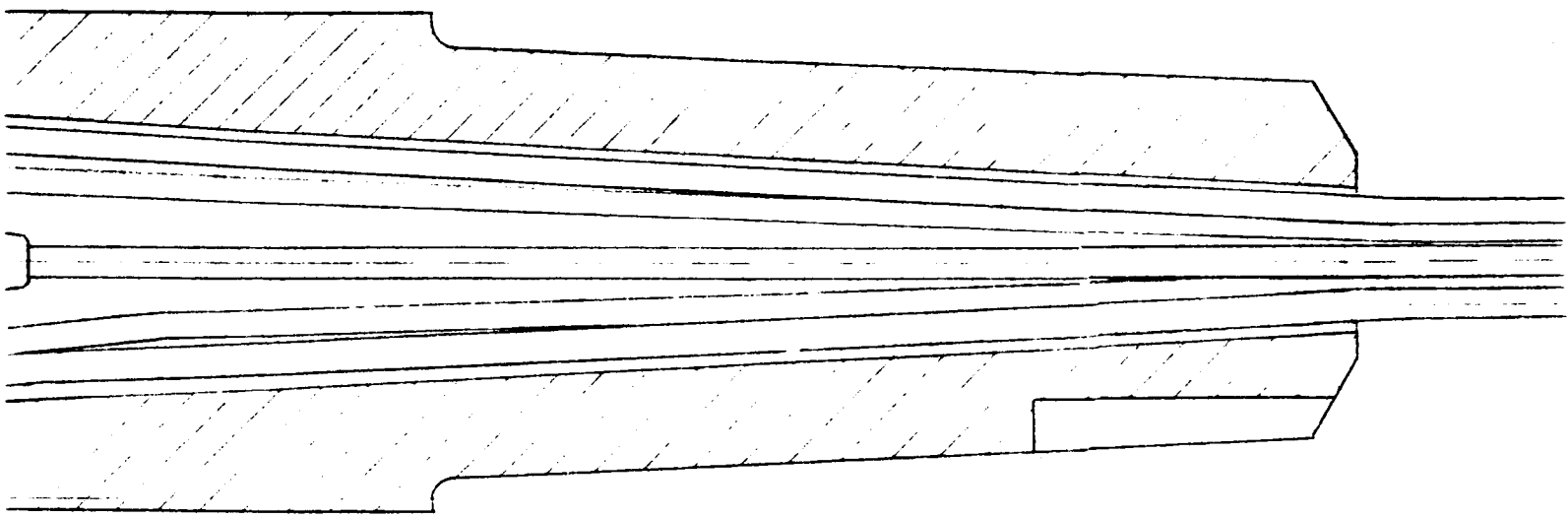

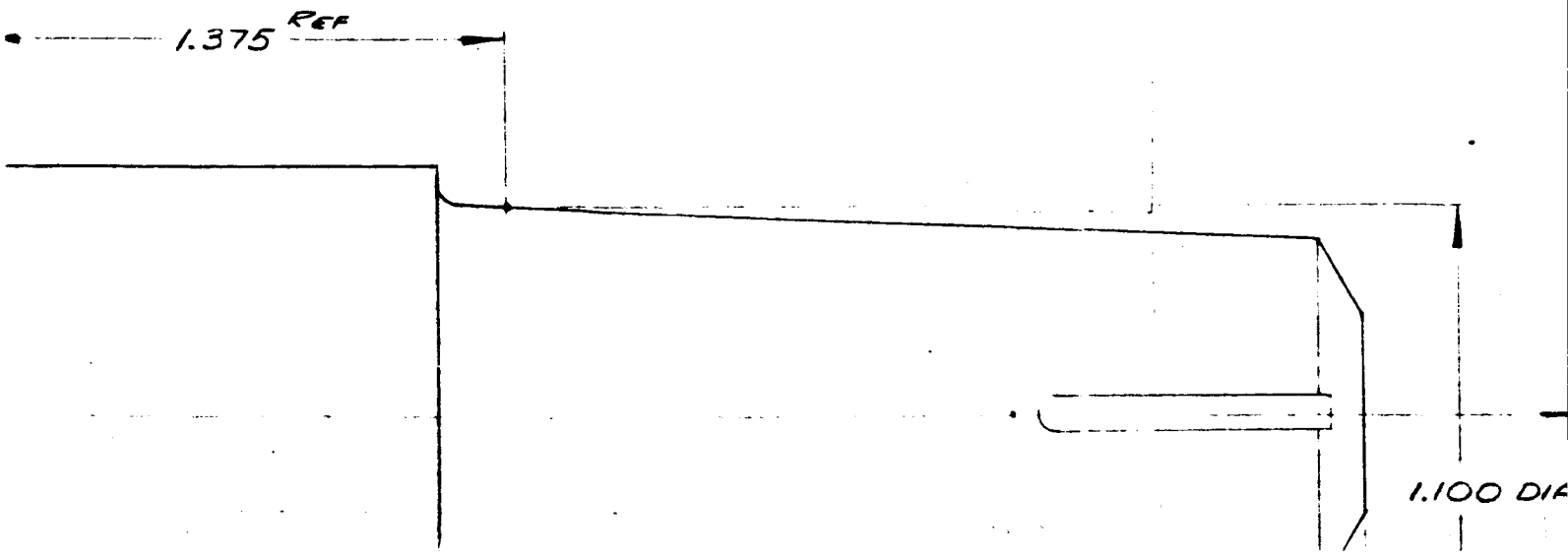

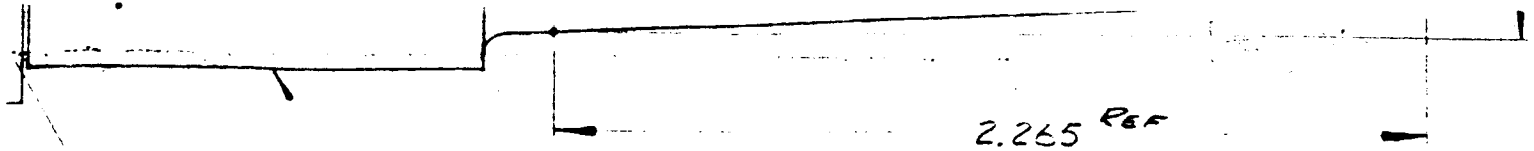

4 5 6

ITEM NO.	
9	CONNEC
8	CABLE-
7	LOAD
6	BALANC
5	SADDL
4	SHOUL
3	SHOUL
2	LC
1	AC

SEE ENGINEERING RECORDS	
NEXT ASSY	USED ON
APPLICATION	

UNLESS OTHERWISE SPECIFIED

DIMENSIONS ARE IN INCHES

TOLERANCES ON FRACTIONS ____ DECIMALS ____ ANGLES ____

MATERIAL ____

HEAT TREATMENT ____

FINAL PROTECTIVE FINISH ____

D.	M F	REVISIONS				
		ZONE	SYM	DESCRIPTION	DATE	APPROVAL

F-41 D

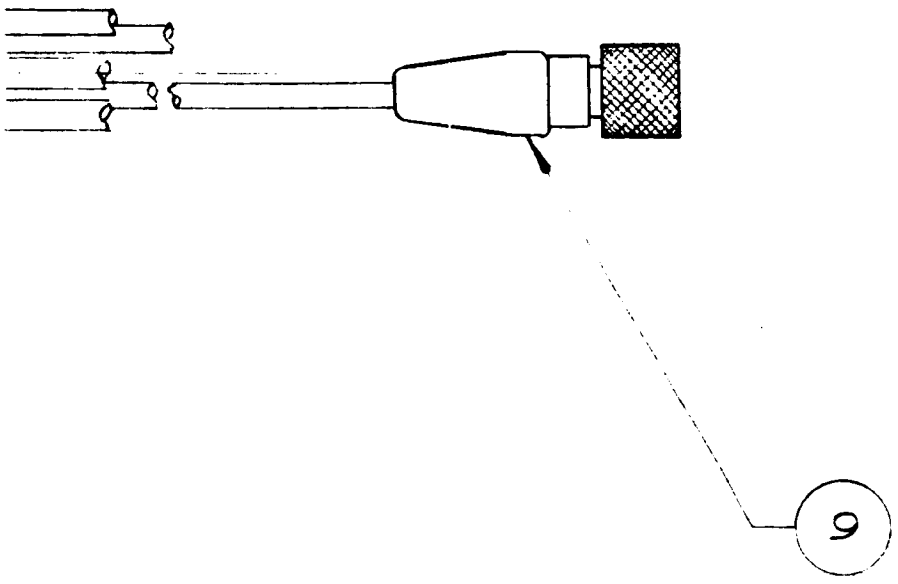

DESCRIPTION	NO. REQ'D	PART NO. / DWG NO.	MATERIAL	REMARKS
2 - MINIATURE	7	32-21		◁3
TLDED	2	121M5 OR EQUIV.		◁2
SHER	1	901M1101		◁2
ISE ASSY.	1	80M41665		
ASSY	1	80M41664		
SCREW	2	80M21179-1		
SCREW	1	80M21179-2		
WASHER	2	901		◁2
ROMETER	2	AA310502		◁1

LIST OF MATERIAL

DISTR CODE

IGINAL DATE DRAWING	23 SEPT. 65
F. LOUGHEAD / FTSMAN	CHECKER
CKER	STRESS
INEER	ENGINEER
IMITTED	
ROVED	
DIRECTOR	

FINAL ASSY. — BALANCE 199

WEIGHT CHECKER	DATE	CODE
SCALE 2-1	UNIT WEIGHT	

GEORGE C. MARSHALL SPACE FLIGHT CENTER
NATIONAL AERONAUTICS AND SPACE ADMINISTRATION
HUNTSVILLE, ALABAMA

DWG SIZE D — 80M41670

SHEET 1 OF 1

F-41 H FIG. 41

E-42

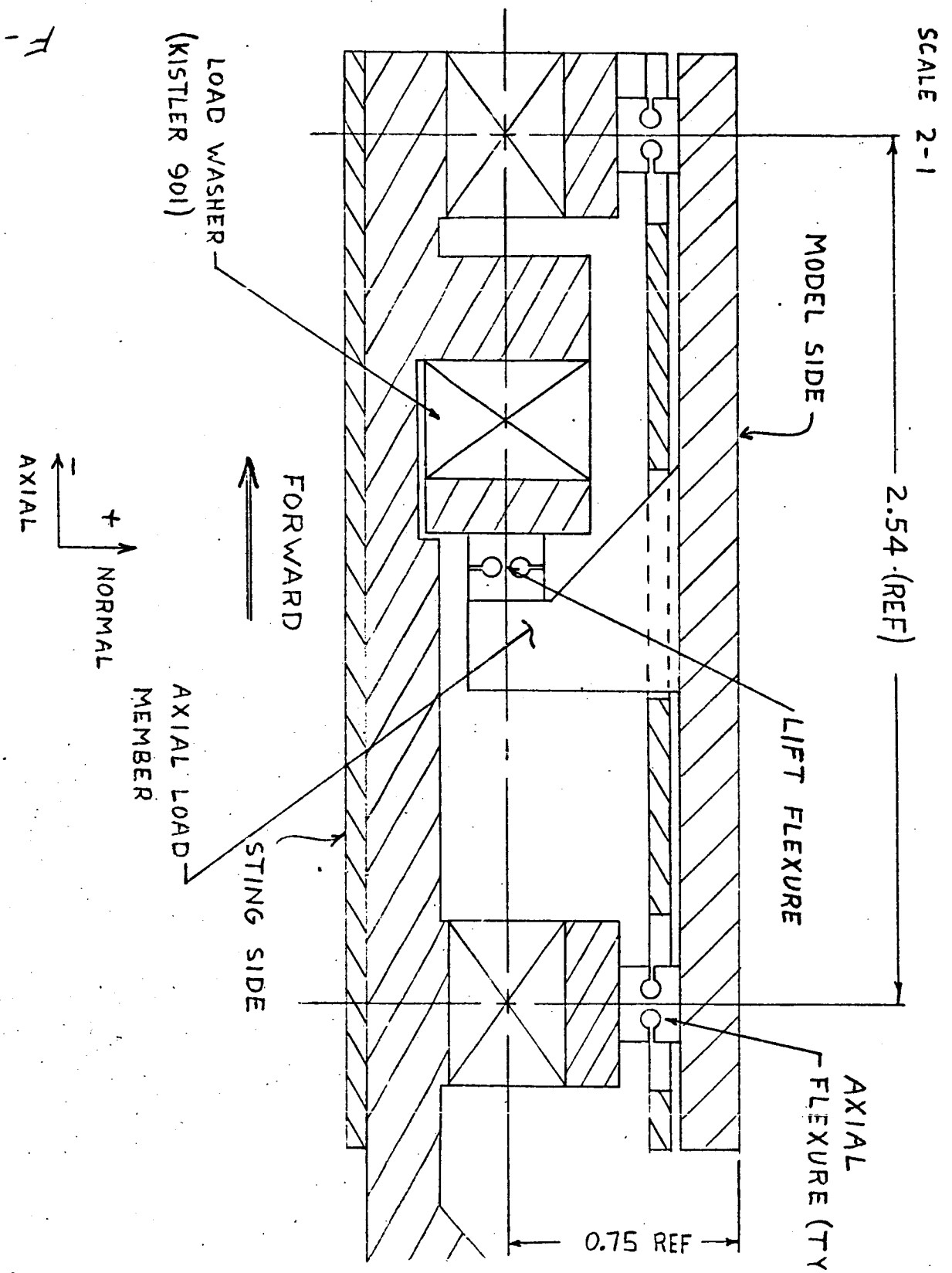

SIDE VIEW - BALANCE ASSEMBLY

FIG. 42

Notice — When Government drawings, specifications, or other data are used for any purpose other than in connection with a definitely related Government procurement operation, the United States Government thereby incurs no responsibility nor any obligation whatsoever; and the fact that the Government may have formulated, furnished, or in any way supplied the said drawings, specifications or other data is not to be regarded by implication or otherwise as in any manner licensing the holder or any other person or corporation, or conveying any rights or permission to manufacture, use, or sell any patented invention that may in any way be related thereto.

PART No.	MF	REVISIONS				
		ZONE	SYM	DESCRIPTION	DATE	APPROVAL

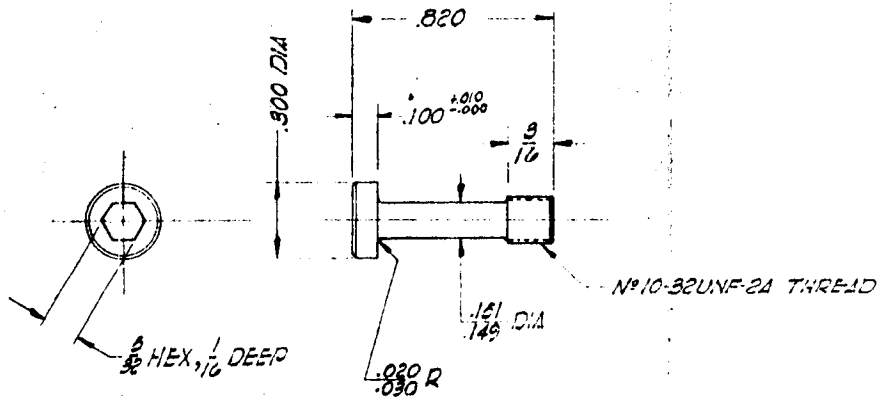

GENERAL NOTES

1. REMOVE BURRS & BREAK SHARP EDGES .010 R. MAX.
2. 63 ALL OVER

DISTR CODE

		UNLESS OTHERWISE SPECIFIED	ORIGINAL DATE OF DRAWING 4 JAN 66	SHOULDER SCREW BALANCE Nº 199	GEORGE C. MARSHALL SPACE FLIGHT CENTER
		DIMENSIONS ARE IN INCHES	DRAFTSMAN WEEKS / CHECKER		NATIONAL AERONAUTICS AND SPACE ADMINISTRATION
SEE ENGINEERING RECORDS		TOLERANCES ON FRACTIONS ±1/64 DECIMALS ±.004 ANGLES ±1°	CHECKER / STRESS		HUNTSVILLE, ALABAMA
			ENGINEER / ENGINEER		
		MATERIAL BERYLLIUM COPPER	SUBMITTED		DWG SIZE B 80M21179
NEXT ASSY	USED ON	HEAT TREATMENT	APPROVED		
APPLICATION		FINAL PROTECTIVE FINISH	DIRECTOR	WEIGHT CHECKER / DATE / CODE	SHEET 1 OF 1
				SCALE 2=1 / UNIT WEIGHT	

F-43-A F-43-B F-43 2 FIG.43

E. — WHEN GOVERNMENT DRAWINGS, SPECIFICATIONS, OR OTHER DATA
ED FOR ANY PURPOSE OTHER THAN IN CONNECTION WITH A DEFINITELY
D GOVERNMENT PROCUREMENT OPERATION, THE UNITED STATES GOVERN-
HEREBY INCURS NO RESPONSIBILITY NOR ANY OBLIGATION WHATSOEVER;
E FACT THAT THE GOVERNMENT MAY HAVE FORMULATED, FURNISHED, OR
WAY SUPPLIED THE SAID DRAWINGS, SPECIFICATIONS OR OTHER DATA IS
BE REGARDED BY IMPLICATION OR OTHERWISE AS IN ANY MANNER
NG THE HOLDER OR ANY OTHER PERSON OR CORPORATION, OR CONVEY-
Y RIGHTS OR PERMISSION TO MANUFACTURE, USE, OR SELL ANY
ED INVENTION THAT MAY IN ANY WAY BE RELATED THERETO.

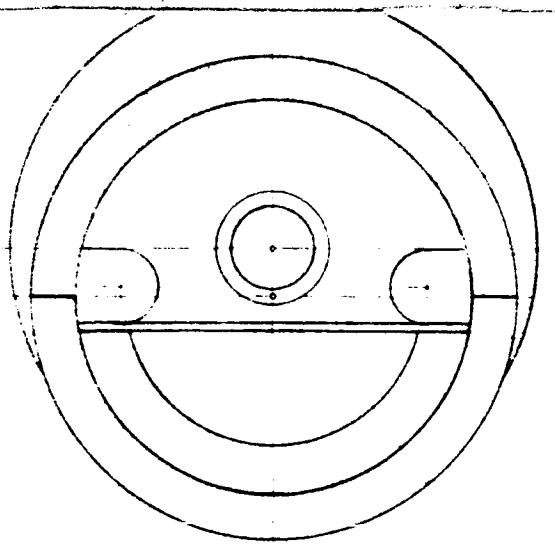

NOTES:

1. FURNISH PART C

2- GRIND ITEM
OF ITEM NO

F-

A

F-44 B

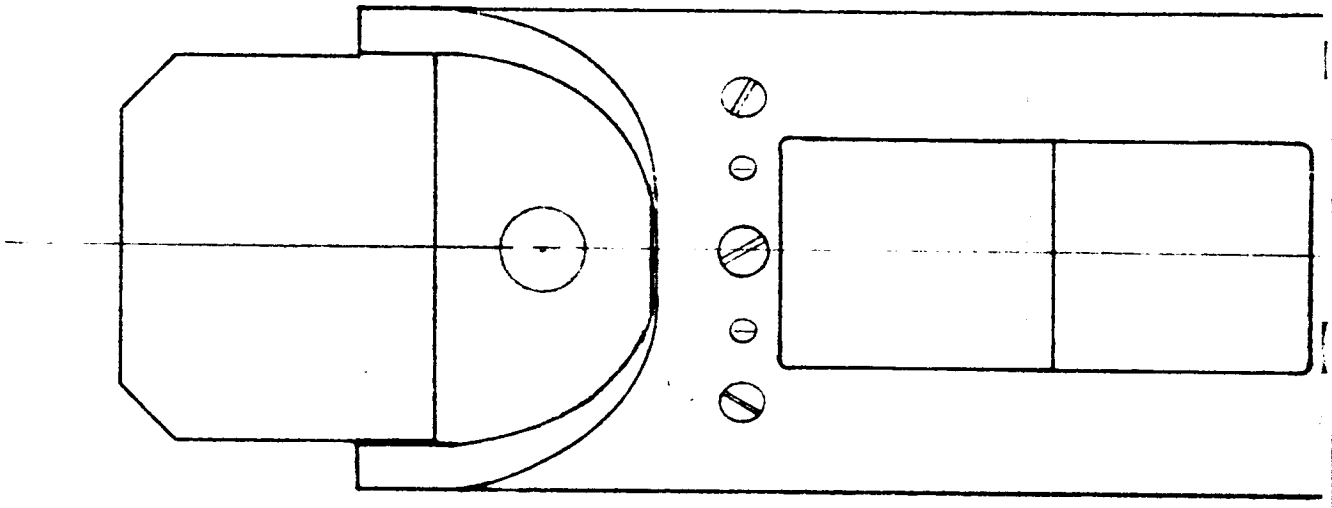

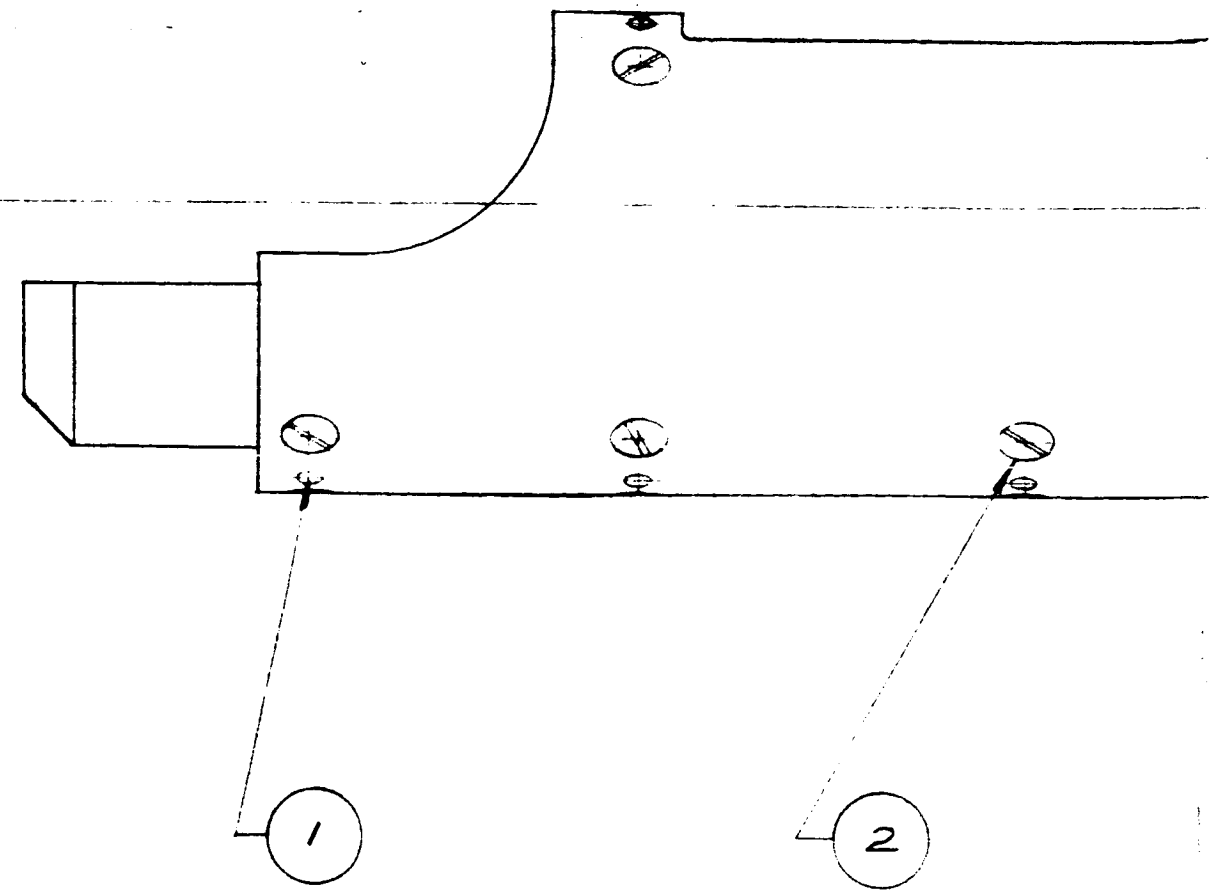

DO NOT INSTALL-.

1) FLUSH WITH SURFACE AFTER FINAL ASSY.

E

F-44 F

PART No.

F-44 C

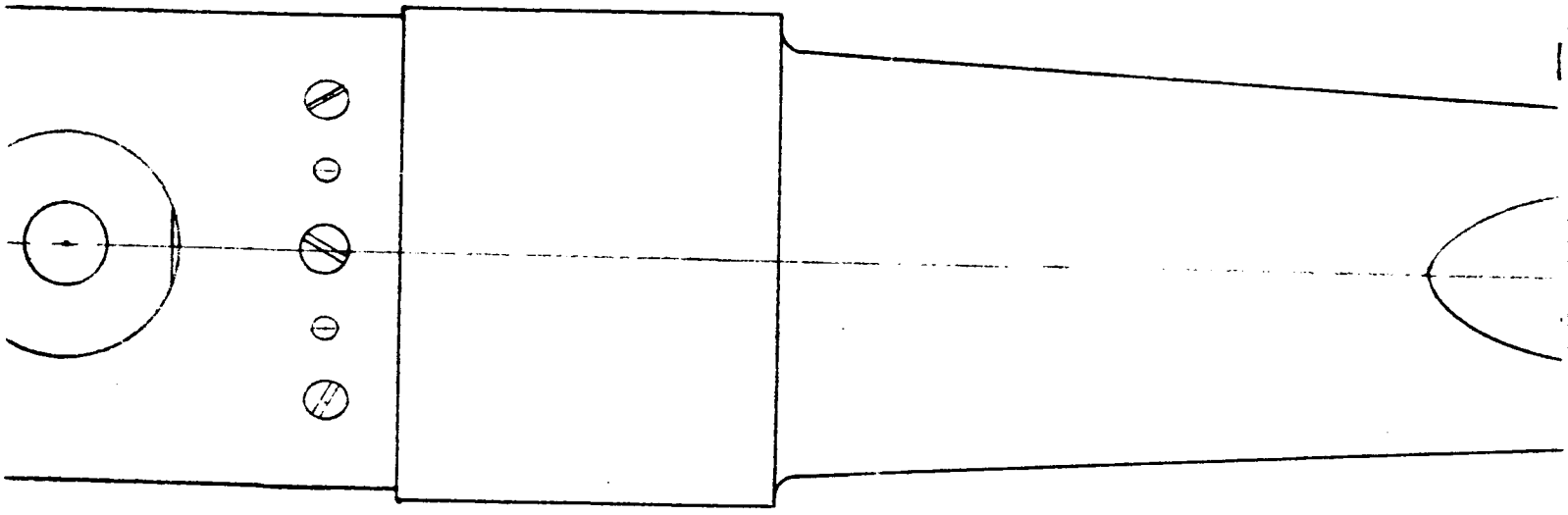

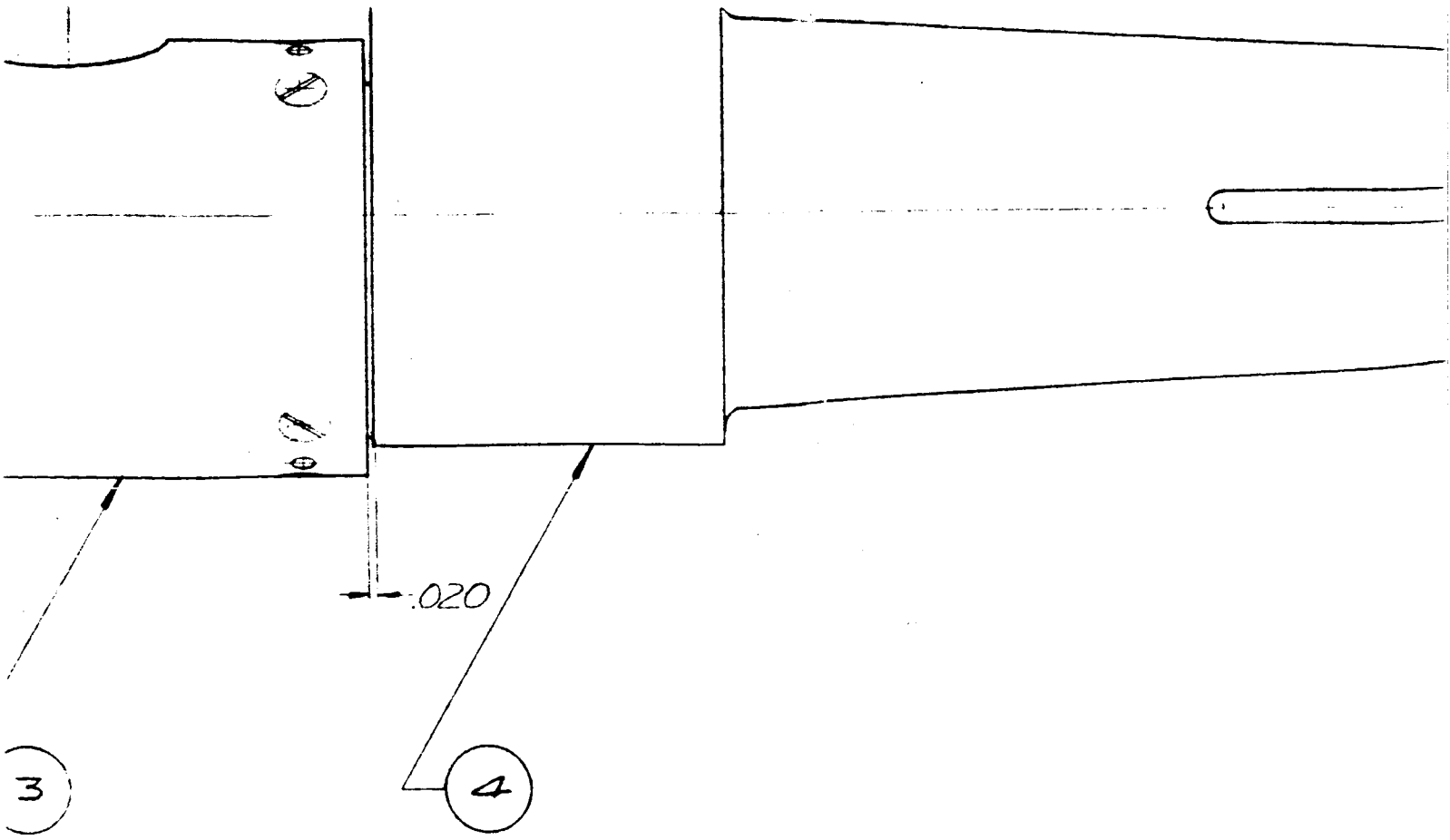

ITEM NO.	DESC
4	BALANCE BASE
3	SLEEVE
2	SCREW-MACH. I
1	DOWEL PIN .062

SEE ENGINEERING RECORDS	
NEXT ASSY	USED ON
APPLICATION	

UNLESS OTHERWISE SPECIFIED

DIMENSIONS ARE IN INCHES

TOLERANCES ON FRACTIONS ——— DECIMALS ±.004 ANGLES ———

MATERIAL ———

HEAT TREATMENT ———

FINAL PROTECTIVE FINISH ———

ORIGIN OF DR.

DRAFTSM. J.E.G.

CHECKER

ENGINEE

SUBMIT

APPRO\

F-44 G

	M F	ZONE	SYM	REVISIONS DESCRIPTION	DATE	APPROVAL
			A	NOTE 2 WAS NOTE 1, ADDED NOTE <1>		
			B	#1-64 WAS #2-56		

F-44D

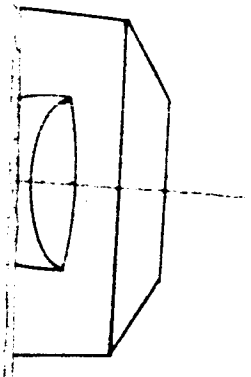

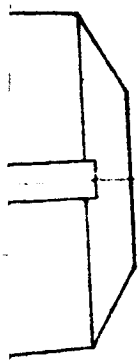

NO. 199	1	80M50787		
	1	80M41660		
H. #1-64NC x 3/16 LG.	19		CRES	
DIA x 3/8 LONG	14		CRES.	
RIPTION	NO REQ'D	PART NO DWG. NO	MATERIAL	REMARKS

LIST OF MATERIAL

DISTR CODE

AL DATE
AWING 17 SEPT, 65

SHEAD | CHECKER
WEEKS | STRESS
ENGINEER

TED

ED

DIRECTOR

BALANCE BASE ASSY. BALANCE 199

WEIGHT CHECKER | DATE | CODE

SCALE 2-1 | UNIT WEIGHT

GEORGE C. MARSHALL SPACE FLIGHT CENTER
NATIONAL AERONAUTICS AND SPACE ADMINISTRATION
HUNTSVILLE, ALABAMA

DWG SIZE D | 80M41665

SHEET 1 OF 1

FIG. 44 F44 H

BY G. Hassett DATE 11-16-65 SUBJECT Balance #199 Load SHEET NO. 1 OF 2
CHKD. BY DATE Design JOB NO. 43003

F-45

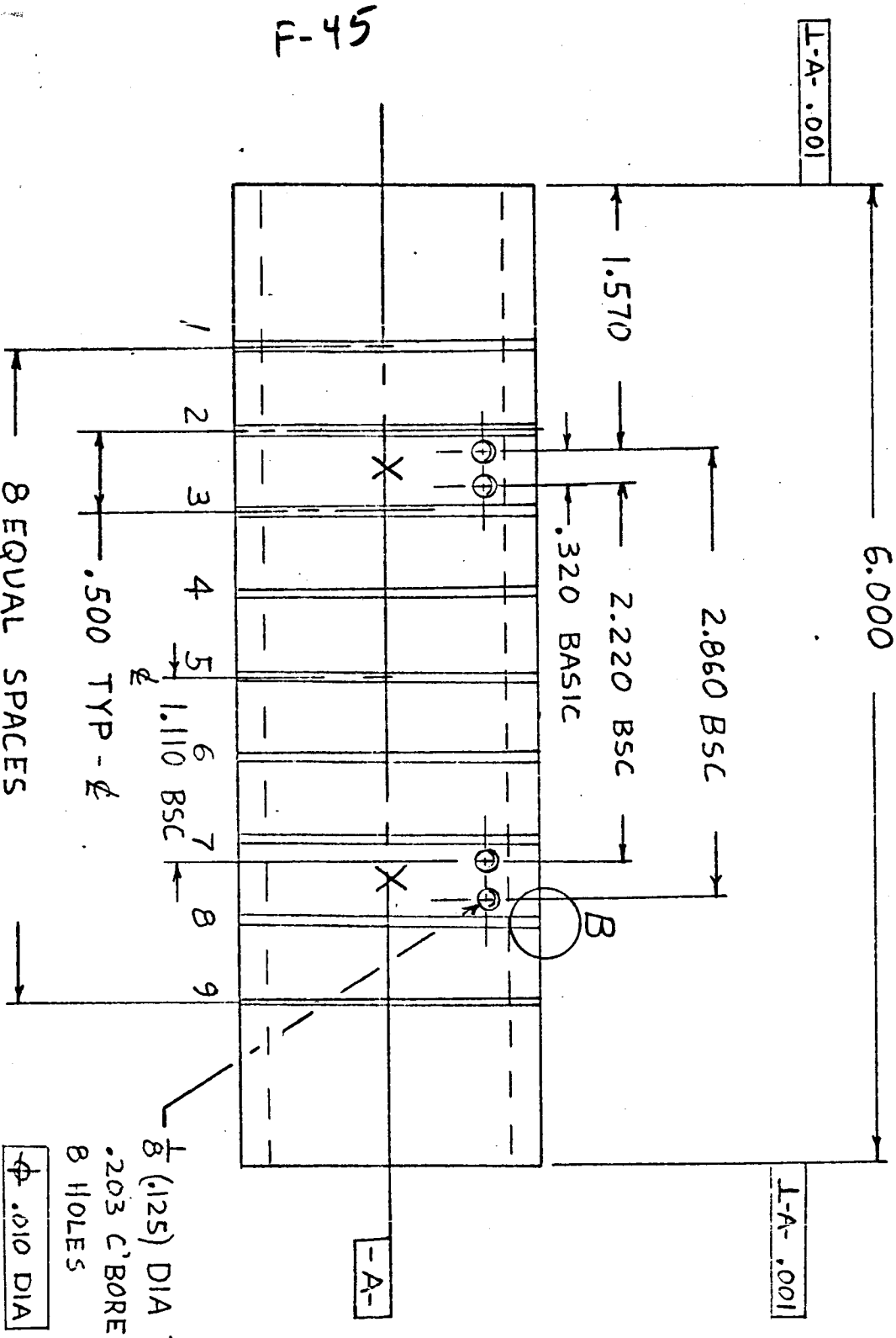

SIDE VIEW

* POSITION 5 IS 3.525 IN. FROM THE 1.10 IN. DIA TAPER REFERENCE

FIGURE #5

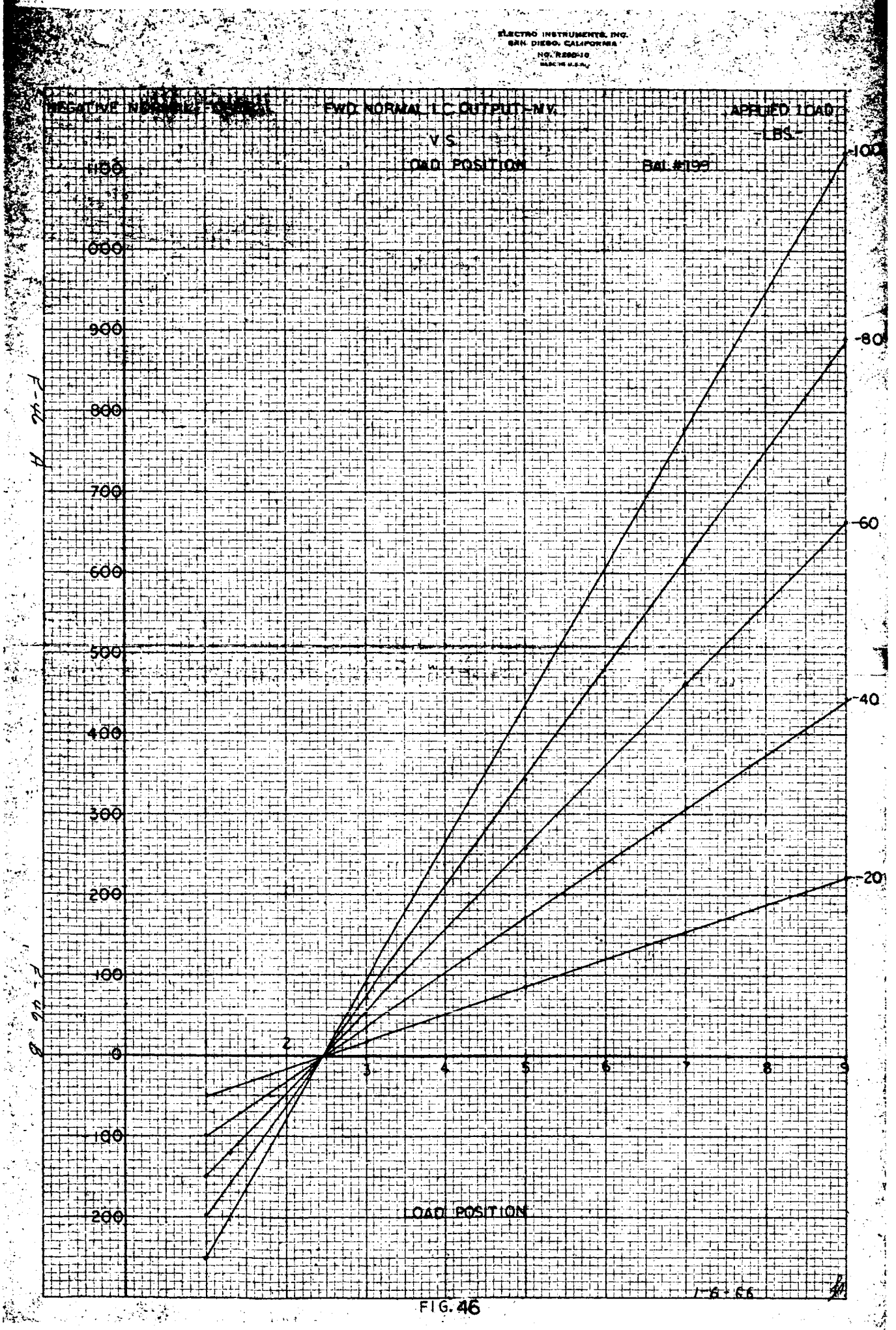
ELECTRO INSTRUMENTS, INC.
SAN DIEGO, CALIFORNIA
NEGATIVE NORMAL FWD. NORMAL L.C. OUTPUT-MV.
V.S.
LOAD POSITION
BAL #195
APPLIED LOAD
-LBS-
-100
-80
-60
-40
-20
1100
1000
900
800
700
600
500
400
300
200
100
0
100
200
1
2
3
4
5
6
7
8
9
LOAD POSITION
1-6-66

FIG. 46

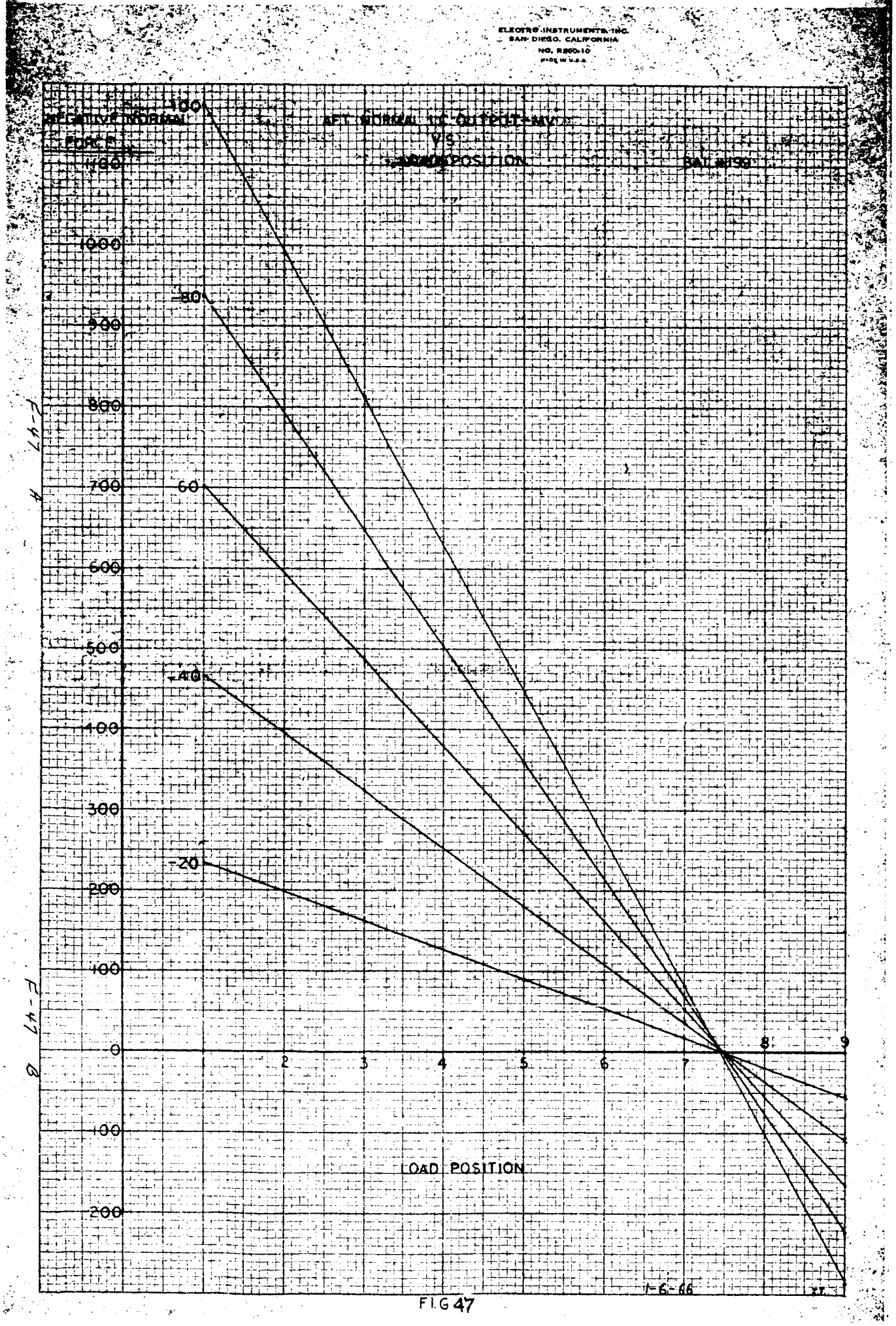
ELECTRO-INSTRUMENTS, INC.
SAN DIEGO, CALIFORNIA
NO. R800-10
MADE IN U.S.A.
AFT NORMAL I/C OUTPUT-MV
VS
LOAD POSITION
BAT #198
NEGATIVE NORMAL
FORCE-#
100
80
60
40
20
1000
900
800
700
600
500
400
300
200
100
0
-100
-200
1
2
3
4
5
6
7
8
9
LOAD POSITION
1-6-66
FIG 47

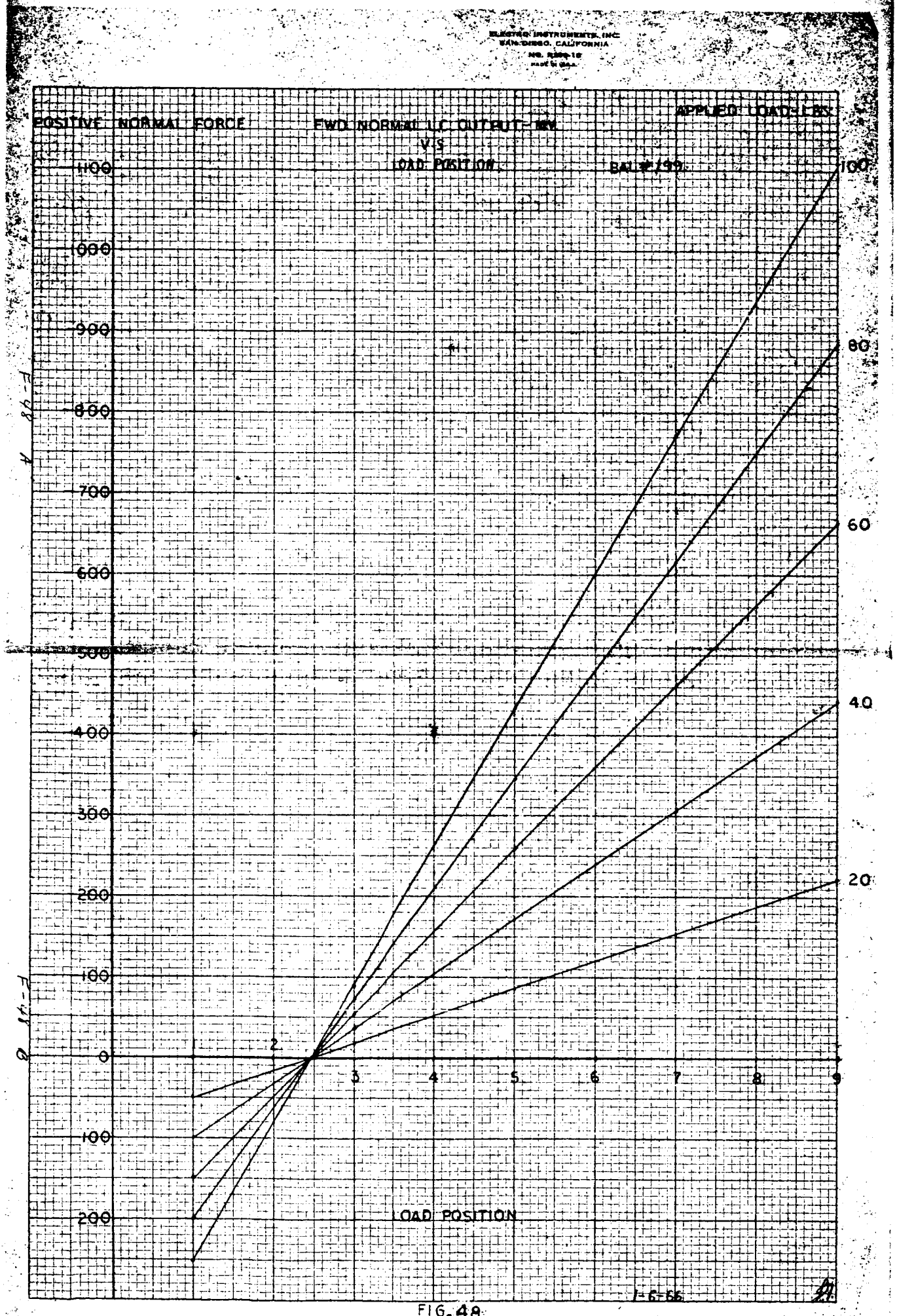
ELECTRO INSTRUMENTS, INC.
SAN DIEGO, CALIFORNIA
POSITIVE NORMAL FORCE
FWD NORMAL LC OUTPUT - MV
VS
LOAD POSITION
BAL # 199
APPLIED LOAD - LBS
100
80
60
40
20
1100
1000
900
800
700
600
500
400
300
200
100
0
100
200
2
3
4
5
6
7
8
9
LOAD POSITION
1-6-56

FIG. 48

ELECTRO INSTRUMENTS, INC.
SAN DIEGO, CALIFORNIA
NO. R200-10
MADE IN U.S.A.

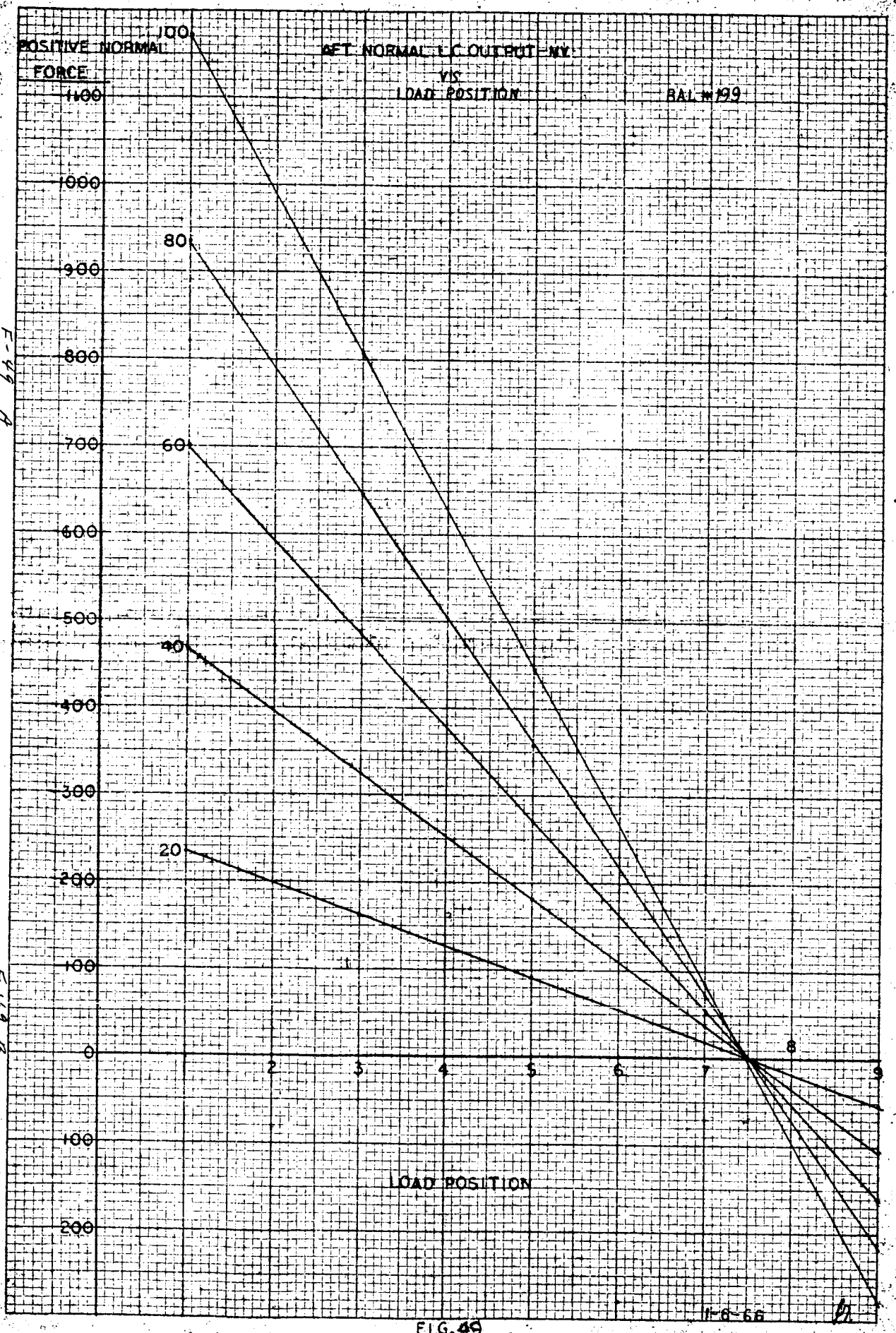

FIG. 49

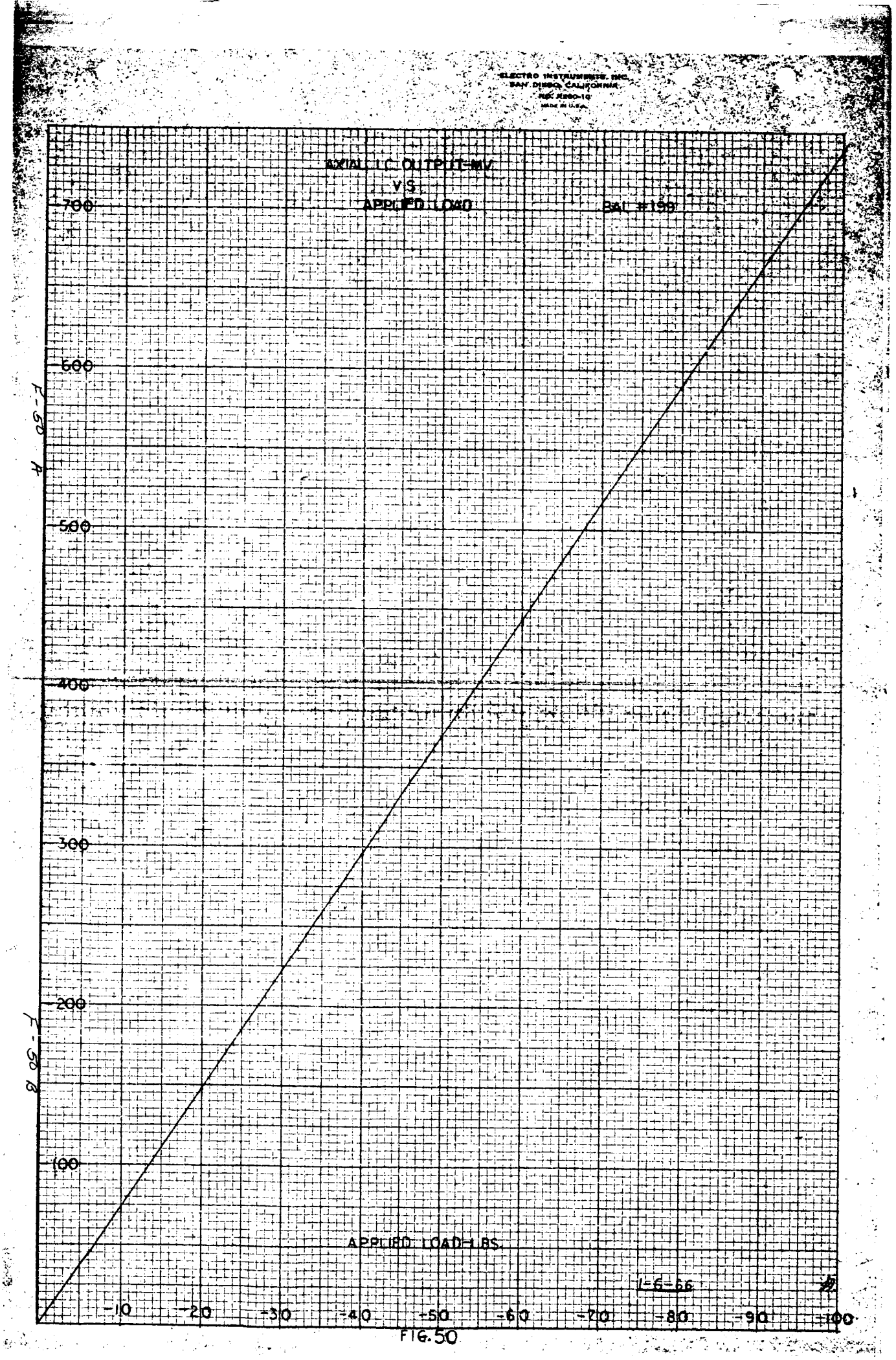
ELECTRO INSTRUMENTS, INC.
SAN DIEGO, CALIFORNIA
AXIAL I.C. OUTPUT-MV
VS.
APPLIED LOAD
BAL #199
700
600
500
400
300
200
100
F-50 A
F-50 B
APPLIED LOAD-LBS.
1-6-66
-10
-20
-30
-40
-50
-60
-70
-80
-90
-100

FIG. 50

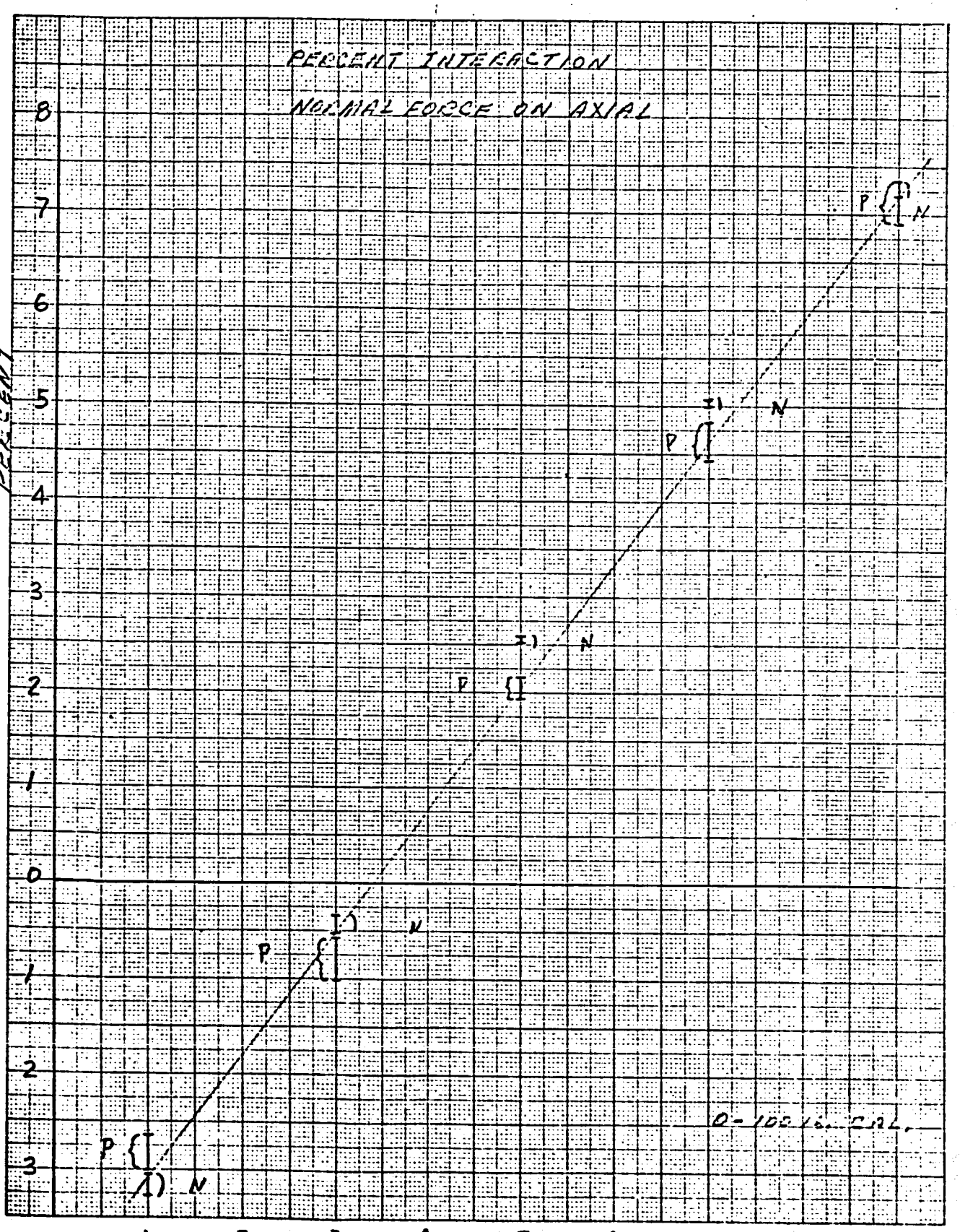

F-51 FIG.51

CLEARPRINT PAPER CO. NO. C301. MILLIMETERS. 200 BY 280 DIVISIONS.
CLEARPRINT CHART
PRINTED IN U.S.A. ON CLEARPRINT TECHNICAL PAPER NO. 1018

ELECTRO INSTRUMENTS, INC.
SAN DIEGO, CALIFORNIA
NO. R200-10
MADE IN U.S.A.

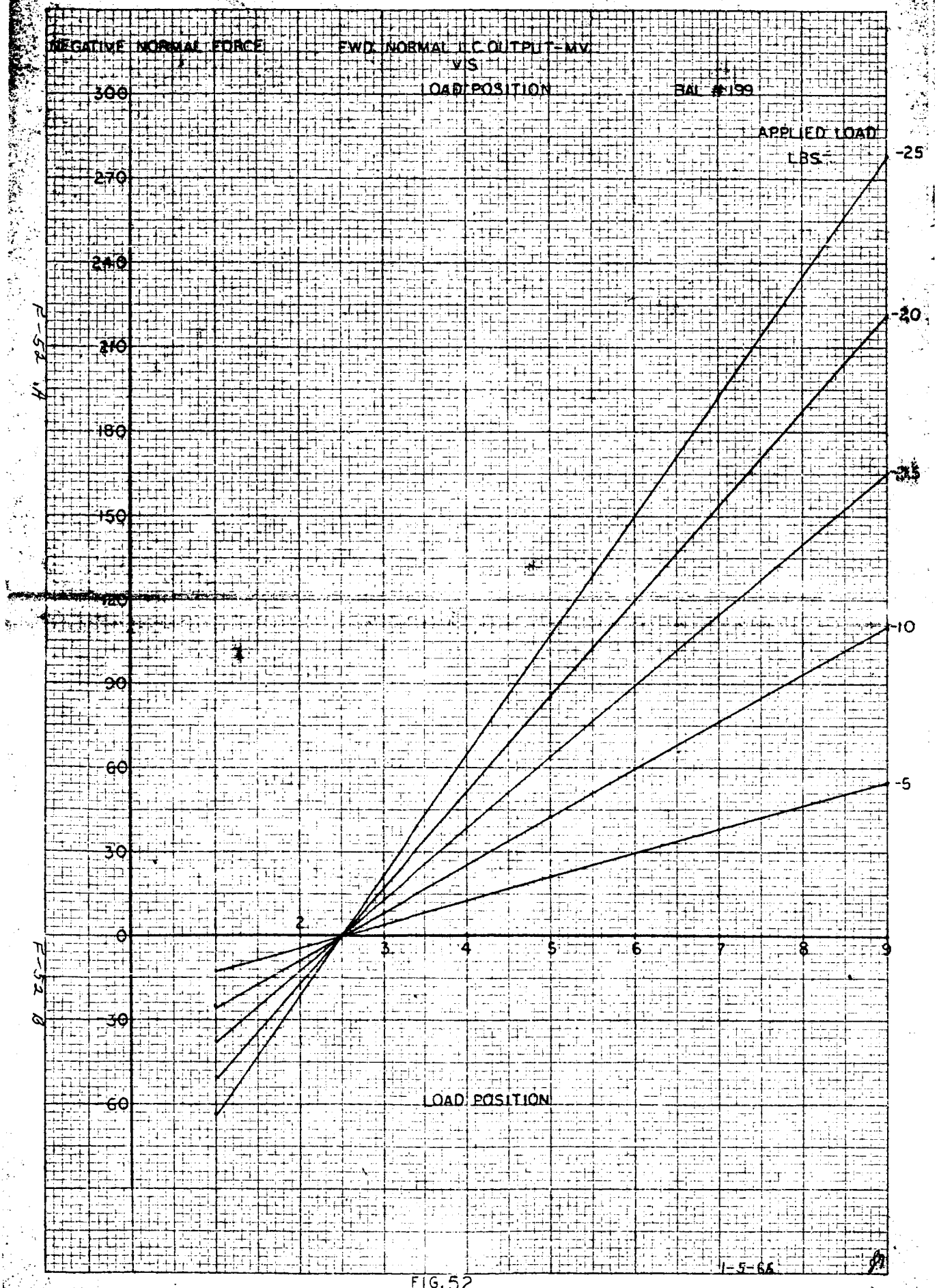

FIG. 52

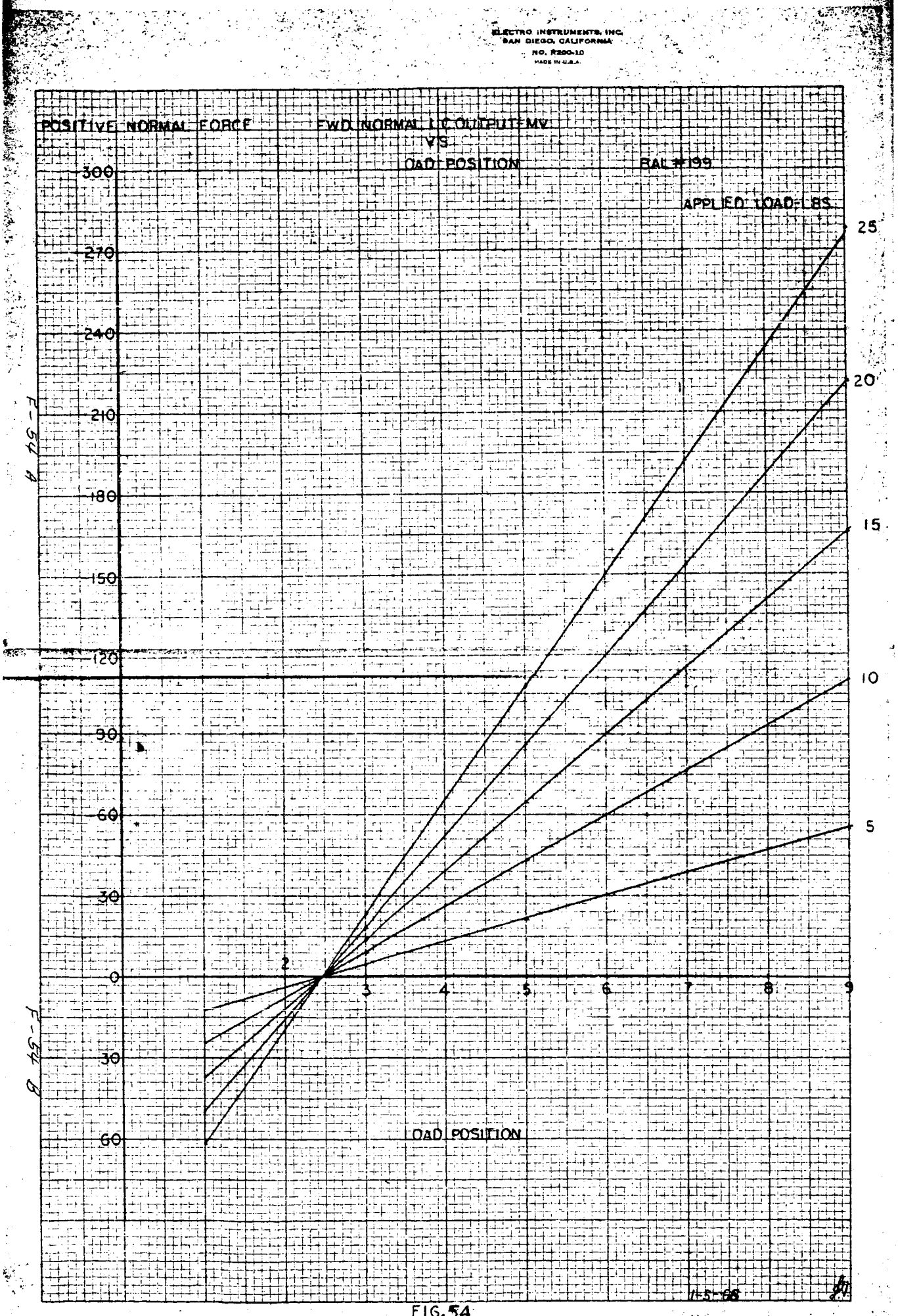
ELECTRO INSTRUMENTS, INC.
SAN DIEGO, CALIFORNIA
NO. P300-10
MADE IN U.S.A.
POSITIVE NORMAL FORCE
FWD NORMAL L.C. OUTPUT=MV.
VS
LOAD POSITION
BAL #199
APPLIED LOAD-LBS.
25
20
15
10
5
300
270
240
210
180
150
120
90
60
30
0
30
60
2
3
4
5
6
7
8
9
F-54 A
F-54 B
LOAD POSITION
1-5-68

FIG. 54

ELECTRO INSTRUMENTS, INC.
SAN DIEGO, CALIFORNIA
NO. R200-10
MADE IN U.S.A.

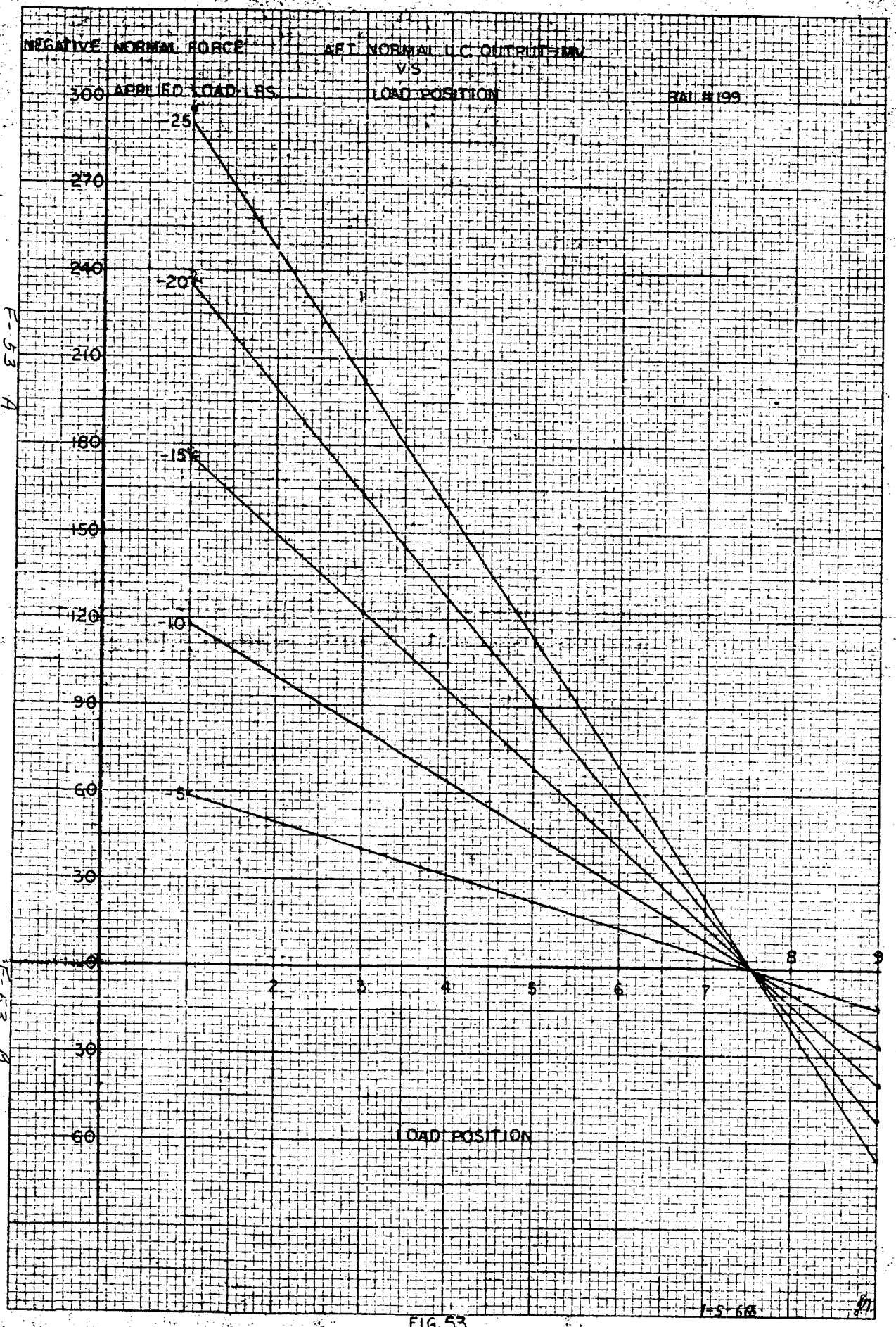

FIG. 53

ELECTRO INSTRUMENTS, INC.
SAN DIEGO, CALIFORNIA
NO. R200-10
MADE IN U.S.A.

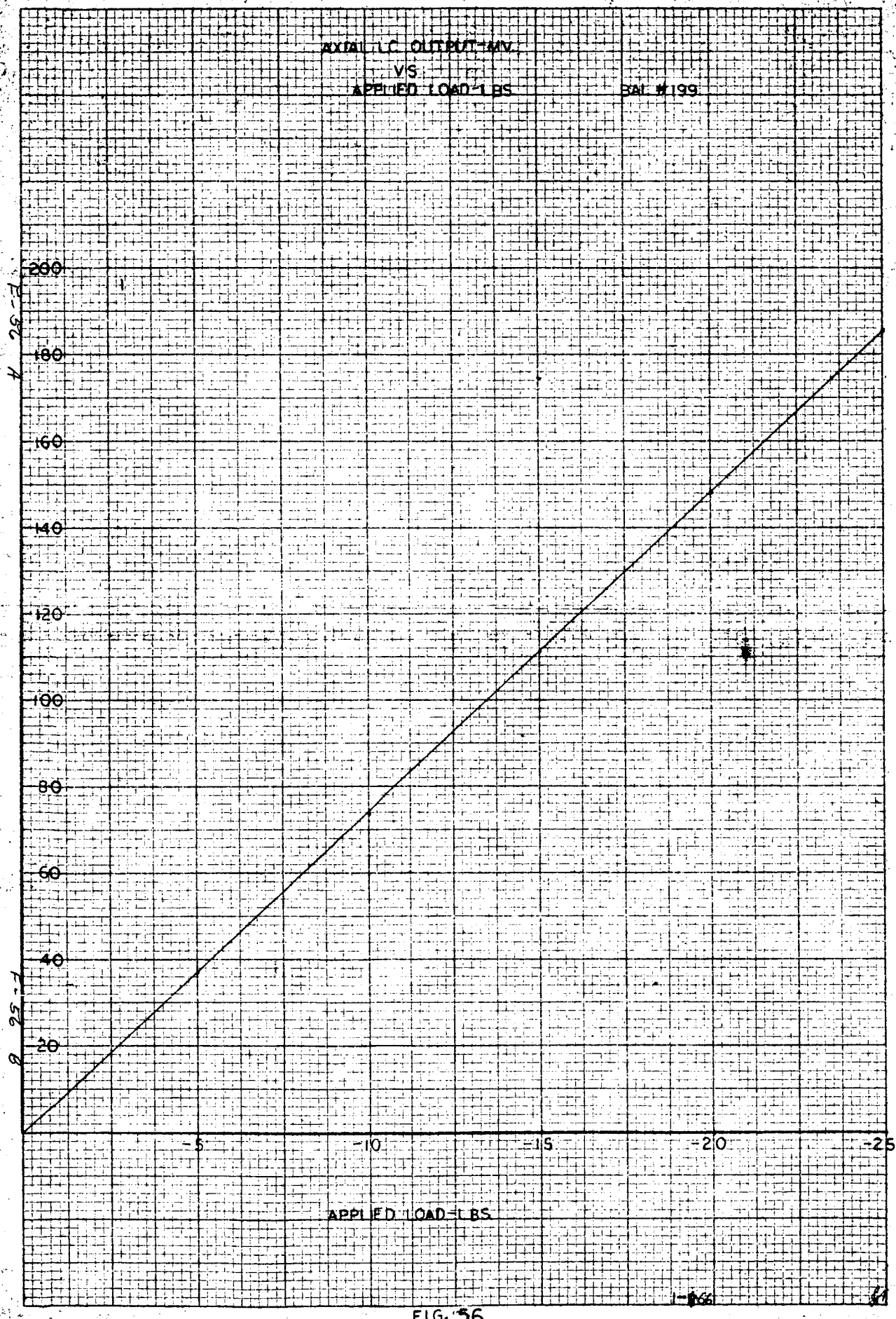

FIG. 56

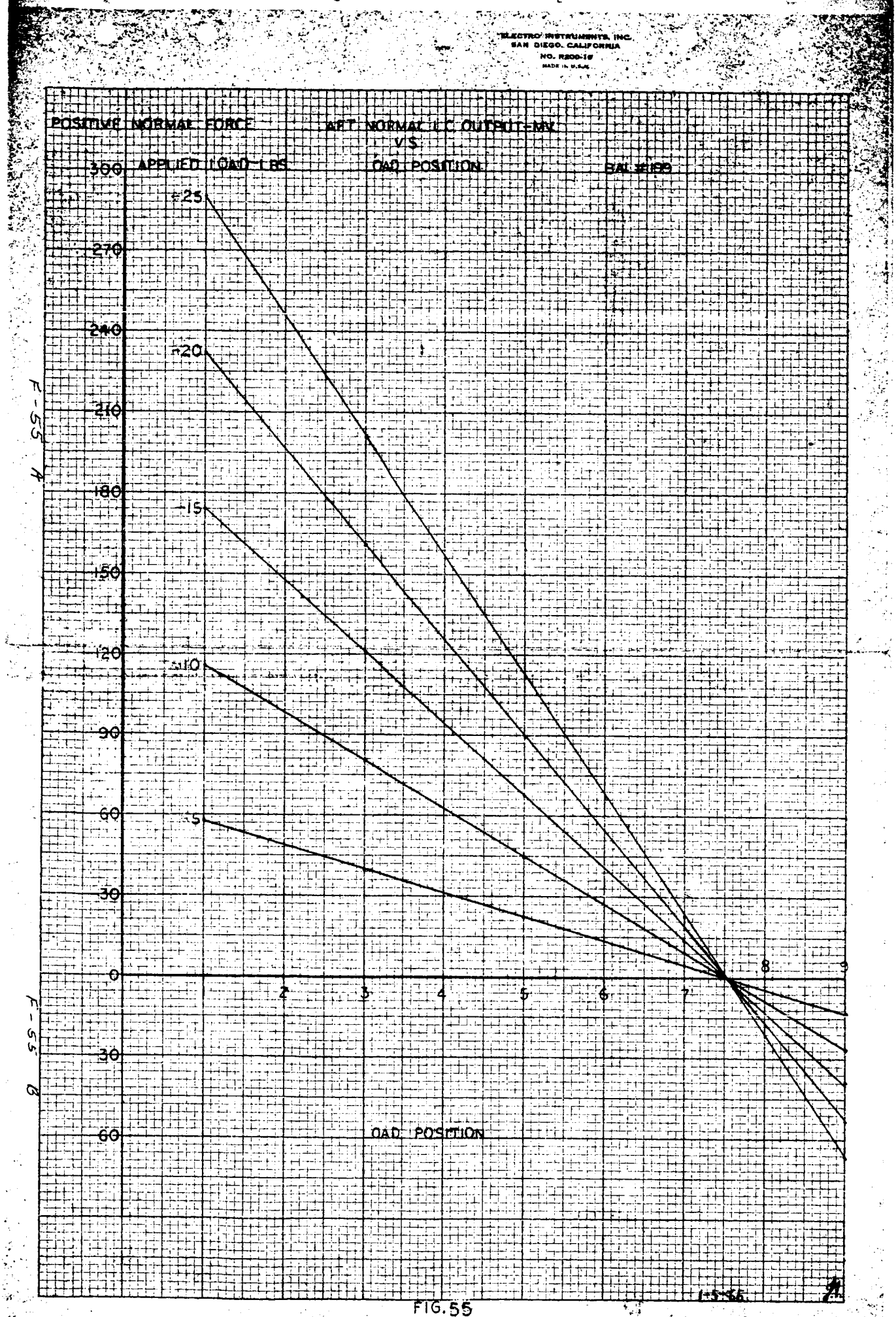
ELECTRO INSTRUMENTS, INC.
SAN DIEGO, CALIFORNIA
NO. R500-19
POSITIVE NORMAL FORCE
APPLIED LOAD-LBS
AFT NORMAL F.C. OUTPUT-MV
VS.
LOAD POSITION
BAL #1199
300
270
240
210
180
150
120
90
60
30
0
30
60
+25
+20
+15
+10
+5
1
2
3
4
5
6
7
8
9
LOAD POSITION
F-55 A
F-55 B
1-5-55

FIG. 55

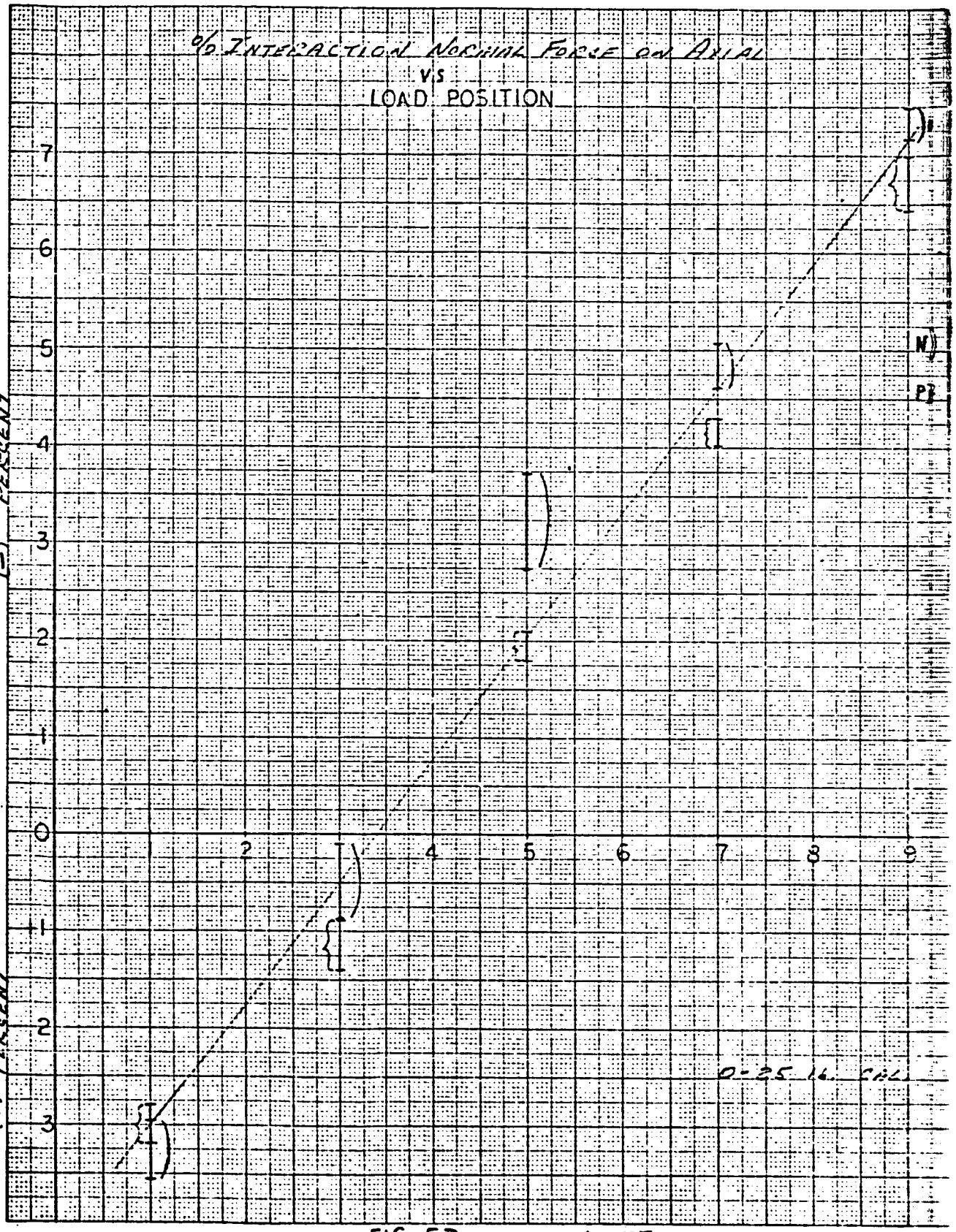

FIG. 57 F-57

PRINTED IN U.S.A. ON CLEARPRINT TECHNICAL PAPER NO. 1018
CLEARPRINT PAPER CO. NO. C252. MILLIMETERS. 200 BY 250 DIVISIONS.

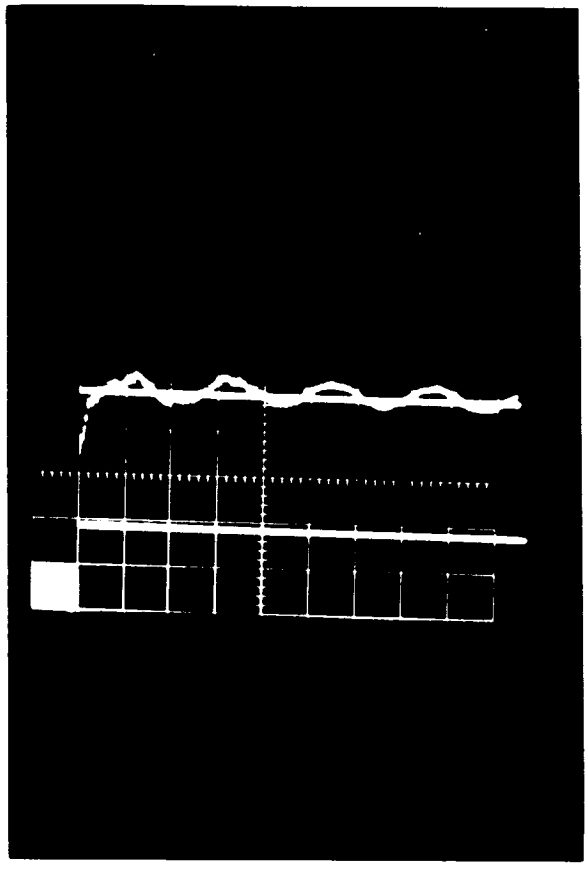

Figure 58 - Uncompensated Forward Load Washer Response Trace

F-58

Figure 59 - Compensated and Filtered
Response Trace

SFC FORM 422-3 (AUGUST 1960)

YTICE. — WHEN GOVERNMENT DRAWINGS, SPECIFICATIONS, OR OTHER DATA
E USED FOR ANY PURPOSE OTHER THAN IN CONNECTION WITH A DEFINITELY
LATED GOVERNMENT PROCUREMENT OPERATION, THE UNITED STATES GOVERN-
NT THEREBY INCURS NO RESPONSIBILITY NOR ANY OBLIGATION WHATSOEVER;
D THE FACT THAT THE GOVERNMENT MAY HAVE FORMULATED, FURNISHED, OR
ANY WAY SUPPLIED THE SAID DRAWINGS, SPECIFICATIONS OR OTHER DATA IS
T TO BE REGARDED BY IMPLICATION OR OTHERWISE AS IN ANY MANNER
ENSING THE HOLDER OR ANY OTHER PERSON OR CORPORATION, OR CONVEY-
ANY RIGHTS OR PERMISSION TO MANUFACTURE, USE, OR SELL ANY
ENTED INVENTION THAT MAY IN ANY WAY BE RELATED THERETO.

F-60-A

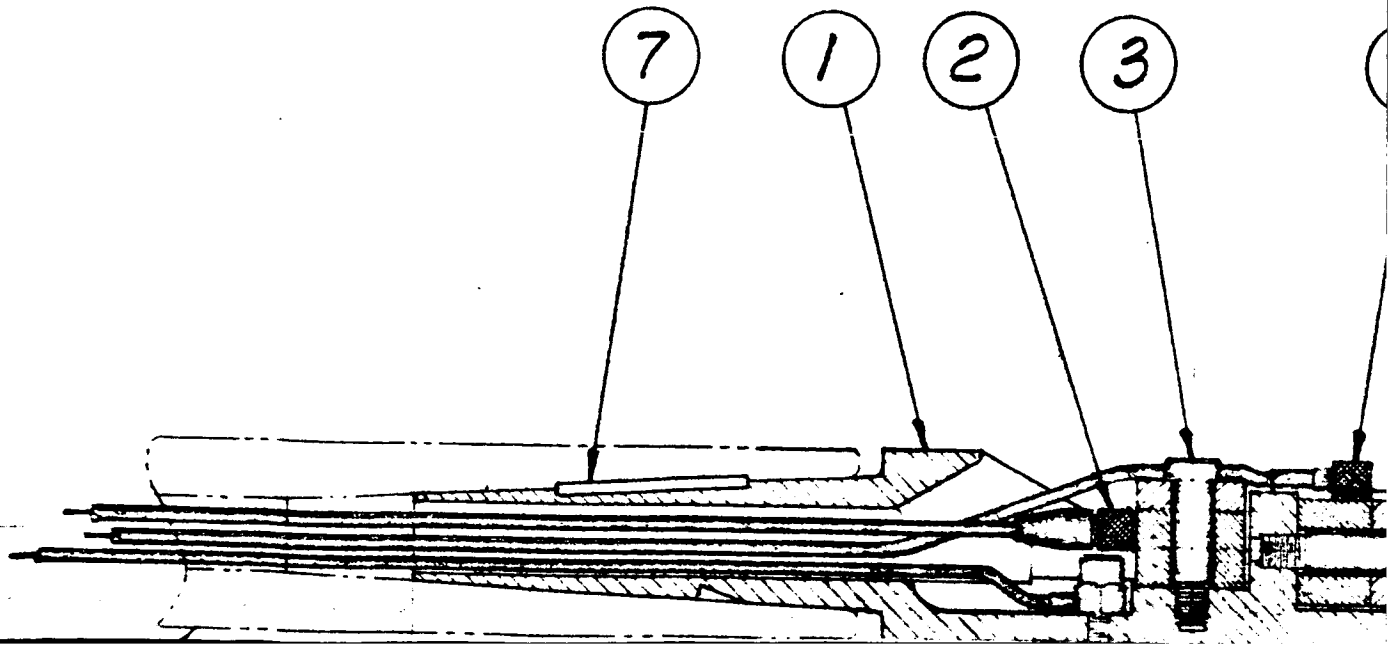

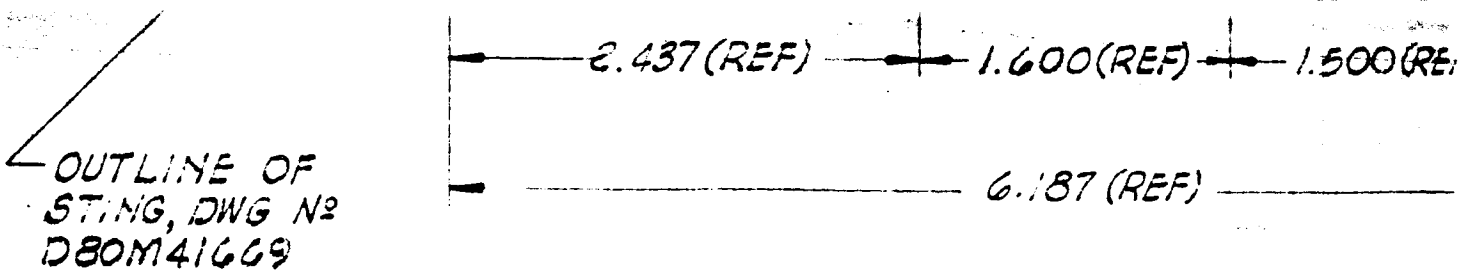
2.437 (REF)
1.600 (REF)
1.500 (RE
6.187 (REF)
OUTLINE OF
STING, DWG Nº
D80M41669

-60-B

	ITEM Nº	DWG Nº	QTY REQD	DESCRIPT
	7	B80M21181	1	KEY
	6		2	ACCELEROMETER, 4-275-0002,
	5	D80M41668	1	LIFT & DRAG FLEXURE SUB
1	4		1	LOAD WASHER, KISTLER MODEL
	3	B80M21180	3	SHOULDER BOLT
1	2		2	LOAD WASHER, KISTLER MOD
	1	D80M41667	1	BASE

SEE ENGINEERING RECORDS

NEXT ASSY | USED ON

APPLICATION

UNLESS OTHERWISE SPECIFIED

DIMENSIONS ARE IN INCHES

TOLERANCES ON

FRACTIONS	DECIMALS	ANGLES
± 1/64	± .004	± 1°

MATERIAL

HEAT TREATMENT

FINAL PROTECTIVE FINISH

	MF	REVISIONS				
		ZONE	SYM	DESCRIPTION	DATE	APPROVAL

F-60 C

GENERAL NOTES

1. KISTLER INSTRUMENT CO., 8989 SHERIDAN DRIVE, CLEARENCE, NEW YORK.

NSOLIDATED ELECTRODYNAMICS, 1500 S. SHAMROCK AVE., MONROVIA, CALIF

SY

: 901M101

Nº 901

O N

MATL

DISTR CODE

GINAL DATE DRAWING 22 OCT 65

TSMAN WEEKS | CHECKER

:KER MILLER | STRESS

NEER | ENGINEER

MITTED

ROVED

DIRECTOR

BALANCE Nº 203 ASSEMBLY

GEORGE C. MARSHALL SPACE FLIGHT CENTER

NATIONAL AERONAUTICS AND SPACE ADMINISTRATION

HUNTSVILLE, ALABAMA

WEIGHT CHECKER	DATE	CODE
SCALE 1:2	UNIT WEIGHT	

DWG SIZE D 80M41666

SHEET OF

F-60 E

FIG. 60

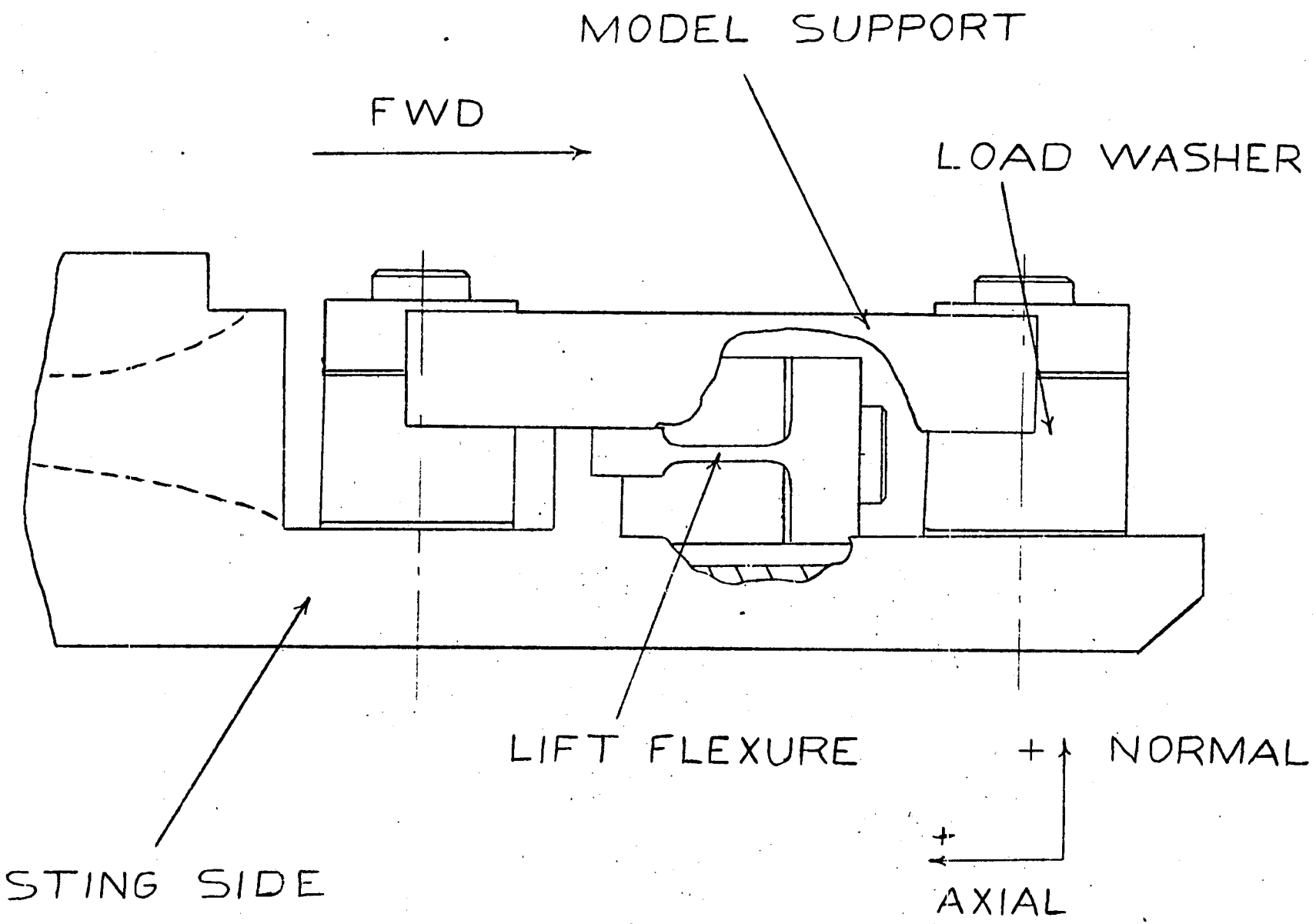

BALANCE #203

FIG. 61

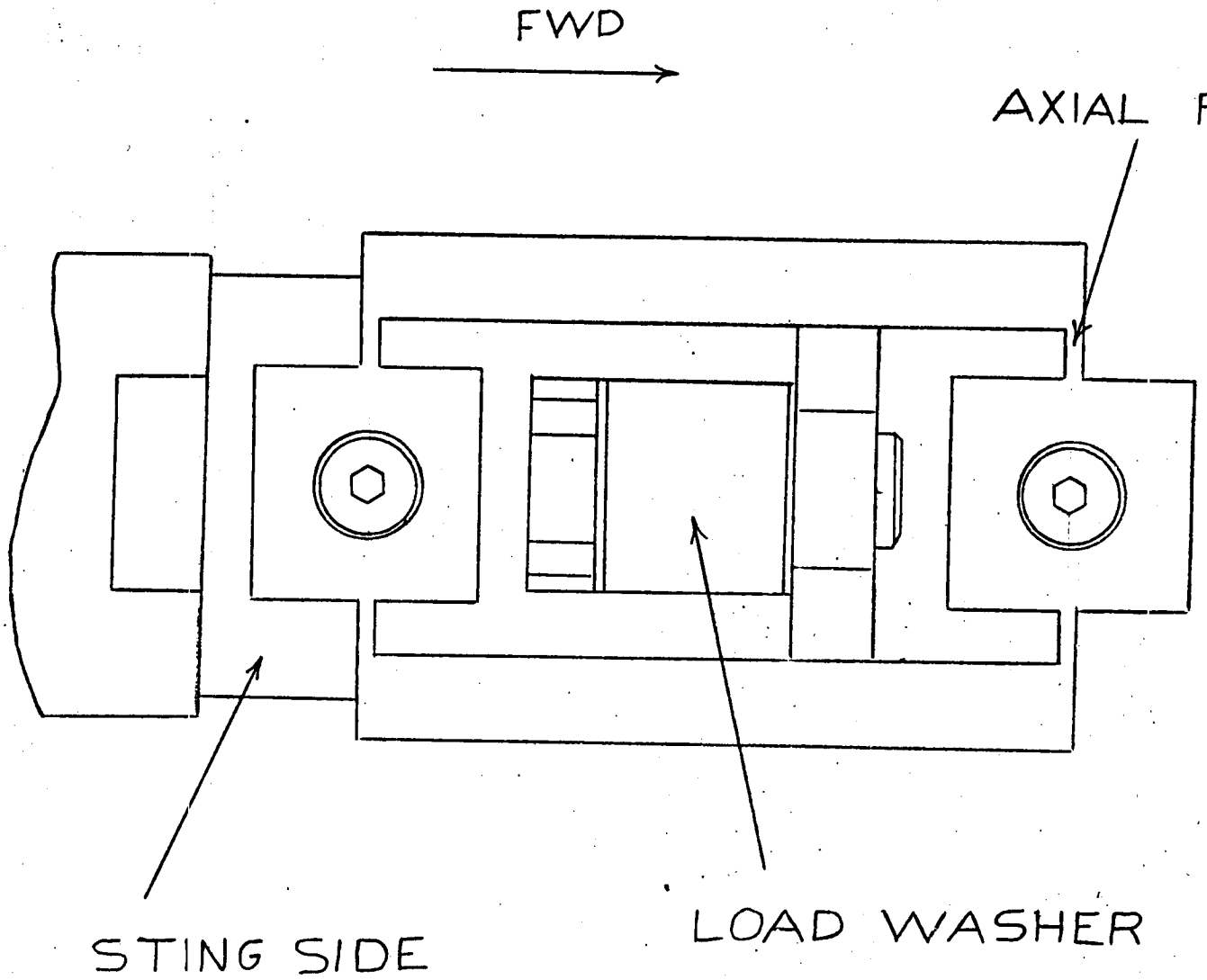

BALANCE #203

FIG. 62

Notice — When Government drawings, specifications, or other data are used for any purpose other than in connection with a definitely related Government procurement operation, the United States Government thereby incurs no responsibility nor any obligation whatsoever and the fact that the Government may have formulated, furnished, or in any way supplied the said drawings, specifications or other data is not to be regarded by implication or otherwise as in any manner licensing the holder or any other person or corporation, or conveying any rights or permission to manufacture, use, or sell any patented invention that may in any way be related thereto.

PART No.	MF

REVISIONS

ZONE	SYM	DESCRIPTION	DATE	APPROVAL
	A	.151/.149 DIA WAS .2180/.2175 DIA	12-17-65	
	A	ADD .020/.030 R	12-17-65	
	A	ADD DIM .70/.60	12-17-65	
	A	REMOVE DIM .300	12-17-65	
	A	REMOVE 1/32 WIDE RELIEF	12-17-65	
	A	REMOVE 1/32 WIDE BY 1/64 DEEP	12-17-65	
	B	ADDED BUSHING	KJan66	

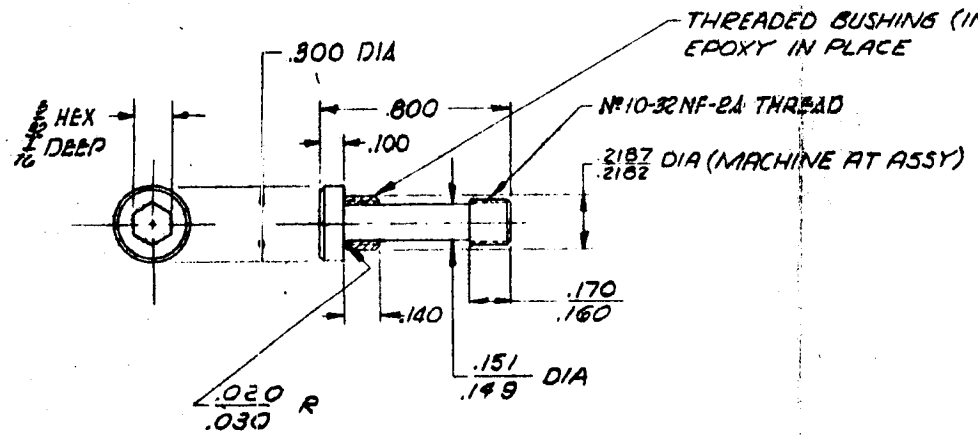

GENERAL NOTES

1. REMOVE BURRS & BREAK SHARP EDGES 1/64 X 45° MAX.
2. (63) UNLESS OTHERWISE SPECIFIED.

SEE ENGINEERING RECORDS	
D80M14666	EAL № 203
NEXT ASSY	USED ON
APPLICATION	

UNLESS OTHERWISE SPECIFIED
DIMENSIONS ARE IN INCHES
TOLERANCES ON FRACTIONS ±1/64 DECIMALS ±.004 ANGLES ±1°

MATERIAL BERYLLIUM COPPER
HEAT TREATMENT
FINAL PROTECTIVE FINISH

ORIGINAL DATE OF DRAWING 22 OCT 65
DRAFTSMAN WEEKS CHECKER
CHECKER MILLER STRESS
ENGINEER L.H. ENGINEER
SUBMITTED
APPROVED
DIRECTOR

SHOULDER BOLT BALANCE № 203

WEIGHT CHECKER	DATE	CODE
SCALE 2=1	UNIT WEIGHT	

DISTR CODE

GEORGE C. MARSHALL SPACE FLIGHT CENTER
NATIONAL AERONAUTICS AND SPACE ADMINISTRATION
HUNTSVILLE, ALABAMA

DWG SIZE B 80M21180
SHEET 1 OF 1

F-63 A F-63 B FIG.63

Figure 64 was not used.

MSFC FORM 422-2 (AUGUST 1960)

Notice — When Government drawings, specifications, or other data are used for any purpose other than in connection with a definitely related Government procurement operation, the United States Government thereby incurs no responsibility nor any obligation whatsoever; and the fact that the Government may have formulated, furnished, or in any way supplied the said drawings, specifications or other data is not to be regarded by implication or otherwise as in any manner licensing the holder or any other person or corporation, or conveying any rights or permission to manufacture, use, or sell any patented invention that may in any way be related thereto.

F-65 A

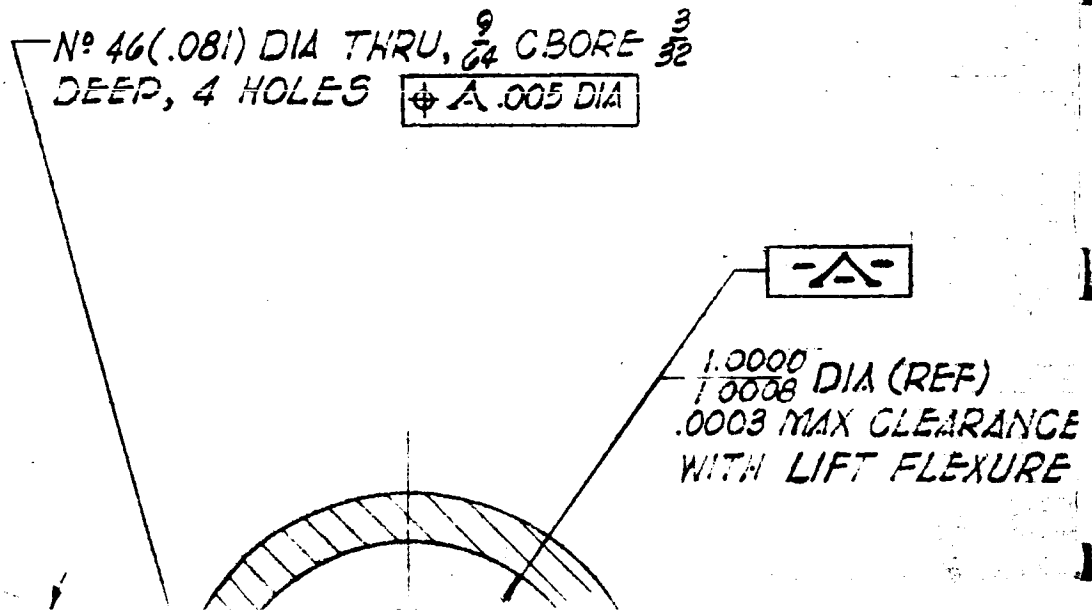

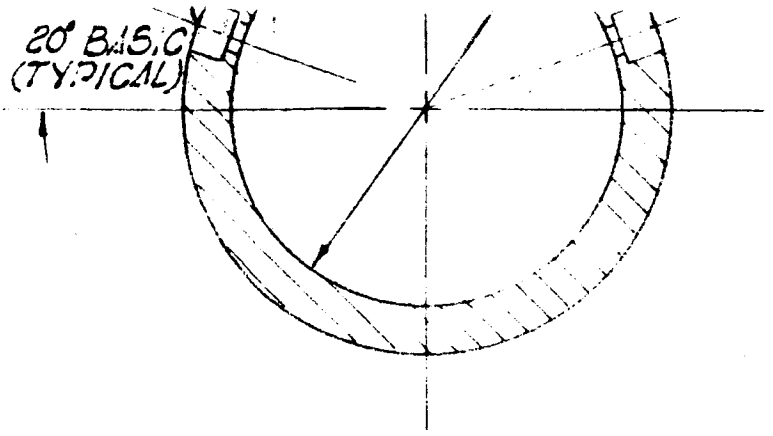

SECTION "A-A"

SEE E
RECOR

NEXT AS

PART No.

F-65 B

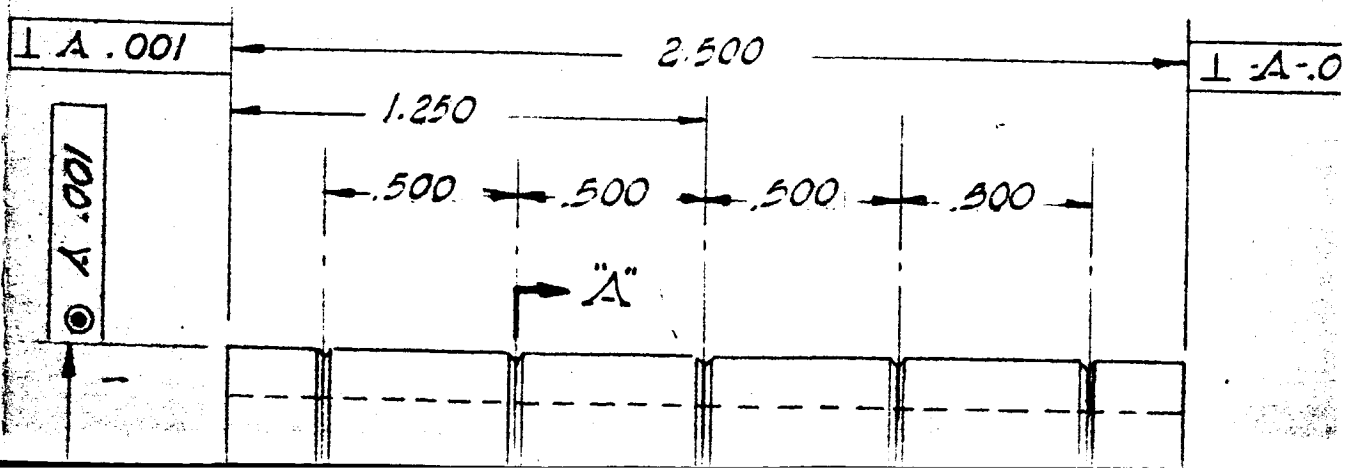

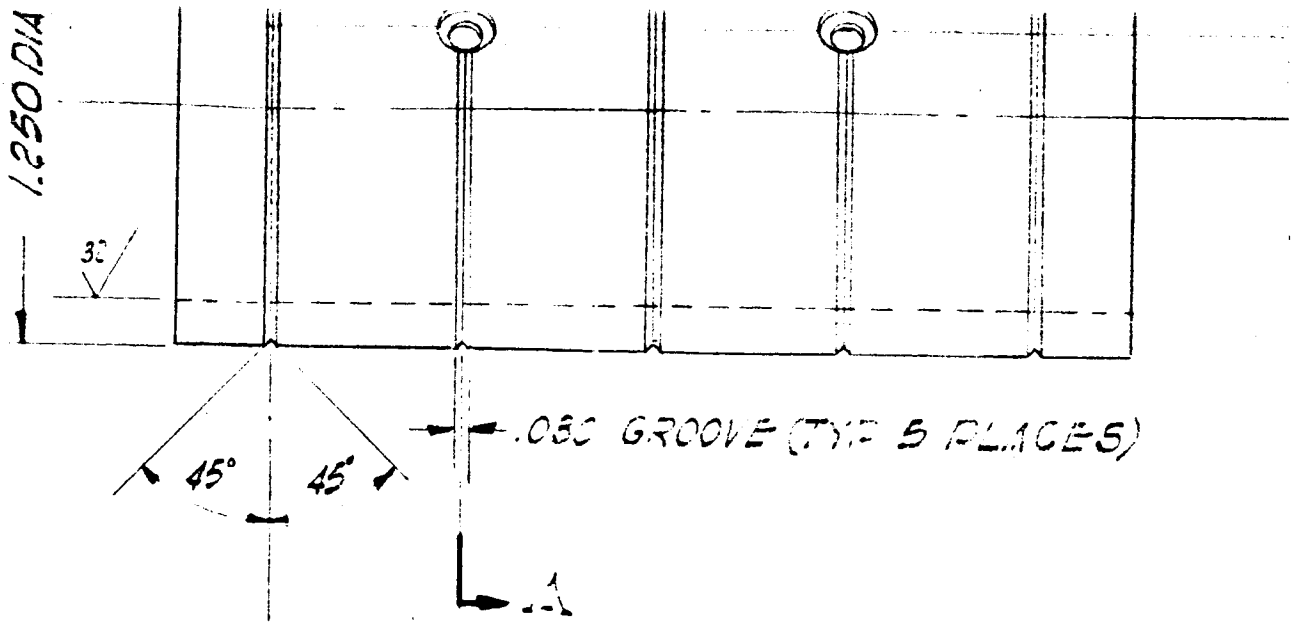

	UNLESS OTHERWISE SPECIFIED		ORIGINAL DATE OF DRAWING 20 DEC
GINEERING)S	DIMENSIONS ARE IN INCHES TOLERANCES ON FRACTIONS ±1/64 DECIMALS ±.005 ANGLES ±1°		DRAFTSMAN WEEKS / CHECKER CHECKER / STRESS ENGINEER / ENGINEER
	MATERIAL 17-4 PH CRES		SUBMITTED
USED ON	HEAT TREATMENT		APPROVED
LICATION	FINAL PROTECTIVE FINISH		DIRECTOR

M F	REVISIONS				
	ZONE	SYM	DESCRIPTION	DATE	APPROVAL

F-65 C

01

GENERAL NOTES

1. REMOVE BURRS AND BREAK SHARP EDGES $\frac{1}{64}$ X 45° MAX.
2. 63 UNLESS OTHERWISE NOTED

DISTR CODE

65

CALIBRATION SLEEVE
BALANCE Nº 203

GEORGE C. MARSHALL SPACE FLIGHT CENTER
NATIONAL AERONAUTICS AND SPACE ADMINISTRATION
HUNTSVILLE, ALABAMA

WEIGHT CHECKER	DATE	CODE	DWG SIZE C	80M31744
SCALE 2=1	UNIT WEIGHT		SHEET	OF

F-65 E FIG.65

CLEARPRINT PAPER CO. NO. C45 10 DIVISIONS PER INCH BOTH WAYS 150 X 100 DIVISIONS. PRINTED IN U.S.A. ON CLEARPRINT TECHNICAL PAPER NO. 1015

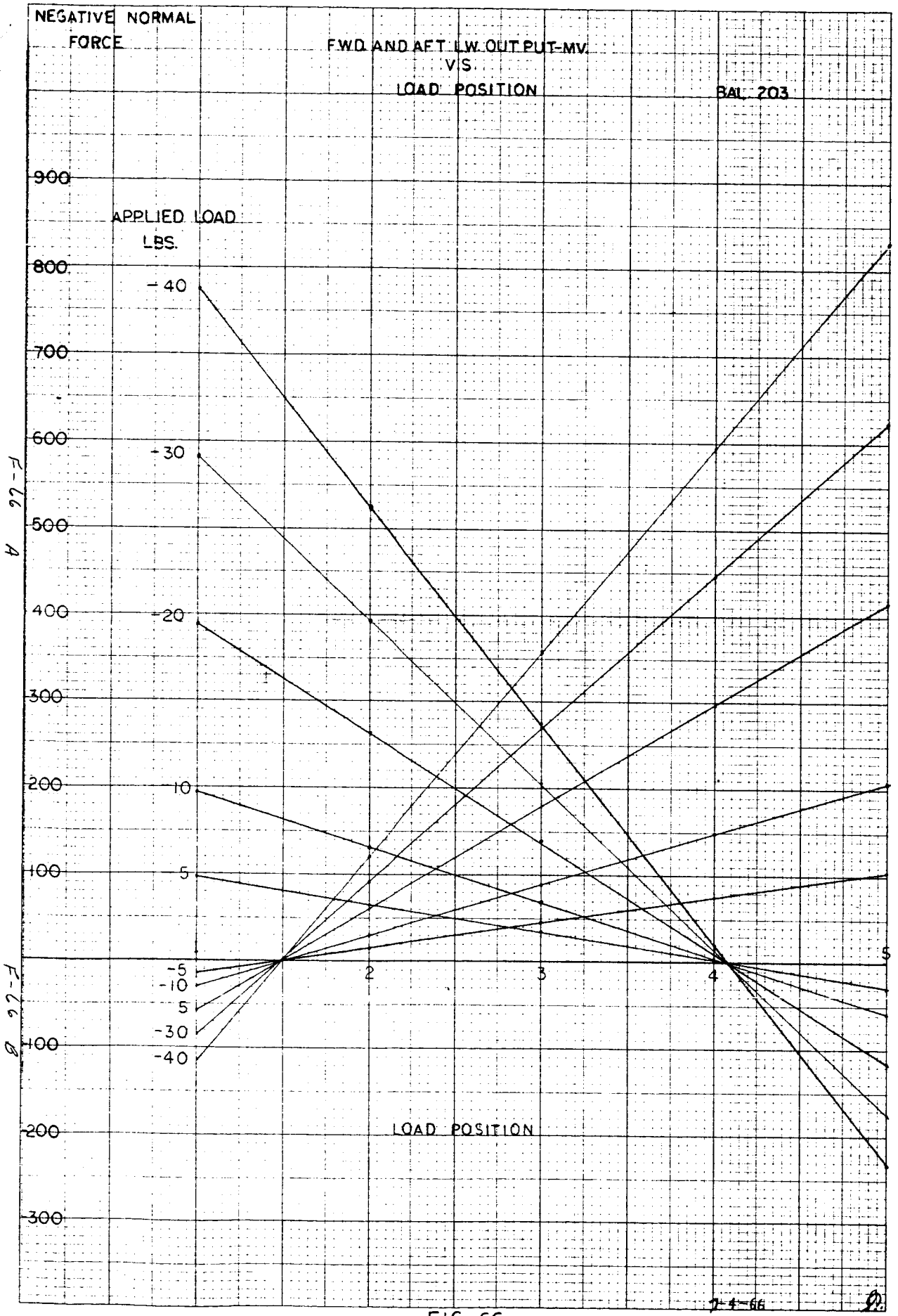

FIG. 66

CLEARPRINT PAPER CO NO. C4S 10 DIVISIONS PER INCH BOTH WAYS 100 & 100 DIVISIONS PRINTED IN U.S.A. ON CLEARPRINT TECHNICAL PAPER NO 1015

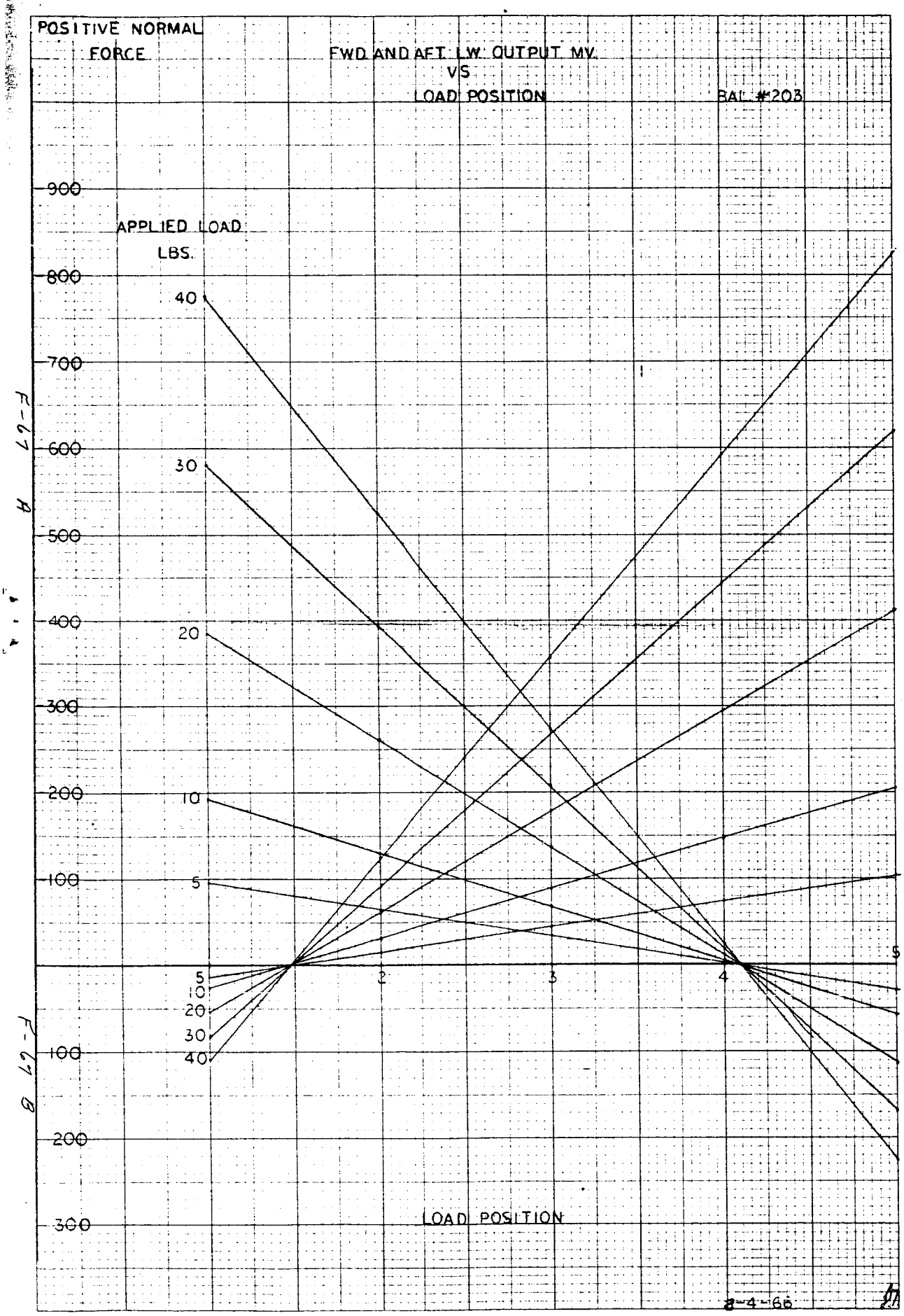

Figure 67

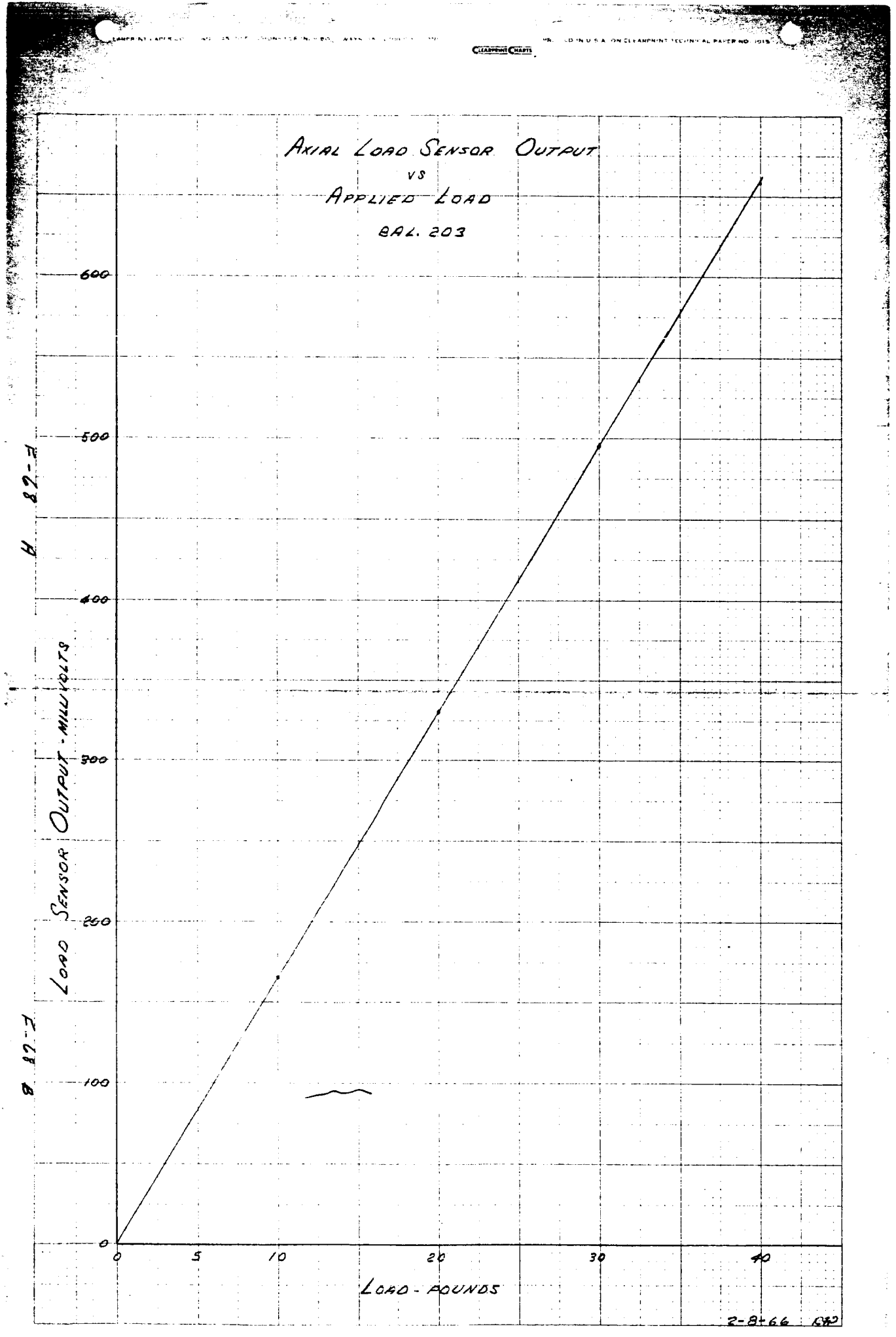
AXIAL LOAD SENSOR OUTPUT
VS
APPLIED LOAD
BAL. 203
600
500
400
300
250
100
0
LOAD SENSOR OUTPUT - MILLIVOLTS
0
5
10
20
30
40
LOAD - POUNDS
2-8-66

Figure 68

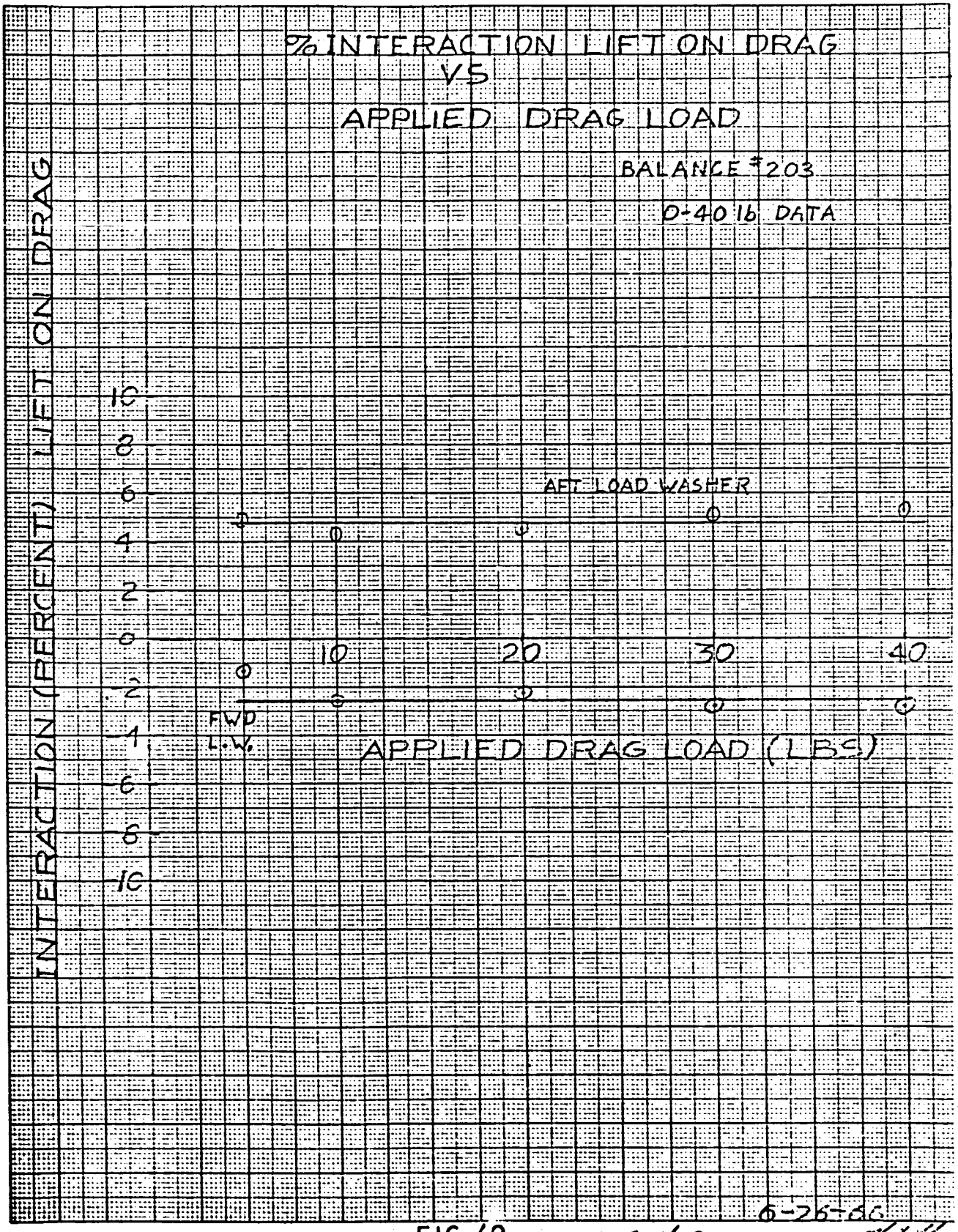
% INTERACTION LIFT ON DRAG
VS
APPLIED DRAG LOAD
BALANCE #203
0-40 lb DATA
AFT LOAD WASHER
INTERACTION (PERCENT) LIFT ON DRAG
10
8
6
4
2
0
-2
-4
-6
-8
-10
10
20
30
40
FWD
L.W.
APPLIED DRAG LOAD (LBS.)
6-26-56

FIG. 69

F-69

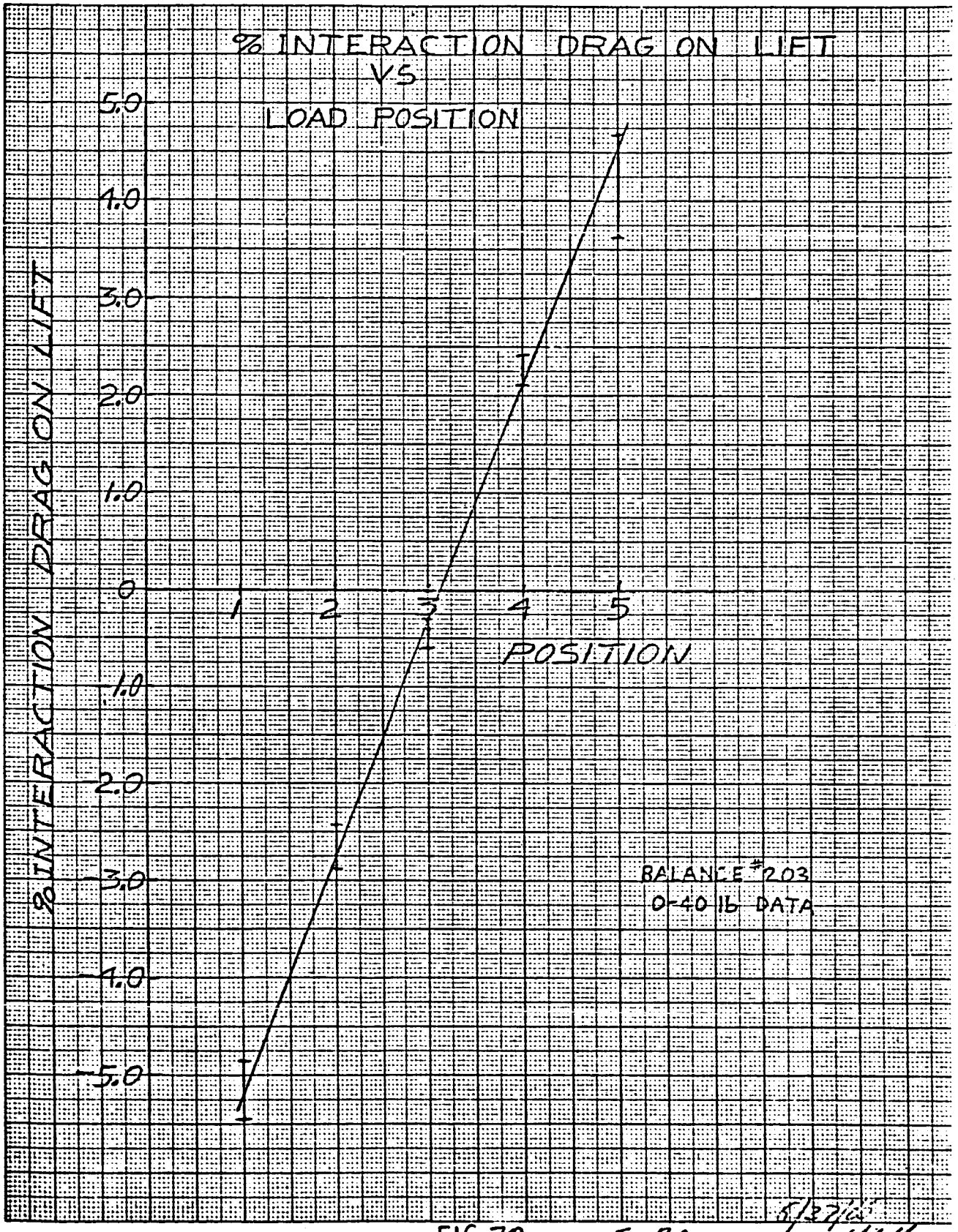
% INTERACTION DRAG ON LIFT
VS
LOAD POSITION
% INTERACTION DRAG ON LIFT
5.0
1.0
3.0
2.0
1.0
0
1.0
2.0
3.0
4.0
5.0
1
2
3
4
5
POSITION
BALANCE #203
0-40 lb DATA

FIG. 70 F-70

CLEARPRINT PAPER CO. NO. CAD. 10 DIVISIONS PER INCH BOTH WAYS. 150 X 100 DIVISIONS.
PRINTED IN U.S.A. ON CLEARPRINT TECHNICAL PAPER NO. 1015

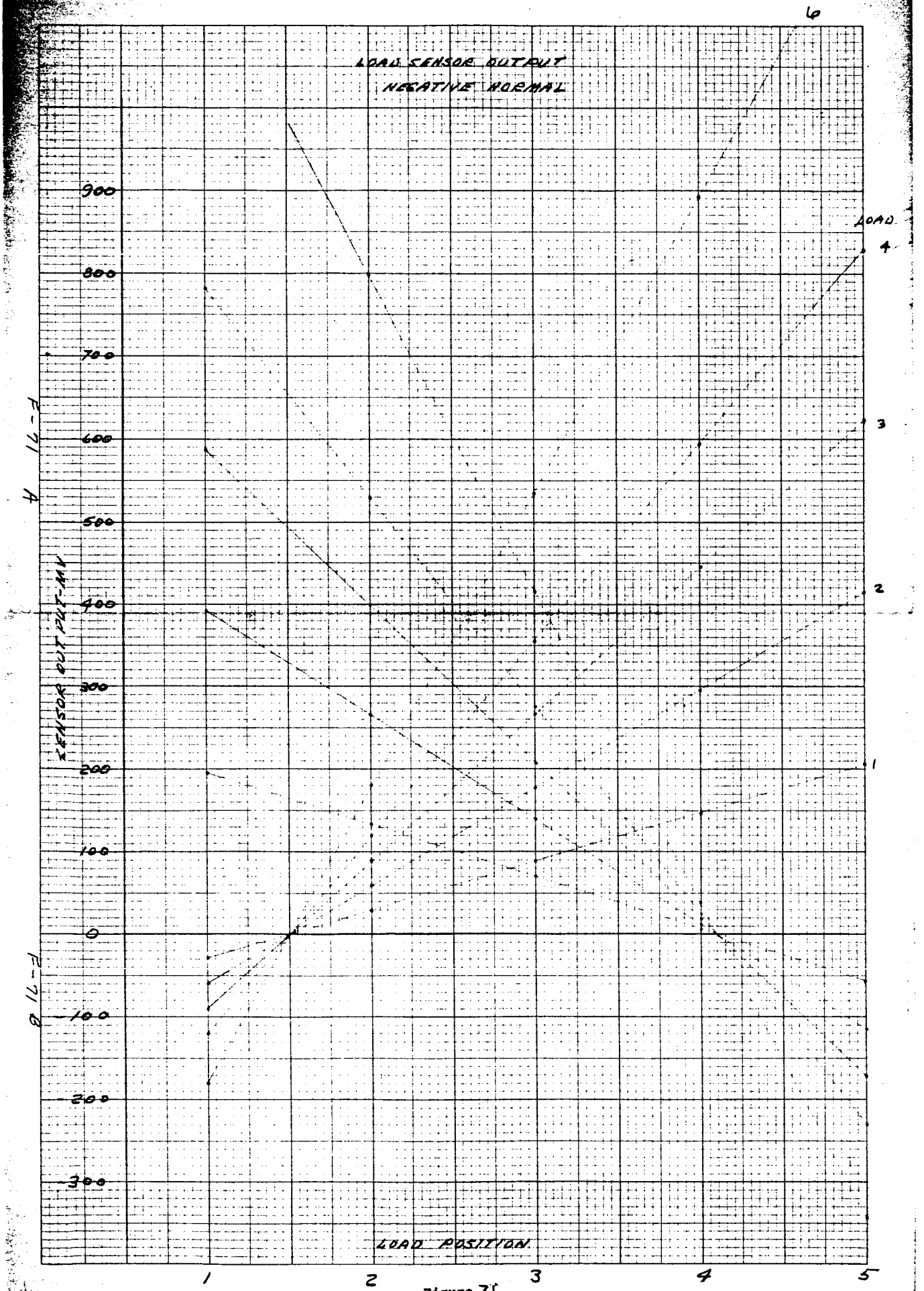

Figure 7

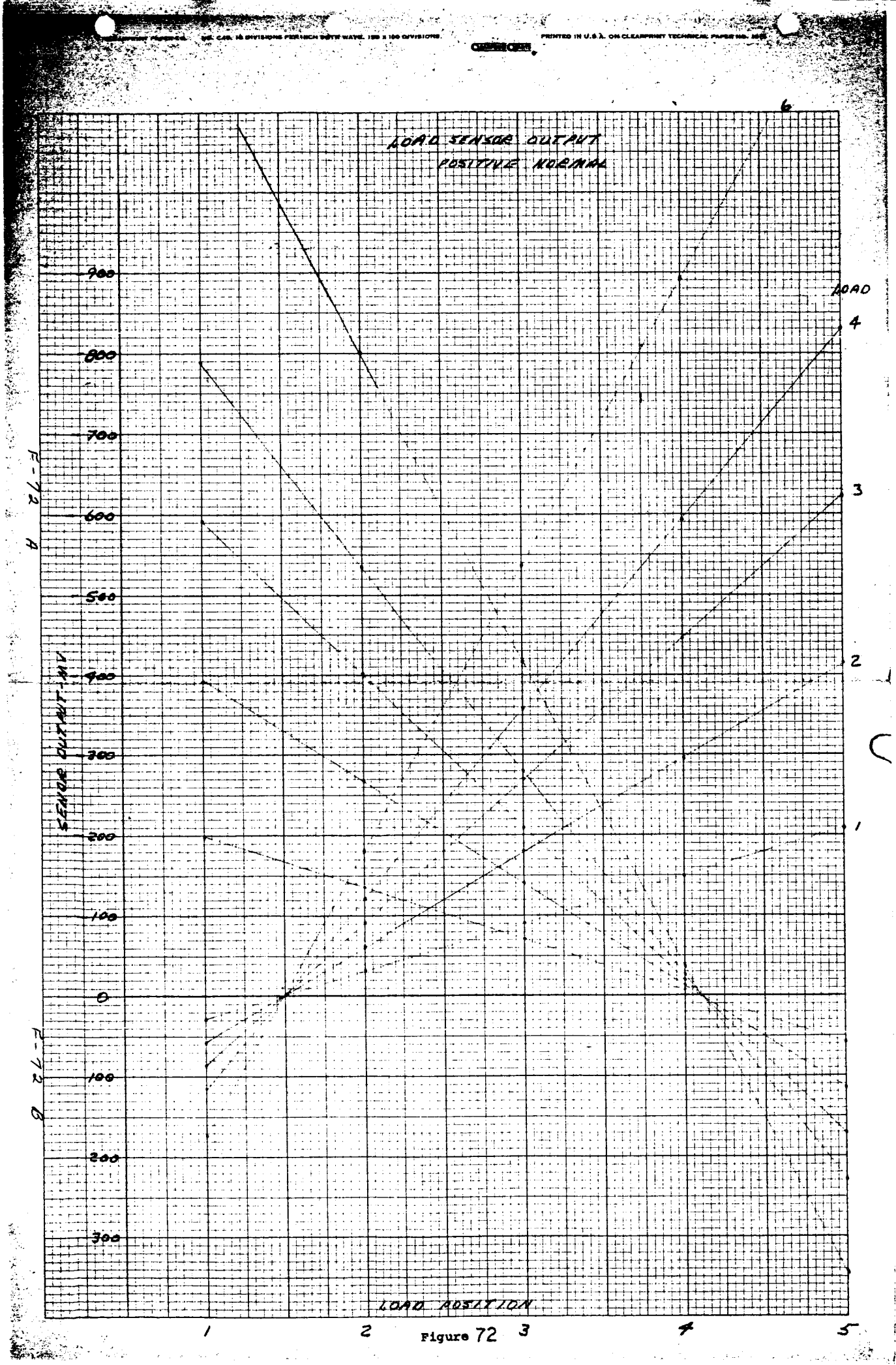
LOAD SENSOR OUTPUT
POSITIVE NORMAL
LOAD
SENSOR OUTPUT-MV
LOAD POSITION
900
800
700
600
500
400
300
200
100
0
100
200
300
1
2
3
4
5
6

Figure 72

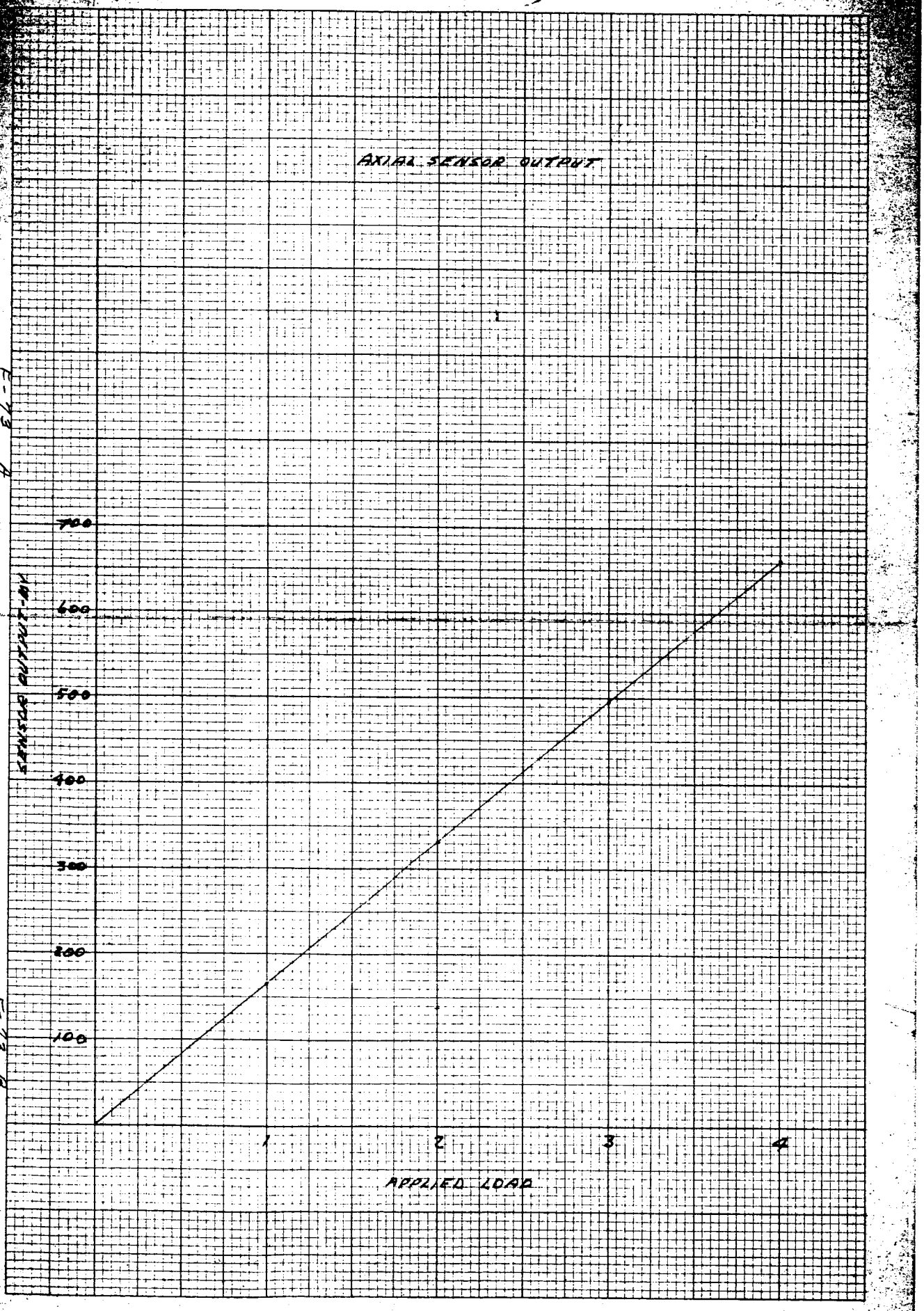
AXIAL SENSOR OUTPUT
E-73 #
SENSOR OUTPUT-AH
700
600
500
400
300
200
100
E-73 B
1
2
3
4
APPLIED LOAD

Figure 73

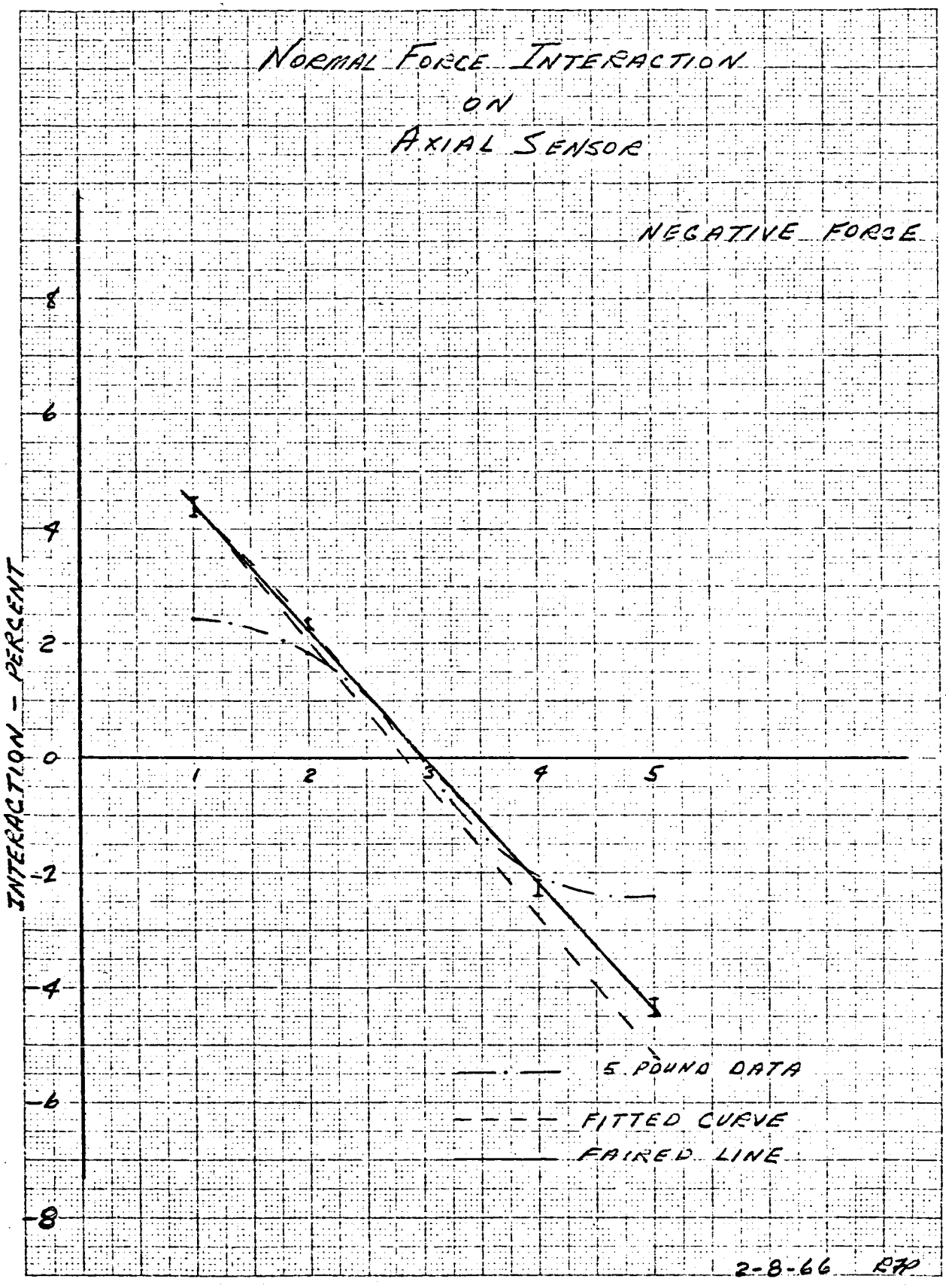
NORMAL FORCE INTERACTION
ON
AXIAL SENSOR
NEGATIVE FORCE
INTERACTION - PERCENT
8
6
4
2
0
-2
-4
-6
-8
1
2
3
4
5
5 POUND DATA
FITTED CURVE
FAIRED LINE
2-8-66 RP

Figure 74